Emulsion-derived (PolyHIPE) foams: optimization of properties and morphology for fluid flow applications

Andrea Barbetta

Emulsion-Derived (PolyHIPE) Foams: Optimization of Properties and Morphology for Fluid Flow Applications

A thesis submitted to the University of Durham in accordance with the regulations governing the award of the degree of Doctor of Philosophy

ANDREA BARBETTA

Department of Chemistry
University of Durham
Durham

September 2002

DECLARATION

The material contained within this thesis has not previously been submitted for a degree at the Univeristy of Durham or any other University. The research reported within this thesis has been conducted by the author unless indicated otherwise.

Andrea Barbetta

September 2002

ABSTRACT

Emulsion-Derived (PolyHIPE) Foams: Optimization of Properties and Morphology for Fluid Flow Applications

ANDREA BARBETTA

The aim of the work described in this thesis is the development of highly porous materials (PolyHIPEs) which could find wide applications in separation science and in solid phase synthesis.

Two systems were developed and studied. In the first one, PolyHIPE materials from divinylbenzene were synthesised in the presence of porogens of different chemical structures. These materials possess two levels of porosity: large pores (1 – 20 μm) which guarantee the flow of fluids under the application of small pressures and a fine porosity (1 – 100 nm) present in the walls of the foams which confer to the materials high surface areas (up to 700 m^2g^{-1}). The chemical nature of the porogens employed has a significant influence on the morphologies of the foams affecting both the dimension of the cavities and the fine porous structure. It was shown that the mechanisms operating at the emulsion stage and thus determining the characteristics of the final foams are the co-adsorption at the oil/water interface of the porogens and/or monomers together with the primary surfactant, and diffusion of the dispersed aqueous phase through the continuous organic phase. The latter phenomenon can be minimized by the appropriate choice of the surfactant system.

The second system consisted of styrene/4-vinylbenzylchloride/divinylbenzene foams. The presence of a chloromethyl group render these PolyHIPE foams amenable to functionalization. Also in this case, the morphologies of the resulting foams were studied. It was shown that emulsion composition is the relevant variable affecting via the interfacial tension and viscosity not only foam morphologies but also their mechanical properties.

LIST OF SYMBOLS AND ABBREVIATIONS

A	total surface or interface area (Eq. 1.1 and 1.8)
a	radius of a hole in a film of continuous phase (Eq. 1.14)
a^*	critical hole radius
Aerosol OT	sodium bis-2-ethylhexylsulfosuccinate
AIBN	α,α'-azoisobutyrronitrile
a_N	isotropic hyperfine splitting constant
APO_2H_2	3-allyloxypropane-1,2-diol
b	thickness of the film of continuous phase separating two droplets of the dispersed phase (Fig. 1.3)
BET	Brunauer, Emmet, Teller
BVE	bis(4,4'-isopropylidene diphenoxyethyl)vinyl ether
BJH	Barret, Joyner, Halenda
BMI-70	bis(3-ethyl-5-methyl-4-maleimide-phenyl)methane
BPPSTE	bipolar pulse pair stimulated echo
CB	chlorobenzene
C_2B	1,2-dichlorobenzene
CEB	(2-chloroethyl)benzene
$C_{eq}(r)$	equilibrium concentration of the solution in the medium attained at the surface of a particle (Eq. 1.15 and 1.21)
$C_m(t)$	concentration of the dispersed phase substance in the medium (Eq. 1.21)
$C_{f,eq}(\infty)$	bulk phase solubility in the surface fim (Eq. 1.22)
$C_{m,eq}(\infty)$	concentration in the medium when $r = \infty$ (the bulk phase solubility)(Eq. 1.22 and 1.23)
CMC	critical micelle concentration
CPP	1-chloro-3-phenylpropane
CTAB	cetyltrimethylammonium bromide
c.μ.c	critical microemulsion concentration
$c.\mu.c_{water}$	critical surfactant concentration in water for microemulsion formation
$c.\mu.c_{oil}$	critical surfactant concentration in oil for microemulsion formation
$c(\infty)$	bulk phase solubility (Eq.1.17)
D	diffusion coefficient of the molecules of the dispersed phase through the

	continuous phase (Eq. 1.17)
D	average cavity dimension in PolyHIPE as determined by TEM
d	average interconnecting hole dimension in PolyHIPE as determined by TEM
d	mesh size (droplet diameter) (Eq. 1.8)
d_0	initial droplet diameter (Eq. 1.11) and polymer-porogen affinity (Eq. 3.8)
D_f	diffusiveness of the dispersed phase substance in the dispersion medium.
D_m	diffusiveness of the dispersed phase substance in the surfactant membrane at interface
DDBSS	dodecylbenzensulfonic acid, sodium salt
DSC	Differential Scanning Caloremeter
DVB (55 or 80%)	divinylbenzene (55 or 80 % vol. of *m* and *p* isomers)
E_f	foam modulus (Eq. 4.2)
EHA	2-ethylhexylacrylate
EHMA	2-ethylhexylmethacrylate
E_p	polymer modulus (Eq. 4.2)
ESR	Electron Spin Resonance
f	frequency of film rupture per unit area (Eq. 1.8)
F^*	activation energy for the hole nucleation event (Eq. 1.13)
FMA	perfluorooctylethyl acrylate
FT-PGSE	Fourier Transform Pulse Gradient Spin-Echo
FTIR	Fourier Transform Infrared
HAAEMA	2-(methacryloyloxy)ethyl acetoacetate
HDPE	high density poly(ethylene)
HIPE	High Internal Phase Emulsion
HLB	Hydrophile-Lihpophile Balance
G	gradient amplitude (Eq. 3.1)
G_A	free energy associated with van der Waals forces (Fig. 1.4)
G_E	free energy associated with electrostatic forces (Fig. 1.4)
G_i	total interaction free energy as a function of interdroplet distance b (Fig. 1.4)
G_{max}	maximum in the potential energy *vs* distance diagram (Fig. 1.4)

G'_{min}	absolute minimum in the potential energy *vs* distance diagram (Fig. 1.4)
G''_{min}	relative minimum in the potential energy *vs* distance diagram (Fig. 1.4)
$g(u)$	quasi-steady droplet size distribution (Eq. 1.8)
I	second moment of area of the cell edge (Eq. 4.7 and Fig. 4.9)
I_0	intensity in the absence of a gradient pulse (Eq. 3.1)
IPN	interpenetrating polymer network
ISEC	inverse size exclusion chromatography
$k(\phi)$	degree of interaction among diffusion fields (Eq. 1.20)
K	distribution coefficient of the dispersed phase substance between the adsorption film and the medium (Eq. 1.23)
l	length of a beam (Eq. 4.6, 4.7 and Fig. 4.9)
L	tube length (Eq. 4.1)
L_α	lamellar phase formed by a surfactant or mixture of surfactants
LSW	Lifshitz, Slezof, Wagner
MPS	methacryloxypropyltrimethoxy silane
O/W	oil-in-water emulsion
$N(t)$	number of cubic cells (Eq. 1.8)
N	number of bilayers (Eq. 1.14)
$p(b)$	normal pressure in a film of continuous phase of thickness b (Fig. 1.3)
$p(\infty)$	normal pressure at infinite inter droplet distance
$P_0 - P_L$	pressure drop along a tube of length L (Eq. 4.1)
PCL	poly(ε-caprolactone)
PEO	poly(ethylene oxide)
PES	poly(aryl ether sulfone)
PHP	polyHIPE
PIT	phase inversion temperature
PPO	poly(propylene oxide)
PSDVB	poly(styrene-co-divinylbenzene)
PV	pore volume
PVA	poly(vinylalchool)
q	scattering vector
R	molar gas constant and radius of a tube (Eq. 4.1)
r_c	critical radius of a droplet (Eq. 1.17)

R_m	diffusion resistance of the dispersion medium (Eq. 1.22 and 1.23)
R_f	diffusion resistance of the adsorption film (Eq. 1.22 and 1.23)
S	order parameter
S	styrene
S_i	solubility of a particle of radius r_i (Eq. 1.16)
SAXS	Small Angle X-Ray Scattering
SDS	sodium dodecyl sulfate
SEM	Scanning Electron Microscopy
SPAN 20	sorbitan monolaurate
SPAN 80	sorbitan monooleate
SPC	self-supported channel
t	square cross section of a beam (Eq. 4.6 and 4.7)
T	absolute temperature or toluene
T_d	temperature of decomposition
TEM	Transmission Electron Microscopy
T_g	glass transition temperature
TGA	thermogravimetry analysis
THF	tetrahydrofurane
Triton X-405	polyoxyethylene(40)isooctylphenyl ether
u	reduced radius (= r/r_c)(Eq. 1.18)
V	volume of a stack of cubic cells (Eq. 1.9)
VBC	4-vinylbenzylchloride
V_i	molar volume of a solvent (Eq. 3.4)
V_m	molar volume of the dispersed phase (Eq. 1.15)
W/O	water-in-oil emulsion
x_i	molar fraction of a component in a mixture of components (Eq. 3.4)
Z	coordination number of an element of volume (Eq. 1.9)
α	characteristic length scale (Eq. 1.15)
δ	thickness of a surfactant layer at the interface (Fig. 1.3) or duration of the bipolar gradient pulse pair (Eq. 3.1) or remote stress (Eq. 4.7)
δ_i	solubility parameter (Eq. 3.2 and 3.4)
δ_d	contribution of dispersion interaction to solubility parameter (Eq. 3.7)
δ_h	contribution of hydrogen bonding interaction to solubility parameter

	(Eq. 3.7)
δ_{mix}	solubility parameter of a mixture of solvents (Eq. 3.4)
δ_p	contribution of polar interaction to solubility parameter (Eq. 3.7)
δ_s	solubility parameter of a substrate
δ_t	total solubility parameter (Eq. 3.7)
Δ	diffusion delay time (Eq. 3.1)
Δ	average cavity and interconnecting hole dimension as determined by intrusion mercury porosimetry
$\Delta\delta$	difference between solubility parameters of polymer and solvent
ΔG_m	free energy of mixing (Eq. 3.2)
ΔH_m	free enthalpy of mixing (Eq. 3.2 and 3.3)
ΔS_m	free entropy of mixing (Eq. 3.3)
ΔG_f	free energy of emulsion formation (Eq. 1.1)
ΔS_f	entropy of emulsion or microemulsion formation (Eq. 1.1)
ε	remote strain (Eq. 4.7)
ϕ	volume fraction of the dispersed phase
ϕ_c	critical value of ϕ (= 0.74) (Eq. 1.1 and 1.2)
γ	interfacial tension between phases or gyromagnetic ratio (Eq. 3.1)
γ_c	value of interfacial tension at and post-c.μ.c.
Γ_s	surface or interface surfactant excess (Eq. 1.2)
μ	viscosity of a solvent (Eq. 4.1)
μ_s	surfactant chemical potential (Eq. 1.2)
ν	flow rate of a liquid in a tube (Eq. 4.1)
θ	contact angle between the two phases composing an emulsion (Fig. 1.3)
π	surface pressure
π_A	contribution of van der Waals forces to the disjoining pressure
$\pi(b)$	disjoining pressure (Eq. 1.3, 1.4 and 1.5)
π_E	contribution of electrostatic forces to the disjoining pressure
π_γ	contribution of changes in interfacial tension to the disjoining pressure (Eq. 1.7)
π_S	contribution of short range forces to the disjoining pressure
τ_{film}	lifetime of an emulsion film (Eq. 1.8)

ρ_f	foam density (Eq. 4.2 and 4.7)
ρ_p	polymer density (Eq. 4.2 and 4.7)
ω_0	rate of Ostwald ripening predicted by the LSW theory (Eq. 1.20)
ω	rate of Ostwald ripening (Eq. 1.17 and 1.20)

CONTENT

CHAPTER 1	**THEORETICAL BACKGROUND**	
1.1	Emulsions	1
1.2	Coalescence	9
1.2.1	Disjoining pressure	11
1.3	Ostwald ripening in emulsions	16
1.4	Gel emulsions	23
Bibliography		28
CHAPTER 2	**LITERATURE REVIEW**	
2.1	Recent advances in PolyHIPE science	33
2.2	PolyHIPE high performances materials	33
2.3	PolyHIPE materials as supports for chemical synthesis and separation media	40
2.4	PolyHIPE materials in technological applications	46
Bibliography		51
CHAPTER 3	**PREPARATION AND CHARACTERIZATION OF DVB polyHIPE FOAMS**	
3.1	Introduction	53
3.2	Experimental section	53
3.2.1	Materials	53
3.2.2	PolyHIPE preparation	54
3.2.3	PolyHIPE coding system	55
3.2.4	Bulk polymerisation	55
3.2.5	Surface area/Pore size distribution	55
3.2.6	Mercury porosimetry	56
3.2.7	Electron microscopy	56
3.2.8	Solid-state ^{13}C NMR	57
3.2.9	Determination of the diffusion coefficient of water in emulsions using ^{1}H NMR	57
3.2.1	Surface pressure-area measurements	57

3.3	Results and discussion	58
3.3.1	Foams obtained by using SPAN 80	58
3.3.2	Single component porogenic solvents	58
3.3.3	Mixed porogenic solvents	69
3.3.4	Influence of Pore Volume on foam characteristics	73
3.3.5	Macroporous resins from DVB 80%	84
3.3.6	PolyHIPE foams prepared with a mixture of surfactants	89
3.3.7	Conclusions	112
Bibliography		113

CHAPTER 4	**PREPARATION AND CHARACTERIXATION OF 4-VINYLBENZYL CHLORIDE AND DVB PolyHIPE MATERIALS**	
4.1	Introduction	116
4.2	Experimental section	117
4.2.1	Materials	117
4.2.2	PolyHIPE preparation	117
4.2.3	PolyHIPE coding system	117
4.2.4	Mercury porosimetry	118
4.2.5	Electron microscopy	118
4.2.6	Surface pressure-area measurements	118
4.2.7	Compression moduli measurements	118
4.3	Results and discussion	119
4.3.1	Morphology	119
4.3.2	Intrusion mercury porosimetry results	123
4.3.3	Surface pressure measurements	126
4.3.4	Mechanical properties	133
4.3.5	Conclusions	138
Bibliography		139

CONCLUSION AND FUTURE WORK		142
Bibliography		146

THEORETICAL BACKGROUND

Chapter 1

THEORETICAL BACKGROUND

1.1 Emulsions

An emulsion may be defined as an opaque, heterogeneous system of two immiscible liquid phases (oil and water) where one of the phases is dispersed in the other as drops of microscopic or colloidal size (typically around 1 μm). There are two kinds of simple emulsions, oil-in-water (O/W) and water-in-oil (W/O), depending on which phase comprises the drops [1]. Emulsions made by agitation of the pure immiscible liquids are very unstable and break rapidly to the bulk phases. Such emulsions may be stabilised by the addition of surface-active material which protects the newly formed drops from re-coalescence. An emulsifier is a surfactant which facilitates emulsion formation and aids in stabilization through a combination of surface activity and possible structure formation at the interface.

As stated above, emulsions are thermodynamically unstable systems, that is to say their free energy of formation (ΔG_f) is greater than zero and as such will show a tendency to break. This instability is a result of the energy associated with the large interfacial area of the droplets within the emulsion, given by $A\gamma$, where A is the total surface area of the drops and γ the interfacial tension existing between the aqueous and non-aqueous phases. This energy term outweighs the entropy of formation (ΔS_f) associated with the formation of the droplets from the bulk constituents. The free energy of formation of the emulsion in simple term is given by:

$$\Delta G_f = \gamma A - T\Delta S_f \qquad (1)$$

The interfacial tension in emulsions is generally of the order of 1-10 mN m^{-1}, this in conjunction with the large interfacial area results in a large positive interfacial energy term. The entropy of formation in emulsions is relatively small due to the number of droplets formed being small in entropic terms. These two factors result in $\Delta G_f \geq 0$, leading to the thermodynamic instability of the emulsions. Emulsions are, however, kinetically stable due to the presence of an adsorbed layer at the O/W interface, this barrier may be electrostatic in nature (adsorption of an ionic surface active agent), or steric (adsorption of a non-ionic surface active agent or polymer). These barriers not only prevent emulsion droplets from coming into direct contact but also serve to stabilize the thin film of liquid between two adjacent droplets. The presence of adsorbed surfactants can reduce the likelihood of rupture through the Gibbs-Marangoni effect: as the lamellar film between adjacent droplets is stretched new surface will be formed at some locations in the film having a lower instantaneous surfactant concentration, and a local surface tension increase will occur.

A surface tension gradient along the film will be produced, causing liquid to flow from regions of low γ toward the new stretched surface, thereby opposing film thinning. Reduction in interfacial tension may also play a significant role in emulsion stability. In the case of polymers other factors may also come into play, such as the viscoelastic properties of the adsorbed layer.

Conversely, microemulsions are thermodynamically stable [2-4] since the interfacial energy term is now very small owing to the very low interfacial tensions (typically 10^{-4}-10^{-5} Nm^{-1}) obtained by the use of mixed emulsifier systems at high concentrations. Moreover, as a result of their very small size (and hence greater number), the positive entropy of formation of microemulsion droplets may be an order of magnitude larger than that in emulsions. This term dominates the free energy of formation of microemulsions and these systems are thermodynamically stable.

Surfactant molecules, which are used to stabilise emulsions, consist of two blocks, one with an affinity to water and the other to oil. When added to the mixture of oil and water, they self-assemble at the oil water interface, so that the hydrophilic block stays in water and the hydrophobic one remains in the oil.

As the surfactant concentration increases, the monolayer at the oil-water interface becomes more densely populated and the interfacial tension decreases, as predicted by the Gibbs equation

$$d\gamma = - \Gamma_s d\mu_s \qquad (2)$$

where γ is the interfacial tension, Γ_s is the surface concentration of surfactant and μ_s is the surfactant chemical potential. Both Γ_s and μ_s increase with surfactant concentration, c.

At a certain concentration (or in a very narrow concentration range), reached simultaneously in both phases, surfactant molecules start to self-associate in the bulk of one of the phases, forming supramolecular aggregates, *e.g.* spherical micelles. After reaching this point, which is called the critical micelle concentration regardless of the particular form of the aggregates, the surfactant chemical potential stays essentially constant, because all the surfactant added is consumed by the micelles (Fig. 1.1). The interfacial tension at the CMC is the lowest possible under given experimental conditions.

Consider now the microscopic structure of micelles. In three-component oil-water-surfactant systems, the core of a micelle contains a solubilizate, which is the oil, if the micelles are formed in water, and water if the micelles are formed in oil. The oil-water interface is therefore present not only between the macroscopic phases, but also on the microscopic level

within the micelles. From this standpoint, the surfactant monolayer can be considered as a basic construction block of both the macroscopic oil-water interface and the microscopic micellar interface.

For a non-ionic surfactant, at low temperatures, the aggregates are oil-in-water (O/W) microemulsion droplets which form in the water phase present in equilibrium with an excess oil phase containing only monomeric surfactant. This type of two-phase system is designated a Winsor I system. At high temperatures, the aggregated surfactant forms water-in-oil microemulsion droplets in the oil phase with an excess water phase giving a Winsor II system. At intermediate temperatures, the aggregated surfactant is entirely located in a third phase present at equilibrium with both excess oil and water phases [5]. The structure of the third, surfactant-rich phase may be either a bicontinuous microemulsion or a lamellar liquid crystalline phase [6]. The temperature at which the inversion of the microemulsion occurs is called the phase inversion temperature (PIT). Since the aggregates formed are microemulsion,

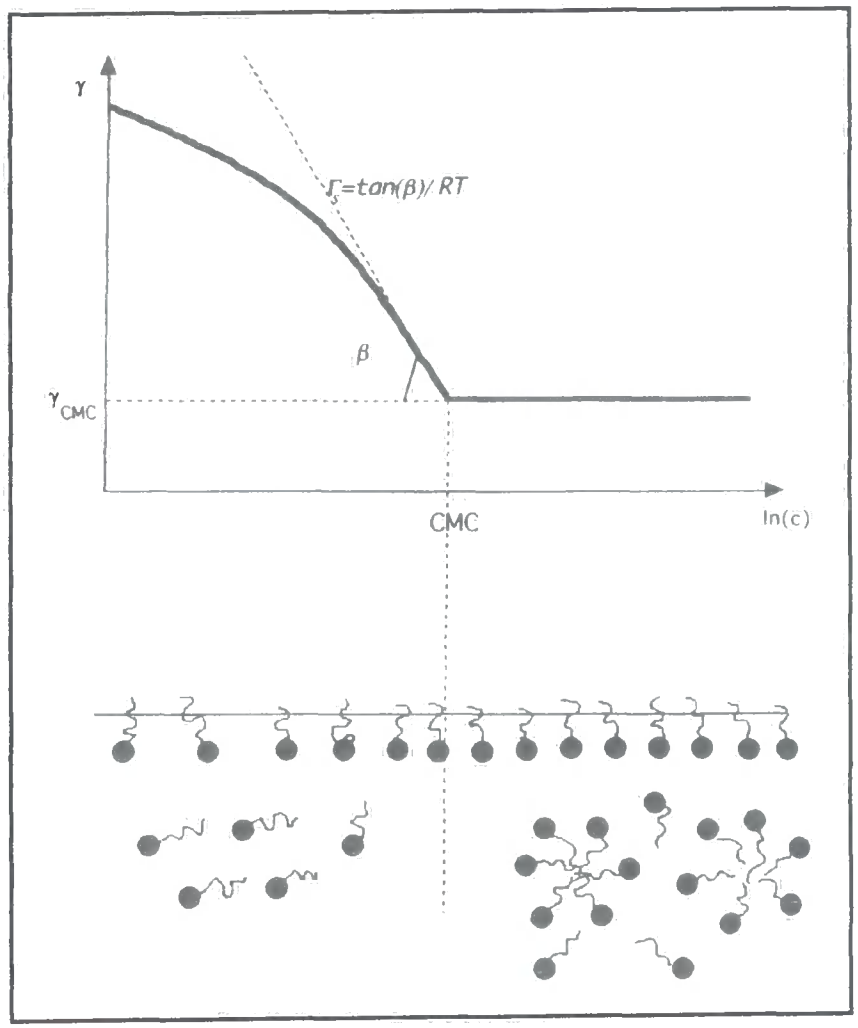

Figure 1.1. Interfacial tension isotherm of a micelle-forming nonionic surfactant.

the critical concentration of surfactant required for their formation is referred to as the critical concentration (c.μ.c.). For non-ionic surfactants the c.μ.c. in oil is typically of the order of 0.1 *M* whereas the value in the corresponding aqueous phase is of the order of 10^{-5} *M*. The oil-water interfacial tension (γ) reaches a virtually constant value above the c.μ.c (Fig. 1.1). The value of the constant, post-c.μ.c. tension (γ_c) passes through a minimum with increasing temperature and the temperature of minimum γ_c coincides with the microemulsion PIT [7].

The surfactant c.μ.c. has been shown to be affected markedly by the polarity of the oil phase in a W/O emulsion. For non-ionic surfactants the c.μ.c. increases as the polarity of the oil phase increases [8].

Emulsions can be stabilised against breakdown by one or more mechanisms: charge stabilization and stabilization by adsorbed particles at the liquid/liquid interface. In emulsion systems employing normal surfactants, the effectiveness of steric stabilization processes is limited by the fluidity and deformability of the dispersed phase, as well as by the fact that monomeric surfactant layers are not generally rigid. Adsorbed molecules may move around relatively freely, especially under the influence of the force developed during drop approach. Emulsion stability can be enhanced by the presence of less fluid interfacial structures such as "molecular complexes" and liquid structures.

When surfactants are added together in water, several physicochemical properties of the mixed systems compared to those of the single surfactants are changed due to the fact that there is a net interaction between the amphiphiles, *i.e.* due to non-ideal mixing. It is well known that many amphiphilic self-assemblies and interfaces, biological or synthetic-based, consist of surfactant mixtures. The existence of these interfacial surfactant structures is distinct from the situation of simple coadsorption of oil-soluble and water-soluble surfactants. In the case of co-adsorption, each component will be competing for available space in the interfacial region and will contribute a weighted effect to the overall energetics of the system. As early as the 1940s, Schulman and co-workers [9, 10] discovered that using two surfactants of the opposite packing type (*i.e.* a mixture of 'oil soluble' and 'water soluble' surfactants) could drastically improve emulsion stability. The authors attributed it to the formation of 'molecular complexes' between the surfactant at the oil-water interface. It was discovered that the two surfactants together reduced the interfacial tension to very low values (~0.1 mNm^{-1}), much lower than each of them separately [11]. Many years later the studies of the phase behaviour of similar systems revealed that the idea of 'molecular complexes' was incorrect. The surfactants do not form stochiometric complexes, but self associate into a mixed bilayer and form a lamellar phase, which co-exists with oil and water in a three-phase equilibrium. The idea of

mixing of two surfactants with an opposite packing type for making emulsions is widely used in practice. After a system containing two surfactants with an opposite packing type is selected, their ratio in the mixture is optimised by trial and error. In most cases, the emulsion stability, as judged by the dispersed phase separation, passes through a maximum at some surfactant ratio [12]. At high concentrations the emulsion solidifies because of the lamellar phase present, which is called the 'self-bodying action' of the surfactant mixture.

Although many emulsions are stabilised by one nearly saturated monolayer, this is not always the case. If the surfactant is balanced, it can form a lamellar phase (L_α), co-existing with oil and water. If emulsification is performed in such a system, the emulsion droplets are often covered by several monolayers back to back, which drastically improves the emulsion stability [13-16].

The molecular structure of the surfactants (headgroups and tails), the presence of additives (salt, co-surfactants) and experimental variables (pH, temperature) can be manipulated in order to induce changes in interfacial activity and in intra- and inter-aggregated forces. The mixed system almost invariably yields enhanced interfacial properties (e.g. decreased CMC, higher interfacial activity) with respect to the individuals surfactants, in what is termed synergism.

A possible beneficial effect of surfactant mixtures, in addition to improved surface energetics, is that such structures may possess a greater mechanical strength than a simple mixed interfacial layer. The closer molecular packing density and greater extent of lateral interactions between hydrophobic chains may result in significant decreases in the mobility of molecules at the interface and a decrease in the rate of drop coalescence. Such an effect has often been mentioned in terms of increased interfacial viscosity or elasticity.

Whether an emulsion is O/W or W/O depends on a number of variables including oil:water ratio, electrolyte concentration, temperature, *etc.* It was realized at the early stages of emulsion research that the volume fractions of oil and water were not that important and that emulsion type and stability were determined primarily by the nature of surfactant. There are three cornerstones guiding practical emulsion formulation which address this problem: the Bancroft rule [17, 18], the Griffin HLB (hydrophile-lipophile balance) scale [19, 20], and the Shinoda phase inversion temperature (PIT) concept [21]. According to Bancroft, the phase in which the surfactant is predominantly dissolved tends to be the continuous phase: water-soluble surfactants (e.g., sodium oleate) tend to stabilise oil-in-water (O/W) emulsions, while oil-soluble surfactants (e.g. calcium dioleate) stabilize water-in-oil (W/O) emulsions. The word 'soluble' is misleading, however, for two reasons. Firstly, a surfactant may be more

soluble in, say, oil than in water in a binary system, but in the ternary system of oil + surfactant it may partition more into water. A good example of this is with the anionic surfactant Aerosol OT (sodium bis-2-ethylhexylsulfosuccinate) which dissolves in heptane at 25 °C up to at least 0.5 M but has a solubility limit in water of only ~0.03 M [22]. An emulsion made from Aerosol OT and equal volumes of water and heptane at 25 °C is O/W, however [23]. Secondly, no distinction is made between the solubility of monomeric or aggregated surfactant in oil or water. We will see that this is an important omission.

The first quantitative measure of the balance between the hydrophilic and hydrophobic moieties within a particular surfactant came from Griffin who introduced the concept of the HLB, as a way of predicting emulsion type from surfactant molecular composition [19]. Surfactants with low HLB values (~4) tend to stabilize W/O emulsions, while those with high HLB values (~20) stabilize O/W emulsions. Surfactants with intermediate HLB values (~10) are usually ineffective stabilisers of either O/W or W/O emulsions. Later Davies [24-26] suggested a simple group contribution method to evaluate the HLB of different surfactants from their molecular structure. A major problem of the HLB concept is that the HLB numbers assigned to the neat surfactant take no account of the effective HLB of a surfactant *in situ* adsorbed at an oil-water interface. Thus for example, a non-ionic surfactant of low HLB number (and hence predicted to stabilise W/O emulsions) may form O/W emulsions at low enough temperatures. It therefore became clear that the prevailing conditions of temperature, electrolyte concentration, oil type and chain length and cosurfactant concentration can all modify the geometry of the surfactant at an interface [27] and thus change the curvature of the surfactant monolayer, which in some way affects the preferred emulsion type [28, 29].

There have been developments in understandings of how the type of emulsion is related to the phase diagram of mixtures of oil + water + surfactant at equilibrium [30-33]. These have come from studies with microemulsions and as an example we take the case of a nonionic surfactant of the polyoxyethylene glycol ether type, C_nE_m (C_n indicates the number of carbons of the hydrocarbonic moiety, E_m the number of oxyethylenic units). Let us consider equilibrium systems of heptane and water (equal volumes) containing $C_{12}E_5$. At low surfactant concentrations, monomer distributes between oil and water but heavily in favour of the oil [34]. The partition coefficient defined as (molar concentration in heptane)/(molar concentration in water) increases from ~130 at 10 °C to ~1500 at 50 °C. Above a critical surfactant concentration, reached in both phases and designated $c\mu c_{water}$ (typically $5*10^{-5}$ M) and $c\mu c_{oil}$ (typically $6–60*10^{-3}$ M), all additional surfactant in excess of this concentration is present in

the form of aggregates, hence the symbol μ for 'microemulsion'. At low temperatures (<28 °C) the aggregates are oil-in-water microemulsion droplets formed in the water phase, in equilibrium with excess oil containing monomeric surfactant (Winsor I system). The preferred curvature of the monolayer is around oil and may be termed positive. At higher temperatures (> 30 °C), aggregation occurs in the oil phase in the form of water-in-oil microemulsion droplets which are in equilibrium with monomeric surfactant in the aqueous phase (Winsor II system). The monolayer curvature is now negative. At intermediate temperatures (28-30 °C), three phases are formed (Winsor III system) consisting of a surfactant rich phase and both excess oil and aqueous phases [35]. Here a monolayer has, on average, zero net curvature.

It is frequently observed that the type of emulsion (O/W, W/O or intermediate) formed by homogenisation of the Winsor system is the same as that of the equilibrium microemulsion [36-38], *e.g.* emulsification of an O/W microemulsion plus excess oil generally gives an O/W emulsion, the continuous phase of which is itself an O/W microemulsion. It is not obvious why this should be so, since in the case of microemulsions their behaviour is determined in part by the spontaneous curvature of the surfactant monolayer stabilising the nanometer-sized droplets. For emulsions the radii of curvature of micrometer-sized drops are of the order of 1000 times the molecular dimensions and so it is difficult to see how curvature effects are implicated. In order to test and understand Bancroft's rule, the type of emulsion at different temperatures must be determined at various fixed surfactant concentrations. By means of conductivity measurements it was seen that at high $C_{12}E_5$ concentrations, sufficient to form microemulsion aggregates in equilibrium systems, emulsions invert from O/W to W/O at temperatures around the Winsor III region [39]. Thus, Bancroft's rule holds but it is impossible to say whether the preferred emulsion type is determined by the distribution of monomeric or aggregated surfactant. At low $C_{12}E_5$ concentrations, where only monomer surfactant exists, emulsions are O/W at low temperatures and remain O/W even at temperatures where Winsor II systems would form in systems of higher surfactant concentration. Thus, we see an apparent violation of Bancroft's rule since despite the surfactant monomer distribution being in favour of oil, the stable emulsions are O/W. Similar findings were reported by Harusawa *et. al.* [40, 41] using nonylphenol ethoxylated surfactants.

A more useful concept than that of the HLB number is that of the system HLB, related to the locus of aggregate formation. Thus 'high' HLB systems are those in which the aggregates (micellar or O/W microemulsions) form in the water phase, whereas 'low' HLB systems are those in which aggregation occurs in the oil phase, either as reverse micelles or W/O microemulsion droplets. It is now more correct to say that the phase containing the surfactant

aggregates becomes the continuous phase of an emulsion. From the foregoing discussion it is clear that the continuous phase of an emulsion is not necessarily the phase containing the highest concentration of surfactant. Bancroft's rule and the system HLB apply to surfactant aggregates rather that to total surfactant present in the system.

These effects are naturally incorporated into Shinoda's PIT concept [21, 42-46], which correlates (macro)emulsion stability with the phase behaviour of oil-water-polyethoxylated non-ionic surfactants (O-W-S) mixtures. According to Shinoda *et. al.*, O/W macroemulsions are stable in the Winsor I region at temperatures ca. 20 °C below the "phase inversion" temperature of the O-W-S microemulsion phase diagram. At this temperature, micellar solution coexists with excess oil. Conversely, W/O emulsions are stable ~20 °C above the PIT, where the system is the Winsor II region, and excess water coexists with inverse micelles. In the vicinity of the PIT point (Winsor III region), where oil, water, and bicontinuous microemulsion phases coexist in a three-phase equilibrium, neither emulsion is stable.

Emulsions may degrade in a number of different mechanisms and these are listed below and are shown schematically in Fig. 1.2:

1. creaming with or without aggregation and decrease in droplet number;
2. aggregation with or without creaming;

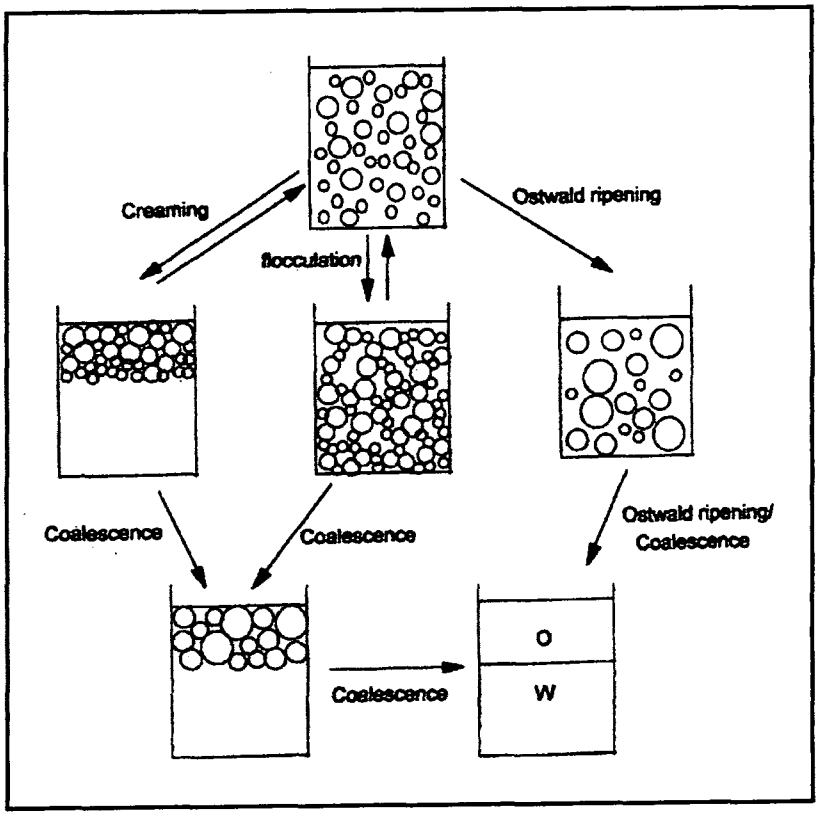

Fig. 1.2. Schematic representation of the emulsion breakdown.

3. increase in the droplet diameter through Ostwald ripening; and

4. droplet coalescence leading to the production of a separate oil phase.

As a result of their thermodynamic instability, emulsions will tend to reduce their total free energy through an increase in droplet diameter, so reducing their total interfacial area.

Processes (1) and (2) do not involve the increase in the size of the droplets, but are precursors to coalescence since this process requires the droplets to be in close proximity. Ostwald ripening on the other hand does not require the droplets to be close, since the process occurs by transport of dissolved matter through the dispersion medium.

In what follows only degradation processes 3 and 4 which are relevant in concentrated emulsions, are described in some detail.

1.2 Coalescence

Coalescence is the process in which two or more emulsion drops fuse together to form a single larger drop, and is irreversible. For coalescence to occur, the force between the drops surfaces must be such that film of continuous phase separating them can become sufficiently thin that film rupture becomes a likely possibility.

The film thinning stage depends on fluctuation in film thickness and on the mechanical properties of the film. As illustrated in Fig. 1.3, when two droplets come in contact, e.g., in a cream or a floc, a thin liquid film or lamellae forms between them. Coalescence results from the rupture of this film. This is on the assumption that the two droplets are formed of the same liquid or, at least, of miscible liquids. Film rupture usually commences at a specified spot in the lamella, arising from thinning in that region. In order to understand the behaviour of these films we need to consider two aspects of their physics: (1) the nature of the forces acting across the film (these determine whether the film is thermodynamically stable, metastable, or unstable) and (2) the kinetic aspects associated with local (thermal or mechanical) fluctuations in the film thickness. The coalescence of emulsion droplets is thus governed by the behaviour of the thin film between the droplets.

Figure 1.3 shows the general features of the lamella between two droplets of the phase (α) in a continuous phase (β). The thin film region, as discussed above, consist of two flat, parallel interfaces separated by a distance b. At the end of the film there is a border or transition region where the interfaces have a high curvature, *i.e.*, compared to the curvature of the droplets themselves. Eventually, however, at larger values of b (effectively beyond the range of the forces operating across the film) the curvature decreases to that of the droplets in the 1-

μm region. One may define a macroscopic contact angle θ as shown in the diagram (Fig. 1.3). In considering the forces acting across the film, two ranges of value of separation b are of interest: $b > 2\delta$. In the first region, the forces acting are long-range van der Waals forces (G_A) and the electrical double layer interactions (G_E). The total interaction free energy G_i is obtained by summing the G_A and G_E contributions.

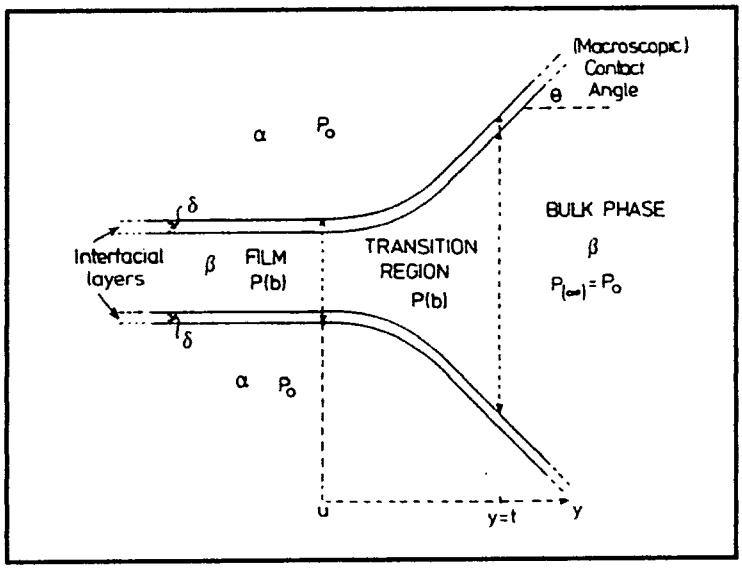

Figure 1.3. Diagrammatic representation of the thin film and border regions between two liquid droplets (α) in a continuous phase (β).

A schematic representation of the G_i curve *vs* the inter droplet distance, b, is given in Fig. 1.4. This curve is characterized by a primary minimum (G'_{min}) at close contact of the drops, a maximum (G_{max}), and a secondary minimum (G''_{min}) at large interdroplet separations. When a

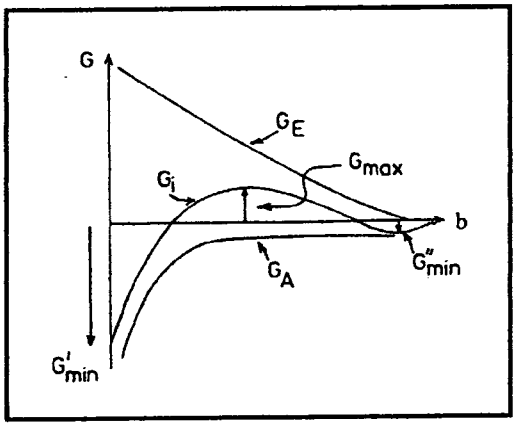

Figure 1.4. Schematic representation of *G(b) vs* interdroplet distance.

film is in the primary minimum we have to consider what happens if it tries to thin further (*i.e.* $b < 2\delta$). Here the so called steric interactions come into play. These constitute a very steep repulsion force, associated with the distortion of the adsorbed polymer or surfactant in the interfacial layers. Film rupture requires the breakdown of these steric interactions. The stability of thin films may be analysed in terms of the relevant interaction free energies. Various alternative descriptions are, however, possible. An example of these is the disjoining pressure concept [47].

1.2.1 Disjoining Pressure

The disjoining pressure $\pi(b)$ is the net force, per unit area, acting in the direction normal to the two flat, parallel interfaces (Fig. 1.3). At any given value of b, $\pi(b)$ balances the excess normal pressures $p(b) - p(\infty)$ in the film. The quantity $p(b)$ is the normal pressure in a film of thickness b, and $p(\infty)$ the normal pressure in a film of sufficient thickness so that $G_i(b) = 0$, *i.e.*, the interaction free energy of the film is zero. Thus, $p(\infty)$ is equivalent, for a plane-parallel film, to the isotropic pressure in the adjacent bulk phase p_0. Thus,

$$\pi(b) = p(b) - p_0 \tag{3}$$

As mentioned above, $\pi(b)$ will contain three contributions, *i.e.*, from the London-van der Waals (dispersion) forces (π_A), from the electrostatic forces (π_E), and from short- range forces (π_S). It is assumed that gravitational forces can be neglected. The short-range forces include the steric interactions plus other van der Waals forces (Keesom and Debye), H-bonding, solvation forces associated with solvent structure at the interface, *etc.* Thus,

$$\pi(b) = \pi_A + \pi_E + \pi_S \tag{4}$$

π_A is generally negative; π_E and π_S are positive. Thus, the net disjoining pressure may be positive (repulsive) or negative (attractive) at any given value of b. $\pi(b)$ is formally related to $\overline{G_i}(b)$ the specific excess free energy of the film, associated with these interactions through the relationship

$$\pi(b) = -\frac{d\overline{G}(b)_i}{db} \tag{5}$$

At the primary and secondary minima $\pi(b) = 0$, and then $p(b) = P_0$, (Eq. (1.3)), *i.e.*, the normal pressure in the film equals the bulk hydrostatic pressure in the continuous phase. A film will tend to thin spontaneously, therefore, until it reaches a thickness where this condition holds. The film is then in mechanical equilibrium but is thermodynamically metastable.

Note that in the transition zone (Fig. 1.3), $p(b)$ is always less than p_0 (i.e., $\pi(b)$ is negative) because of the high curvature of the interface. Because $p(b)$ here is also lower than $p(b)$ in the flat film region, there is a tendency for liquid to be sucked into the transition region from the film, *i.e.*, there is a capillary force acting in the direction parallel to the flat interfaces. This force is responsible for the draining of the film, but it does not enter into a discussion of the disjoining pressure, which acts in the direction normal to the interfaces as we have seen.

The question of film rupture has been considered by various authors, *e.g.* Scheludko [48, 49] and Vrij [50]. A detailed account has been given by Sonntag and Strenge [51]. Film rupture is a non-equilibrium effect and is associated with local thermal or mechanical fluctuations in the film thickness b. A necessary condition for rupture to occur, *i.e.*, for a spontaneous fluctuation to grow, is that

$$\frac{d\pi_A}{db} > \frac{d\pi_E}{db} \tag{6}$$

However, this would assume that, at given value of b, there are no changes in $\gamma(b)$ due to fluctuations. This not so, however, since a local fluctuation is necessarily accompanied by a local increase in interfacial area, a consequent deficiency in surfactant or polymer adsorption in that region, and therefore, a local rise in interfacial tension. This effect, the so-called Gibbs-Marangoni effect, in fact opposes fluctuations. It also means that we need to add a term to the right-hand side of Eq. (6) to take into account of this fluctuation effect in the local interfacial tension, i.e., Eq. (6) now reads

$$\frac{d\pi_A}{db} > \frac{d\pi_E}{db} + \frac{d\pi_\gamma}{db} \tag{7}$$

As a film thins locally due to fluctuations, if the condition expressed by Eq. (7) is met at some critical thickness, then the film becomes unstable and the fluctuation grows leading to rupture. The kinetics of the rupture of single films and the evaluation of the emulsion lifetime can be obtained on the basis of a simple model [52]. Consider the coalescence in a creamed O/W emulsion layer. We can model the system as a stack of monodisperse cubic cells. Each cell has six facets separating it from its neighbours. If rupture is a completely random process, one can expect that the probability of rupture is proportional to the surface area of the film:

$$\tau_{film} \approx \frac{1}{Af} \tag{8}$$

where A is the surface area of the film, τ_{film} is the film lifetime, and f is the frequency of rupture per unit area [$m^{-2}s^{-1}$]. It is very difficult to measure the lifetime of one emulsion film. However, one can measure the mesh size d of the emulsion as a function of time t. Let us

assume that the thickness of films separating the oil droplet is very low, so that the total volume of the system V is equal to:

$$V = N(t)d^3(t) = const \tag{9}$$

where N is the number of cells in the system. The total number of coalescence acts per unit time can be evaluated as:

$$-\frac{dN}{dt} = f \times A_{total} = \frac{Z}{2} N(t)d^2(t)f \tag{10}$$

where $Z = 6$ is the coordination number of the cubic cell. From Eqs. 9 and 10 one concludes that the mesh size in the emulsion increases with time according to the following law:

$$\frac{1}{d_0^2} - \frac{1}{d^2(t)} = \frac{Z}{3} ft \tag{11}$$

where d_0 is the initial droplet diameter. The time to complete coalescence ($d = \infty$) therefore equals:

$$\tau = \frac{3}{Zd_0^2 f} \approx \frac{1}{2d_0^2 f} \tag{12}$$

According to this equation, the emulsion lifetime decreases with an increase in the frequency of the hole nucleation and in emulsion droplet size.

Experimentally, the rate of coalescence if determined by following the rate at which the layer of free oil is formed at the top of the vessel. It is easy to show that the time for separation of half of the volume of the oil, $\tau_{1/2}$, is close to τ predicted by Eq. 12.

The problem of the evaluation of the emulsion lifetime is therefore reduced to determining the rupture frequency f. This quantity can be regarded as the product of a pre-exponent f_o and an exponent:

$$f = f_0 \exp\left(\frac{F^*}{k_b T}\right) \tag{13}$$

Where F^* is the activation energy. The exponent is essentially the rate-controlling term. The pre-exponent term is less dependent on the external conditions.

Two theoretical approaches have been developed for the evaluation of the activation energy of the hole nucleation process: the de Vries theory and that of Kabalnov and Wennestrom. According to de Vries the behaviour of macroemulsions is related to the nucleation behaviour of the emulsion film rupture event: for the coalescence act to occur, a nucleation hole must be formed, which involves overcoming a free energy penalty [53]. Consider a flat-parallel liquid film of half thickness b. The liquid is under interfacial tension γ. Assume a hole of radius a

has been formed; the edge of the hole is round (Fig. 1.5). The emulsion film rupture is driven by reducing the surface area of the planar part of the emulsion film.

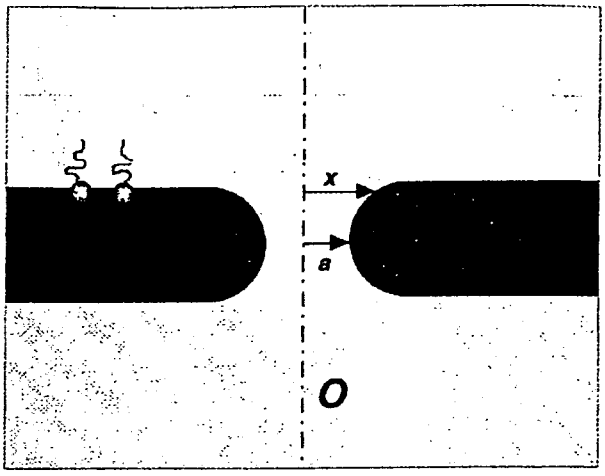

Figure 1.5. Geometry of nucleation hole according to de Vries (53).

On the other hand, the edge of the nucleation hole creates an extra surface area, and, therefore a free energy penalty. The energy barrier of nucleation comes from an interplay of the free energy penalty at the edge of the hole and the free energy gain at the planar part. Assume first that the interfacial tensions of the curved and planar parts are the same. The free energy balance of the nucleation pore in a liquid film states that:

$$F = \gamma(A_1 + A_2) = -2\pi a^2\gamma + 2\pi a[\gamma(\pi - 2)b] + (2\pi^2 - 6\pi)b^2\gamma \qquad (14)$$

At constant film thickness, the excess surface area as a function of the hole radius a passes through the maximum $A = 2.9b^2$ at $a^* = 0.57b$, after which it decreases to negative values. After passing through the maximum, the hole growth become spontaneous, the maximum, however can be reached by a thermal fluctuation. Naturally, the activation barrier for the film to break is equal to the free energy at the maximum, $F^* = \gamma A^* = 2.94\gamma b^2$.

Consider now the hole nucleation in a stack of N liquid films (for instance, in a lamellar liquid crystalline film composed of N bilayers). If the hole pierces all the N bilayers, the unfavourable edge is formed on all the N bilayers. On the other hand, the unfavourable reduction of the total surface area is the same as in the case of only one film. The total balance of the surface area states that

$$\Delta A = A_1 + NA_2 \qquad (14)$$

The excess free energy has a maximum at $a^* = b(N\pi/2 - 1)$ equal to $F^* = \gamma b^2(N^2\pi^3/2 - 4\pi N)$. One can see that the coalescence energy barrier drastically increases with the number of films

to be pierced. Note that the bilayers cannot just pop one after another: there is no free energy gain in this process, only the free energy penalty [54].

The analysis of de Vries is based on the assumption that the interfacial tension of the edge of the film is the same as that of the planar part of the film. The theory of Kabalnov and Wennerström [55] of coalescence in emulsions makes use of the concept of oriented wedge of a surfactant at the interface of Langmuir and Harkins [56, 57]. According to the authors, surfactants with bulky alkyl chains and small head groups stabilise W/O emulsions due to packing constraints at the oil-water interface of the emulsion drop, while single-tailed Harkins

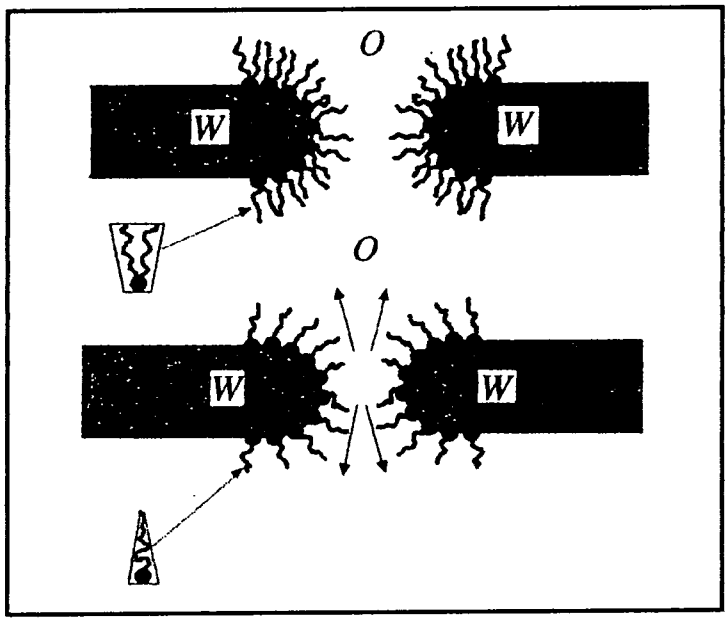

Figure 1.6. Oriented wedge theory. (top) Monolayer spontaneous curvature fits that of the hole edge and the rupture occurs without a barrier. (bottom) Monolayer at the edge of the hole nucleus is "frustrated" and the hole nucleation is suppressed. Arrows indicate the frustration stress in the bent monolayer.

and Langmuir, the monolayer bending energy affects the free energy of the droplets themselves. Although the oriented wedge theory has been used successfully as an empirical correlation, it stands on a rather shaky physical basis. Consider the spontaneous curvature of the surfactant monolayer, which is controlled by the shape of the surfactant molecules.

For unbalanced surfactants, the radius of curvatures has an order of $\sim 10^{-7}$ cm and is several orders magnitude smaller than the radius of the emulsion droplets themselves. As a result, the monolayer "frustration" energy at the interface of both O/W and W/O drops is essentially the

same: for the monolayer, both O/W and W/O interfaces are essentially planar on a molecular scale.

In the theory of Kabalnov and Wennerström it is argued that the monolayer bending properties, in particular the spontaneous curvature, controls the rates of coalescence of W/O and O/W emulsions via the values of the corresponding coalescence energy barriers. To create a passage in an emulsion film, one has to pay a monolayer bending energy penalty, because the surfactant monolayer must be strongly curved at the edge of the passage (Fig. 1.6). This penalty is dramatically different between W/O/W and O/W/O lamellae. The monolayer bending energy affects not the free energy of the droplets themselves but the free energy of the coalescence transition state-the nucleation pore in the bilayer. The theory has been developed under the assumption that the coalescence process is film-rupture controlled, which corresponds to the coalescence in creamed emulsions layers and high internal phase ratio emulsions.

1.3 Ostwald ripening in emulsions

Irreversible coarsening in emulsions can occur by two distinct mechanisms: coalescence and Ostwald ripening. Coalescence is the process by which two or more droplets fuse to form a single larger droplet, the fusion being controlled by hole nucleation within the thin film separating droplets. Conversely, Ostwald ripening is the process by which large droplets grow at the expense of smaller ones due to differences in their chemical potential. In Ostwald ripening the growth occurs by diffusion of the dispersed phase through the continuous phase one molecule at a time.

In simple terms Ostwald ripening is the growth of one emulsion droplet at the expense of a smaller one as a result of the difference in chemical potential of the material within the droplets. This difference arises from the difference in the radius of curvature of the drops.

$$c(r) = c(\infty)\exp\frac{2\gamma^{i}V_m}{rRT} \approx c(\infty)\left(1+\frac{2\gamma^{i}V_m}{rRT}\right) = c(\infty)\left(1+\frac{\alpha}{r}\right) \qquad (15)$$

where $c(r)$ is the solubility surrounding a particle of radius r, $c(\infty)$ is the bulk phase solubility, γ^{i} is the interfacial tension between the dispersed and continuous phases, V_m is the molar volume of the dispersed phase, R is the molar gas constant, and T is the absolute temperature. The quantity $\alpha = 2\gamma^{i} V_m/RT$ is termed the characteristic length scale. It has an order of $\approx$ 1 nm or less, indicating that the differences in solubility for a 1 nm droplet is of the order of only 0.1 %.

In terms of the Kelvin equation and solubility, the effect of radius can be given as [59]

$$\ln\frac{S_1}{S_2} = \frac{\gamma' V_m}{RT}\left(\frac{1}{r_1} - \frac{1}{r_2}\right) \tag{16}$$

where S_1 and S_2 are the solubilities of the particles of radii r_1 and r_2 and the other quantities have the meaning stated above.

Alternatively, one may view the process purely in terms of the reduction in free energy of the system through the destruction of the interfacial area. Overall, the effect is an increase in the average radius of the emulsion droplets with time as the smaller droplets dissolve and re-deposit their material onto the larger droplets. It is possible to calculate the rate of Ostwald ripening, i.e. the rate at which the radius of the emulsions increase with time.

Theoretically, Ostwald ripening should lead to the condensation of all droplets into a single droplet (*i.e.* phase separation). This is not observed in practice, however, due to a significant decrease in the rate of growth with increasing droplet size.

The kinetics of Ostwald ripening is most often described in terms of the theory developed by Lifshitz, Slezof and Wagner [58, 59](*i.e.* LSW theory). The LSW theory is based upon the following assumptions:

(i) the mass transport is due to molecular diffusion through the continuous phase;

(ii) the dispersed phase particles are spherical and fixed in space;

(iii) there are no interactions between neighbouring particles, *i.e.* the particles are separated by distances much larger than the diameter of the droplets (the volume fraction of the dispersed phase $\phi \rightarrow 0$); and

(iv) the concentration of the molecularly dissolved species is constant except adjacent to the particle boundaries.

It follows then that the rate of Ostwald ripening, ω, is given by:

$$\omega = \frac{d}{dr}(r_c^3) = \frac{8\gamma^i Dc(\infty)V_m}{9RT} = \frac{4Dc(\infty)\alpha}{9} \tag{17}$$

where r_c is the critical radius of a droplet which is neither growing nor decreasing in size, and D is the diffusion coefficient for the dispersed phase in the continuous phase. Droplets with $r > r_c$ grow at the expense of smaller ones, while droplets with $r < r_c$ tend to disappear.

Let us summarize the major results of the LSW theory for the stationary stage of the process:

1. The distribution function of the ratio of the radius at a given moment of time $g(u)$ is time invariant (Eq. 18). A characteristic feature of the function is its cut-off for $r/r_c > 1.5$, *i.e.* at the stationary stage of the process there are no particles in the system greater than the critical radius multiplied by a factor of 1.5. At the stationary stage, the value of the critical radius r_c

coincides with its number average value r.

$$g(u) = \frac{81e}{\sqrt{32}} u^2 (3+u)^{-7/3} (1.5-u)^{-11/3} \exp\left[\frac{1}{\left(\frac{2u}{3}-1\right)}\right] \tag{18}$$

for $u < 1.5$ and

$$g(u) = 0 \quad \text{for } u \geq 1.5 \tag{19}$$

The normalised form of this distribution is shown in Fig. 1.7.

This size distribution is time invariant so that whilst the critical radius increases with time, the

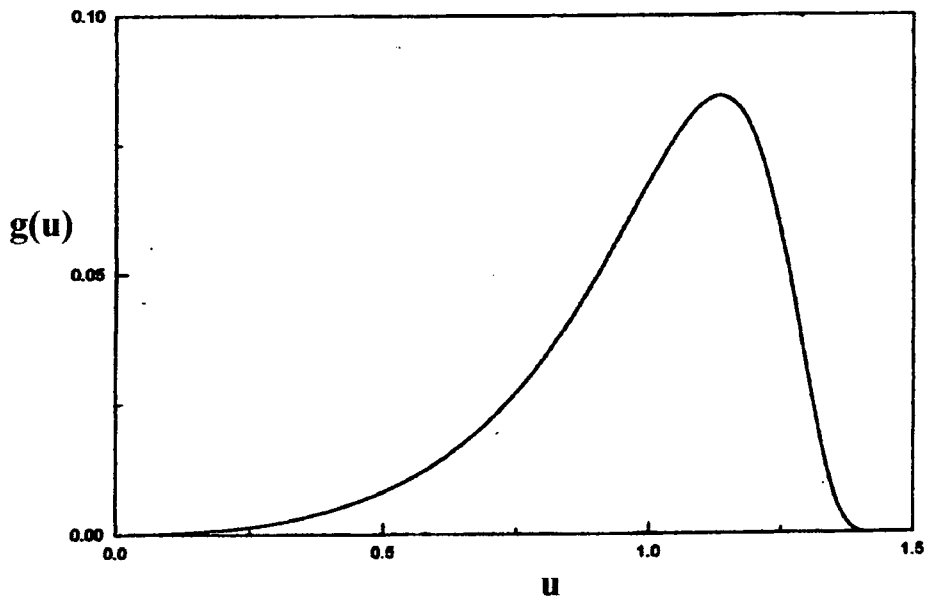

Figure 1.7. Quasi-steady size distribution, *g(u)*, as a function of reduced radius, *u(=r/r$_c$)*.

form of the size distribution as a function of u does not change. The rate of ripening will be affected by the droplet size distribution if the steady state regime has not been reached where Eq. 17 holds true. A wider distribution of sizes will lead to an enhanced rate. Eq. 17 demonstrates why Ostwald ripening has been neglected in emulsions to a large extent.

The linearity of the cube of the average radius with time means that $(dr/dt) \propto r^{-2}\omega$, thus for agiven rate of ripening the rate of change in the average radius decreases inversely with the square of the average radius. In macroemulsions with radii of ≥ 1 μm, the rate of increase in the average radius is very much less than in an emulsion of ≤ 0.5 μm.

Consequently, Ostwald ripening is only seen as a major problem in macroemulsions when the

dispersed phase has a high aqueous solubility, for example hexane, toluene and dichloroethane.

The LSW treatment characterises the Ostwald ripening process for systems with a one-component dispersed phase in the steady state regime (ignoring the adsorbed layer of surface active agent). These results, however, strictly only apply to highly dilute emulsions. One main deficiency with the LSW treatment is that it predicts no volume fraction dependence for the rate of ripening and this has been found to be contrary to experimental evidence in suspensions. In addition the size distributions found experimentally in suspensions disagree with the LSW size distribution at higher volume fractions. In suspensions of only 3% discrepancies may be found, with the size distribution being broader than that predicted [60]. One of the assumptions made was that the thickness of the diffusion layer was equal to the droplet radius. This only holds for dilute emulsions in the limit $\phi \rightarrow 0$, that is to say, the diffusion of the dissolved material to or from a droplet is not affected by the presence of any other droplet and is independent of its local surroundings. This not the case in more concentrated systems were the mean separation between neighbouring droplets may be of the same order of magnitude as the droplet radius. In this case the diffusion gradient about any given droplet is modified by the presence of the second drop and the rate would be significantly modified.

This interaction of diffusion fields results in a modest increase in the rate of ripening [61-66], the form of this increase as given by Enamoto et al. [61] is shown in Fig. 1.8 where $k(\phi)$ is simply a multiplication factor such that the rate at a given volume fraction, $\omega(\phi)$, defined by,

$$\omega(\phi) = k(\phi) \cdot \omega(0) \tag{20}$$

where $\omega(0)$ is the rate predicted by the LSW equation. The rate is predicted to increase by a factor of 2.5 in the range of $\phi = 0.01$ to 0.3. Recent results suggest that this equation may not always apply to emulsion systems where the concentration of surfactant and hence solubilized material, is high. In general it is expected that emulsions with higher volume fractions of the dispersed phase will have broader particle size distributions and faster absolute growth rates than those predicted by LSW theory. This in fact has been verified experimentally for cobalt grains [67].

The rate of Ostwald ripening, according to the LSW theory, is directly proportional to the solubility of the disperse phase in the dispersion medium. One of the most convenient ways of investigating this effect is to study a homologous series, for example the *n*-alkanes, in which the solubility is a function of the carbon number. Davis and Smith [68, 69] investigated

emulsions of a number of oils stabilized by sodium dodecyl sulfate (SDS) using photomicrography. They found that increasing the polarity of the oil decreased the stability of

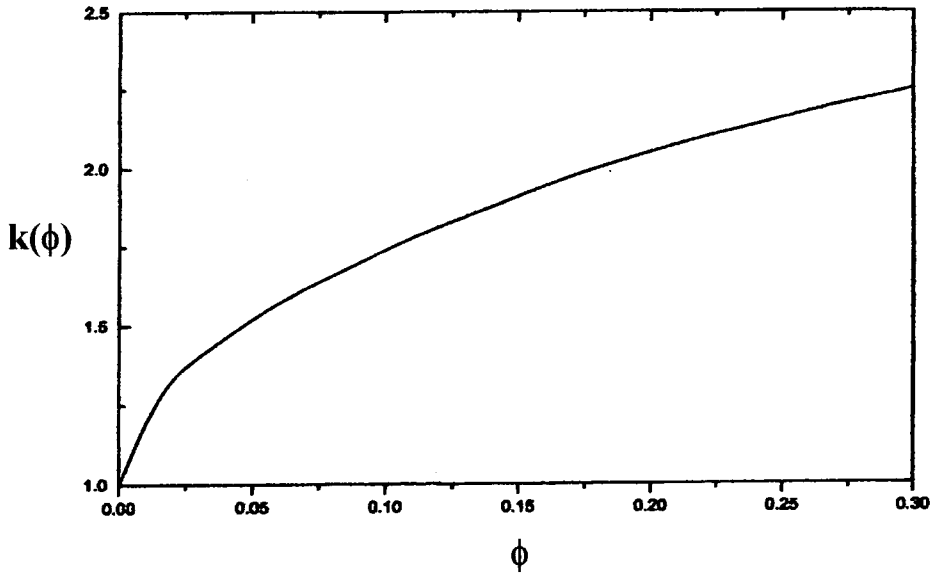

Figure 1.8. Coefficient *K(ϕ)*, as given by the treatment of Enamoto et al. for the increase in the rate of Ostwald ripening as a function of volume fraction (62).

the emulsion. A plot of relative degradation (the cube of the average diameter after 2 days over the cube of the initial diameter) against the carbon number showed the strong dependence of Ostwald ripening on the solubility of the disperse phase.

A comprehensive set of data regarding Ostwald ripening in emulsions has been given by Kabal'nov et al. [70-74].They have investigated the ripening in emulsions in two ways, that is by microscopy examination of emulsions droplets trapped on a microscope slide [72, 73] and also by determining the average size of emulsion droplets using photon correlation spectroscopy (PCS) [70, 71, 74]. Much of their data confirms the prediction of the LSW theory. In the experiments in which the course of the Ostwald ripening was followed by microscopic means the droplets of 1,2-dichloroethane, benzene, toluene, nitrobenzene and *p*-xylene were prepared by passing a saturated aqueous solution of the oil into a narrow channel followed by cooling [71, 74]. When droplets of the correct size were obtained, the solution feed into the channel was stopped and photomicrographs of the droplets were taken. Coalescence was found to be negligible. Micrographs were taken sequentially on the same area of approximately 100-500 drops and the total volume of the drops was measured to check for dissolution due to temperature changes. It was found that for droplets of 1,2-dichloroethane over a 5-min interval [71, 74], the larger droplets grew, small ones diminished and droplets at a

certain radius remained constant in size for a given period. This confirmed the notion of a critical radius at which at a given instance the droplet size remained constant. As the overall average size of the emulsion droplets increased then it would be expected that the critical radius would also increase. This was indeed found and it was observed that droplets which initially grew after a sufficiently long time began themselves to diminish as the critical radius increased. Plots of the cube of the average radius with time were found to be linear and the size distribution of the droplets was found to be close to that predicted by the LSW equation. These results alone strongly support the use of the LSW theory of Ostwald ripening in emulsion systems.

The theory of Ostwald ripening described above assumes that the molecular diffusion through the dispersion medium is the limiting stage of the process. For Ostwald ripening in emulsions the case when the mass transfer is limited by penetration through the adsorption layer is also of great interest. The growth rate of a particle surrounded by a thin membrane is determined by the following expression:

$$\frac{4\pi}{3}\frac{d}{dt}r_c^3(t) = \frac{C_m(t) - C_{eq}(r)}{R_m + R_f} \tag{21}$$

Where R_m and R_f are diffusion resistances of the medium and membrane:

$$R_m = \frac{1}{4\pi a D_m} \quad ; \qquad R_f = \frac{\delta C_{m,eq}(\infty)}{4\pi a^2 D_f C_{f.eq}(\infty)} \tag{22}$$

Here δ is the membrane thickness, D_m and D_f are the diffusiveness of the substance of particles in the membrane and in the dispersion medium, $C_{f,eq}(\infty)$ and $C_{m,eq}(\infty)$ are the solubilities of the substance (ml/ml) in the membrane and in the medium, respectively. The ratio of diffusion resistances of the membrane can be expressed through the following formula:

$$\frac{R_f}{R_m} = \frac{\delta D_m C_{m,eq}(\infty)}{D_f C_{f,eq}(\infty)} = \frac{\delta D_m}{a D_f K} \tag{23}$$

Where K is the distribution coefficient for the substance between membrane and medium. If the ratio shown in Eq. 23 is significantly smaller than 1, the diffusion resistance of the membrane can be neglected and in this case the kinetics of Ostwald ripening is described by Eq. 17 assuming absence of the membrane. In the opposite case the kinetic features of the process should alter dramatically. The linear growth with time will be observed not for the cube but for the square of the average radius [75] and the rate of the growth becomes substantially dependent on the nature of the surfactant used.

Strictly speaking, the theoretical results outlined above are valid for infinite systems. The assumption that there exists a continuum of sizes of particles is only an approximation for finite systems. This gives rise to the question of whether the attainment of the asymptotic regime is valid for real finite systems [76, 77]. It was shown, however, that the effect of a system being finite is negligible under reasonable experimental times owing to a considerable retardation of Ostwald ripening with the increase in the mean particle size [78].

It is clear that the rate of Ostwald ripening may be reduced in emulsions consisting of single component droplets by either a reduction in the interfacial tension or by the use of a less soluble oil. However, when one is constrained to use a particular oil and when a sufficient increase in stability cannot be easily achieved by reduction in the interfacial tension, how may the emulsion be stabilized against Ostwald ripening. Polymeric emulsifiers/stabilizers may help in this respect through the formation of a thick steric barrier at the oil/water interface which may hinder the passage of the oil molecules to and from the droplets. The efficiency of this method is uncertain and a potentially much more reliable method is the use of two component droplets, where one component (the additive) has a substantially lower solubility in the medium than the main constituent of the droplet [68, 69, 79-83]. This method is attractive since the rate of ripening can be reduced by several orders of magnitude, provided a suitable additive is chosen, using only small concentrations of the additive.

The mechanism by which the addition of a less soluble additive to an oil droplet reduces the rate of ripening is based on the fact that the two components in the droplet show different rates of transfer between droplets as a result of their differences in solubility [82, 83]. Initially the concentration of additive is equal in all droplets, however, as ripening proceeds the more soluble component (referred to as component 1) diffuses from the smaller droplets to the larger droplets. The rate of ripening in this stage is close to that in an emulsion component 1 alone. The less soluble component (component 2) cannot transfer at as high a rate as component 1 and is essentially trapped in the droplet at this stage. The concentrations of both components vary between drop size with the concentration of component 1 being greater in the larger droplets and smaller in the smaller droplets, the converse applying to component 2. As a result of its higher concentration in the larger droplets, the chemical potential of component 1 (due to mixing with component 2) is higher than in the smaller droplets where its concentration is lower. This effect directly counters the chemical potential effect due to the difference in radii of curvature. Eventually a point is reached whereupon the chemical potential of component 1 is equal in all droplets as a result of the competition between the two effects. When this point is reached there is no driving force for further transfer of component

1 and any ripening can only occur through transfer of the less soluble component, which occurs at much reduced rate. This rate is referred to as the pseudo-steady state of ripening. Thus the presence of a less soluble component can significantly reduce the rate of ripening.

1.4 Gel Emulsions

The emulsions described in this section are highly concentrated emulsions which form in either water- or oil-rich regions of water/surfactant/oil systems [84-95]. These emulsions are characterised by their large internal phase volume fraction (as large as 0.99), low surfactant content (as low as 0.5%) and gel-like consistency (the reason why they are referred as gel emulsions). By appropriate selection of composition variables and temperature, optically transparent gel emulsions can be obtained. All these features make them of particular interest for theoretical studies (*i.e* as models for foams) and for specific applications as formulation and novel delivery systems in, say, the cosmetic and pharmaceutical fields. In recent years highly concentrated emulsions have received a great deal of attention as novel reaction media for polymerisation reactions in the continuous and/or dispersed phases to obtain materials with improved properties such as solid foams, composites, *etc.* [96, 97].

Highly concentrated emulsions were described and became the object of study a long time ago [98-103]. The initial research focused on the geometrical packing [104, 105] and rheology of oil-in-water (O/W) type emulsions [105-107]. Lately, systematic studies about formation, stability, structure and interfacial properties of both emulsion types (O/W and W/O) have been undertaken [84-95, 108-112].

The internal phase volume fraction in a gel emulsion, ϕ, is larger than the critical value of the most compact arrangement of uniform, undeformed spherical droplets $\phi_c = 0.74$ [99]. Consequently, the droplets in gel emulsions are deformed and/or polydisperse. Typically, the droplet size of gel emulsions with water volume fraction above 0.95 range from sub-micrometer to about 10 μm, while the upper limit of those with volume fraction of the order of 0.90 is of about 1 μm [94]. However, depending on the gel emulsion-forming system and /or the method of preparation, both droplet size and polydispersity can be reduced significantly. The internal or dispersed phase in gel emulsions can be either polar or non-polar and, as ordinary emulsions, they are classified in two types: oil-in-water (O/W) and water-in-oil (W/O). Phase behaviour studies of gel emulsion-forming systems, *i.e.* water/polyoxyethylene non-ionic surfactant/oil systems, indicated that at equilibrium they separate into two isotropic liquid phases [85, 89]. In W/O gel emulsions the nature of these phases are an aqueous phase and a swollen reverse micellar solution phase (or W/O microemulsion) [85]. Considering the

nature of the phases at equilibrium, the emulsions are water (or oil)-in-microemulsion emulsions.

The structure of the equilibrium oil phase of W/O gel emulsions was confirmed by Fourier transform pulse gradient spin-echo (FT-PGSE) NMR determinations [91]. It was found that at high oil/surfactant weight ratios the values of the self-diffusion coefficient for water and surfactant are very low, whereas the corresponding values for oil are high. This means that the continuous phase is non-aqueous and water is confined. Therefore the structure corresponds to a reverse micellar solution or W/O microemulsion. At low oil/surfactant weight ratios, when gel emulsions are extremely unstable or cannot be formed, the self diffusion coefficient of water was found to approach that of the oil, indicating a bicontinuous structure. From these results it was concluded that the continuous phase of W/O gel emulsions should be a reverse micellar solution or W/O microemulsion.

The equilibrium and also the non-equilibrium structure of W/O gel emulsions was also determined by small angle X-ray scattering (SAXS) [94]. The SAXS spectra obtained were explained by the superposition of two spectra: a peak at values of the scattering vector, q, of the order of 0.07 $Å^{-1}$ corresponding to the continuous phase, and an asymptotic part at lower values of q, proportional to q^{-4}, corresponding to the scattering due to the interface between water droplets and the continuous phase [112]. Comparison of SAXS spectra of gel emulsions with those of the continuous phase separated out by centrifugation, indicated that no significant differences exist between the structures of the microemulsion under equilibrium and non-equilibrium conditions [94]. However, theoretical considerations [94, 113] suggest that the number of microemulsion droplets is decreased as the volume fraction of dispersed phase increases. Consequently, at values of water volume fraction close to unity, most of the surfactant molecules would be adsorbed at the interface of water droplets. By comparison of calculated intensities, determined according to the Porod-Auvray equation [112] with experimental absolute intensities, the specific surface and mean droplet radius of gel emulsions was calculated. The droplet size was found to increase on increasing the volume fraction of dispersed phase, oil/surfactant ratio, salinity and temperature. These results were interpreted on the basis of surfactant availability and interfacial tension [94].

The non-equilibrium structure of gel emulsions was also investigated by electron spin resonance (ESR)[113; 114]. The change in apparent order parameter, S, and the isotropic hyperfine splitting constant, a_N, of two amphiphilic and water insoluble spin probes (5- and 16-doxylstearic acids) were determined in gel emulsions, and single oil phases (microemulsion). This type of spin-probe molecule is incorporated with the surfactant

aggregates or in the surfactant molecular layer (water-oil interface). The order parameter provides information regarding the degree of organisation of the surfactant molecules and the hyperfine splitting constant, a_N, is used as a measure of the polarity of the spin label environment. The variation of S and a_N with water concentration in compositions of the system water/$C_{12}EO_3$/cyclohexane and water $C_{16}EO_4$/cyclohexane with a constant oil/surfactant weight ratio follow the following behaviour: up to the solubilization limit, S and a_N increase with increasing water content, indicating that the environment of the spin label changes from an apolar one (surfactant and oil mixtures) to a more polar one (existence of reverse micelles). At water contents higher than the solubilisation limit, W/O type emulsions are formed due to the separation if an excess water phase. If the spin probe is in the same state in a single reverse-micellar solution phase or in a gel emulsion, the order parameter should be equal. The apparent order parameter, S, and the isotropic hyperfine splitting constant, a_N, of 5-doxylstearic acid increase slowly but continuously in an ordinary emulsion region beyond the solubilisation limit and then increase abruptly in the gel emulsion region. However, in the system with 16-doxylstearic acid, both S and a_N remain unchanged over a wide range of water concentrations except in the gel emulsion region. The difference in order parameters at the water droplet film in gel emulsions and the inside of the reverse micelles in the single isotropic phase indicated that the surfactant molecules at the water droplet film are more tightly packed compared to those in reverse micelles. The observed difference in the apparent order parameter between the ordinary emulsions and the gel emulsions suggested that, when the fraction of water in the system is around 0.99, most of the surfactant molecules are adsorbed at the oil-water interface and no reverse micelles are present in the continuous oil phase [113].

In the water rich region, as the water content increases, the water-oil interfacial area increases and the surfactant molecules are preferentially adsorbed at the water-oil interface. Consequently, the number of micelles would decrease and the spin probe would move from reverse micelles to the water-oil interface with the increase in water concentration. The ESR studies [113] suggested that the positions of the spin probes are different in ordinary and highly concentrated emulsions. The surfactant molecules are distributed between the interface and reverse micelles. In the non-equilibrium state, the number of reverse micelles decreases with increasing water content and finally no reverse micelles are present in the continuous media at very high water content. With 5-doxylstearic acid as the spin probe, the order parameter for the longer chain surfactant, $C_{16}EO_4$, is higher than that of the shorter chain surfactant, $C_{12}EO_3$, an indication that it is more tightly packed at the interface.

Gel emulsions are kinetically stable systems, which break into two liquids phases with time. The time taken for separation, which may vary from minutes to months, can be significantly retarded by the appropriate selection of composition variables and temperature.

A relationship between the stability of gel emulsions and the HLB (hydrophilic lipophile balance) temperature of the corresponding water/polyoxyethylene non-ionic surfactant/aliphatic hydrocarbon system was observed [85, 115, 87, 88]. The stability of O/W gel emulsions decreases with increasing temperature, experiencing a pronounced coalescence rate at a temperature approximately 25 °C lower than the HLB temperature [88]. The stability of W/O gel emulsions first increases with temperature, reaching a maximum at 25-30 °C above the HLB temperature, and then decreases [88, 115]. This fact was explained on the basis of FT-PGSE NMR studies [91]. Self-diffusion measurements of the continuous phase of W/O gel emulsions of the water/$C_{12}EO_4$/decane system as a function of temperature showed that the microemulsion structure changed from bicontinuous, at temperatures close to the HLB temperature of the system, to W/O-type at higher temperatures. Therefore, the change in structure of the continuous phase strongly affects gel emulsion stability. As described above, a change in microemulsion structure from bicontinuous to W/O-type was observed in the same system with an increase in the oil/surfactant ratio [91]. Since the bicontinuous structure is highly permeable to the dispersed phase, it cannot stabilise the emulsion. However, when the structure of the continuous phase is of the droplet type, the stability can reach optimum values.

Stability studies of gel emulsions formed with the surfactants $C_{16}EO$ and $C_{12}EO_3$ (which have similar HLB values) and the same oil, cyclohexane (therefore showing the same HLB temperature), revealed that for low and middle-internal phase emulsion the stability is higher in the system with the longer chain surfactant [113].

The presence of additives may influence the stability. In the context of gel emulsions, the effect of electrolytes on gel emulsion stability has been studied in some detail [88, 90, 114]. In general a considerable increase in the stability and the viscosity of gel emulsions is produced with the addition of inorganic salts. Those with a large salting out effect, decreasing the cloud point in binary water/nonionic surfactant/oil systems, are the most effective stabilisers. The stability of emulsions as a function of $NaSO_4$, $CaCl_2$, NaCl and KI concentration, as determined by visual observation, showed that Na_2SO_4, $CaCl_2$ and NaCl stabilised the gel emulsions significantly while KI did not improve gel emulsion stability [88]. The former electrolytes depress the HLB temperature of the system while KI slightly increases it. ESR measurements [114] showed that the apparent order parameter in gel emulsions increased with

the addition of electrolyte.

The increase in the apparent order parameter means that the packing of the surfactant molecules at the interface changes significantly with the addition of salt. The enhanced stability produced by electrolytes might be due to the dehydration of the hydrophilic part of the surfactant [114]. The surfactant-surfactant interactions would increase and consequently the interfacial films become more rigid. Results of rheological studies as well as interfacial tension measurements agreed with these hypotheses [92].

Bibliography

1 B.P. Binks, *Annu. Rep. Prog. Chem., Sect C*, 1996, **92**, 97.

2 J.Th.G. Overbeek in: Th.F. Tadros (Ed.), *Surfactants*, Academic Press, London, 1984.

3 L.M. Prince (Ed.), *Microemulsions: Theory and Practice*, Academic Press, New York, 1977.

4 D. Langevin, *Acc. Chem. Res.* 1988, **21**, 225.

5 R. Aveyard, B.P. Binks, P.D.I Fletcher, *Langmuir*, 1989, **5**, 1210.

6 B.P. Binks, J. Meunier, O. Abillon, D. Langevin, *Langmuir*, 1989, **5**, 415.

7 R. Aveyard, T.A. Lawless *J. Chem. Soc., Faraday Trans. 1*, 1986, **82**, 2951.

8 B.P. Binks, P.D.I. Fletcher, D.I. Horsup, *Colloids Surf.*, 1991, **61**, 291.

9 J.H. Schulman, E.G. Cockbain, *Trans. Faraday Soc.*, 1939, **36**, 651.

10 J.H. Schulman, E.G. Cockbain, *Trans. Faraday Soc.*, 1940, **36**, 661.

11 A.E. Alexander, J.H. Schulman, *Trans. Faraday Soc.*, 1940, **36**, 960.

12 Th.F. Tadros, B. Vincent, in "*Encyclopedia of Emulsion Technology*", Ed. P. Becher, Deker, New York, 1983, vol. 1, p. 129.

13 S. Friberg, L. Mandell and Larson, *J .Colloid and Interface Sci.*, 1969, **29**, 155.

14 S. Friberg, L. Mandell, *J. Pharm. Sci.*, 1970, **59**, 1001.

15 S. Friberg, L. Rydhag, *Colloid Polym, Sci.*, 1971, **244**, 233.

16 N. Krog, N.M. Barfod, R.M. Sanchez, *J. Dis. Sci. Technol.*, 1989, **10**, 483.

17 W.D. Bancroft, *J. Phys. Chem.*, 1913, **17**, 501.

18 W.D. Bancroft, *J. Phys. Chem.*,1915, **19**, 275.

19 W.C. Griffin, L. *Soc. Cosmet. Chem.* 1949, **1**, 311.

20 W.C. Griffin, L. *Soc. Cosmet. Chem.* 1954, **5**, 249.

21 F. Shinoda, S. Friberg, *Emulsions and Solubilisation*, Jonh Wiley & Sons: New York, 1986, p. 174.

22 O. Ghosh, C.M. Miller, *J. Phys. Chem.*, 1987, **91**, 4528.

23 B.P. Binks, *Colloids Surf. A*, 1993, **71**, 167.

24 J.T. Davies In *Proc. 2nd Int. Cong. Surf. Activity*; London, 1957; p. 417.

25 J.T. Davies, E.K. Rideal, *Interfacial Phenomena*; Academic: New York-San Francisco-London, 1963; p. 129.

26 J.T. Davies, In *Progress in Surface Science*; J.F. Danielli, K.G.A. Parkhurst, A.C. Riddford, Eds.; Academic New York, 1964; Vol. 2, p. 129.

27 R. Aveyard, B.P. Binks, P.D.I. Fletcher in "*The Structure, Dynamics and Equilibrium*

Properties of Colloidal Systems", eds. D.M. Bloor and E. Wyn-Jones, Kuwer, Dordrecht, 1990, p. 557.

28 A. Graciaa, J. Lachaise, G. Marion, R.S. Schechter, *Langmuir*, 1989, **5**, 1315.

29 H.T. Davis, *Colloids Surf. A*, 1994, **91**, 9.

30 R. Aveyard, B.P. Binks, T.A. Lawless, J. Mead, *J. Chem. Soc., Faraday Trans. I*, 1985, **81**, 2155.

31 R.D. Hazlett, R.S. Schechter, *Colloids Surf.*, 1988, **29**, 53.

32 D.H. Smith, K.H. Lee, *J. Phys. Chem.* 1990, **94**, 3746.

33 B.P. Binks, *Chem. Ind. (London)*, 1993, **14**, 537.

34 R. Aveyard, B.P. Binks, S. Clarks, P.D.I. Fletcher, *J. Chem. Soc., Faraday Trans. I*, 1990, **86**, 3111.

35 R. Aveyard, B.P. Binks, P.D.I. Fletcher, *Langmuir*, 1989, **5**, 1210.

36 H. Kunieda, K. Shinoda, *J. Colloid Interface Sci.*, 1985, **5**, 1210.

37 J.L. Salager, G. Lopez-Castellanos, M. Miñana-Perez, C. Parra, C. Cucuphat, A. Graciaa, J. Lachaise, *J. Disp. Technol.* , 1991, **12**, 59.

38 A. Kabalanov, T. Tarra, R. Arlauskas, J. Weers, *J. Colloid. Interface Sci.*, 1996, **184**, 227.

39 B.P. Binks, *Langmuir*, 1993, **9**, 25.

40 F. Harusawa, T. Saito, H. Nakajima, S. Fukushima, *J. Colloid Interface Sci.*, 1980, **74**, 435.

41 F. Harusawa, T. Saito, M. Tanaka, *J. Soc. Cosmet. Chem.*, 1982, **33**, 115.

42 K. Shinoda, H. Saito, *J. Colloid Interface Sci.* 1968, **26**, 70.

43 K. Shinoda, H. Saito, *J. Colloid Interface Sci.* 1969, **30**, 258.

44 K. Shinoda, H. Saito, *J. Colloid Interface Sci.*, 1978, **64**, 68;.

45 K. Shinoda, H. Saito, *J. Colloid Interface Sci.*, 1970, **32**, 647.

46 H.T. Davis, *Colloids Surf., A* 1994, **91**, 9.

47 B.V. Derjaguin, E. Obuchar, *J. Colloid Chem.*, 1935, **1**, 385.

48 A. Scheludko, *Adv. Colloid Interface Sci.*, 1967, **1**, 391.

49 A. Scheludko, *Trans. Faraday Soc.*, 1968, **64**, 1123.

50 A. Vrij, *Disc. Faraday Soc.*, 1966, **42**, 23.

51 H. Sonntag, K. Strenge, *Coagulation and Stability of Disperse Systems*, Halstead-Wiley, New York, 1969.

52 B. Deminiere, *Ph.D Thesis*, L'Universite Bordeaux 1, Bordeaux, 1997.

53 A.J. de Vries, *Rec. Trav. Chim.*, 1958, **77**, 3839.

[54] P.G. de Gennes, J. Prost, " *The Physics of Liquid Crystals*", Clarendon Press, Oxford, 1993.

[55] A. Kabalnov, H. Wennerström, *Langmuir*, 1996, **99**, 5605.

[56] W.D. Harkins, E.C.H. Davies, G.L. Clark, *J. Am. Chem. Soc.*, 1917, **39**, 541.

[57] I. Langmuir, *J. Am. Chem. Soc.*, 1917, **39**, 1848.

[58] J.M. Lifshitz, V.V. Slezov, *Sov. Phys. JETP*, 1959, **35**, 331.

[59] C. Wagner, *Z. Electrochem.*, 1961, **35**, 581.

[60] P.W. Vorhees, *J. Stat. Phys.*, 1985, **38**, 231.

[61] Y. Enamoto, M. Tokuyama, K. Kawasaki, *Acta Metall.*, 1986, **34**, 2119.

[62] A.D Brailsford, P. Wynblatt, *Acta Metall.*, 1979, **27**, 489.

[63] A.D Brailsford, *J. Nucl. Mater.*, 1976, **60**, 257.

[64] J.A. Marqusee, J. Ross, *J. Chem. Phys.*, 1984, **80**, 536.

[65] C.H. Kang, D:N: Yoon, *Metall. Trans. A*, 1981, **12**, 65.

[66] A. Niemi, T.H. Courtney, *Acta Metall.*, 1981, **3**, 1393.

[67] C.H. Kang, D:N: Yoon, *Metall. Trans. A*, 1981, **12**, 65.

[68] S.S. Davis, A. Smith in: A.L. Smith (Ed.), *Emulsion Theory and Practice*, Academic Press, London.

[69] S.S. Davis, A. Smith, *J. Pharm. Pharmacol.*, 1973, **25** (Suppl) 117.

[70] A.S. Kabal'nov, A.V. Pertsov, Y.D. Aprosin, E.D. Shchukin, *Kolloidn. Zh.*, 1985, **47**, 898.

[71] A.S. Kabal'nov, K.N. Makarov, *Kolloidn. Zh.*, 1990, **52**, 589.

[72] A.S. Kabal'nov, A.V. Pertsov, E.D. Shchukin, *Kolloidn. Zh.*, 1984, **46**, 965.

[73] A.S. Kabal'nov, A.V. Pertsov, E.D. Shchukin, *J. Colloid Interface Sci.* 1987, **118**, 590.

[74] A.S. Kabal'nov, K.N. Makarov, A.V. Pertsov, E.D. Shchukin, *J. Colloid Interface Sci.* 1990, **138**, 98.

[75] M. Kahlweit, in H. Eyring, D. Henderson and W. Jost (Eds.), *Physical Chemistry*, Vol. 10, Academic Press, New York, 1970.

[76] M. Kahlweit, *Adv. Colloid Interface Sci.*, 1975, **5**, 1.

[77] M. Kahlweit, *Faraday Discuss. Chem. Soc.*, 1976, **61**, 48.

[78] G. Venzl, *Ber. Bunsenges. Phys Chem.*, 1983, **87**, 318.

[79] W.I. Higuchi, J. Misra, *J. Pharm. Sci.*, 1962, **51**, 459.

[80] R. Buscall, S.S. Davis, D.S. Potts, *Colloid. Polym. Sci.*, 1979, **257**, 636.

[81] S.S. Davis, H.P. Round, T.S. Purewal, *J. Colloid Interface Sci.*, 1981, **80**, 508.

[82] A.S. Kabalnov, A.V. Pertzov, E.D. Shchukin, *Colloids Surf.*, 1987, **24**, 19.

[83] P. Taylor, R.H. Ottewill, *Prog. Colloid. Polym. Sci.*, 1995, **97**, 299.

[84] C. Solans, F. Comellez, N Azemer, J. Sanchez, J.L. Parra, *J. Com. Esp. Deterg.*, 1986, **17**, 109.

[85] H. Kunieda, C. Solans, N. Shida, J.L. Parra, *Colloids Surf.*, 1987, **24**, 225.

[86] C. Solans, N. Azemar J.L. Parra, *Prog. Colloid Polym. Sci.*, 1988, **76**, 224.

[87] C. Solans, J.G. Dominguez, J.L. Parra, J. Heuser, S.E. Friberg, *Colloid Polym. Sci.* 1988, **266**, 570.

[88] H. Kunieda, N. Yano, C. Solans, *Colloid Surf.*, 1989, **36**, 313.

[89] H. Kunieda, D.F. Evans, C. Solans, M. Yoshiada, *Colloids Surf.*, 1990, **47**, 35.

[90] R. Pons, C. Solans, M.J. Stebè, P. Erra, J.C. Ravey, *Prog. Colloid Polym. Sci.*, 1992, 110.

[91] C. Solans, R. Pons, S. Zhu, H.T. Davis, D.F. Evans, K. Nakamura, H. Kunieda, *Langmuir*, 1993, **9**, 1479.

[92] R. Pons, P. Erra, C. Solans, J.C. Ravey, M.J. Stebè, *J. Phys. Chem.* 1993, **97**, 12320.

[93] H. Kunieda, A. Cherian John, R. Pons, C. Solans, in "*Structure-Performance Relationships in Surfactants*",. K. Eourni and M. Meno Eds, Dekker, New York, 1997, p. 359.

[94] R. Pons, J.C. Ravey, S. Sauvage, M.J. Stebe, P. Erra, C. Solans, *Colloids Surf.*, 1993, **76**, 171.

[95] R. Pons, J. Carrera, P. Erra, H. Kunieda, C. Solans, *Colloids Surf. A*, 1994, **91**, 259.

[97] E. Ruckenstein, *Adv. Polym. Sci.*, 1997, **127**, 3.

[97] N.R. Cameron, D.C.Sherrington, *Adv. Polym. Sci.*, 1996, **126**, 165.

[98] W. Ostwald, *Kolloid Z.*, 1910, **6**, 103; 1910, **7**, 64.

[99] K.J. Lissant, *J. Colloid Interface Sci.*, 1966, **22**, 462.

[100] K.J. Lissant, K.G. Mayhan, *J. Colloid Interface Sci.*, 1973, **42**, 201.

[101] H.M. Princen, *J. Colloid Interface Sci.*, 1979, **71**, 55.

[102] H.M. Princen, *J. Colloid Interface Sci.*, 1983, **91**, 160.

[103] H.M. Princen A.D. Kiss, *J. Colloid Interface Sci.*, 1986, **112**, 427.

[104] O. Bèlorgey, J.J. Benattar, *Phys. Rev. Lett.*, 1991, **66**, 313.

[105] O. Mondain-Monval, F. Leal-Calderon, J. Bibette, *J. Phys. II*, 1996, **6**, 1313.

[106] M.P. Aronson, H.M Princen, *Nature*, 1980, **286**, 370.

[107] P. Poulin, J. Bibette, *Phys Rev. Lett.*, 1997, **79**, 3290.

[108] J.C. Ravey, M.J. Stèbè, *Physica B*, 1989, **304**, 156.

[109] J.C. Ravey, M.J. Stèbè, *Prog., Colloid Polym. Sci.*, 1990, **82**, 218.

[110] R. Pons, G. Calderò, M.J. Garcia, N. Azemar, I. Carrera C. Solans, *Prog. Colloid Polym. Sci.*, 1996, **100**, 132.

[111] G. Calderò, M.J. Garcia-Celma, C. Solans, M. Plaza, R. Pons, *Langmuir*, 1997, **13**, 385.

[112] L. Auvray, J.P. Cotton, R. Ober, C. Taupin, *J. Phys.*, 1984, **45**, 913.

[113] H. Kunieda, V. Rajagopalan, E. Kimura, C. Solans, *Langmuir*, 1994, **272**, 1166.

[114] V. Rajagopalan, C. Solans, H. Kunieda, *Colloid Polym. Sci.*, 1994, **272**, 1166.

[115] C. Solans, N. Azemar, J.L Parra, *Prog. Colloid Polym. Sci.*, 1988, **76**, 224.

LITERATURE REVIEW

Chapter 2

2 LITERATURE REVIEW

In this chapter, advances in PolyHIPE polymers science and technology published since 1995 are reviewed. For papers published previously, reference is addressed to the review by Cameron and Sherrington [1].

This chapter is subdivided into four sections:

2.1. Recent advances in PolyHIPE science.

2.2. PolyHIPE high performance materials.

2.3. PolyHIPE materials as supports for chemical synthesis and separation media.

2.4. PolyHIPE materials in technological applications.

2.1 Recent advances in PolyHIPE science

N.R. Cameron *et al* have investigated the formation of the interconnected morphology of open cell S/DVB PolyHIPE copolymers by scanning electron microscopy on frozen HIPE samples at different stages of polymerization, a technique known as cryo-SEM [2]. The transition from discrete emulsion droplets to interconnected cells was observed to occur around gel-point of the polymerizing system. This suggested that the formation of holes between adjacent cells was due to the contraction of the thin monomeric films on conversion of monomer to polymer, as a result of the higher density of the latter.

A novel method for the production of porous foams and PolyHIPEs has been proposed by Cooper and collaborators [3]. It involves templating high internal phase emulsions containing supercritical carbon dioxide. The main advantage of this approach is that it does not involve any organic solvent either in the synthesis or in the purification steps. On the other hand it requires the employment of surfactants with fluoroalkyl or fluoroether tails. This method appears to be particularly suitable in applications where solvent residues are undesiderable (e.g. biomedical applications).

2.2 PolyHIPE high performance materials

Porous foams possessing the property of heat resistance have potential in applications for acoustic or thermal insulation within engine compartments and enclosures. With the aim of developing low density, rigid high temperature polyHIPE foams Hoisington *et. al.* [4] copolymerized styrene with N-ethylmaleimide in the presence of either DVB or bis(3-ethyl-5-methyl-4-maleimide-phenyl)methane (BMI-70)(Scheme 1). The preparation of styrene-DVB-ethylmaleimide emulsions in which increasing concentrations of styrene were replaced by

ethylmaleimide produced more and more viscous emulsions and when the concentration of n-ethylmaleimide in the monomer phase reached 50% wt. a HIPE could no longer be obtained. When BMI-70 is used in conjunction with styrene (see Scheme 2.1), emulsions could be

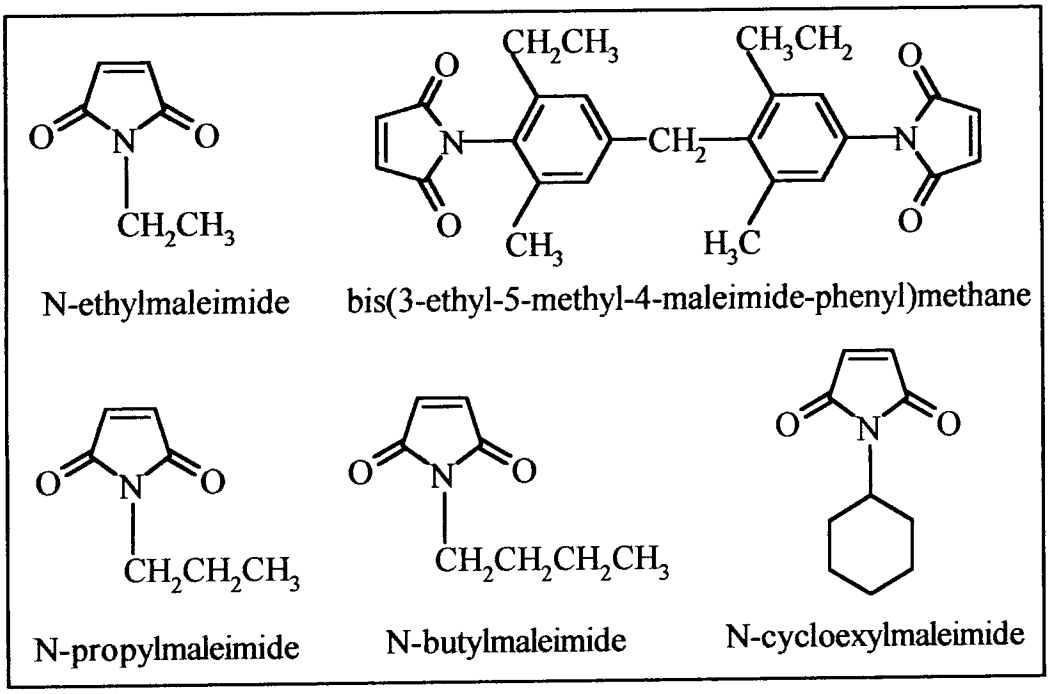

Scheme 2.1. N-maleimide monomers and crosslinkers.

obtained but the corresponding foams were represented by disconnected or poorly connected structures. The influence of ethylmaleimide content on foam morphology showed a tendency to be composed more of a connected strut configuration with larger interconnecting holes. Addition of N-ethylmaleimide appeared to be changing the interaction between the oil and water phase during processing, and therefore, the structure of the final foam cellular structure. The same effect was observed for a combination of ethylmaleimide and BMI-70. The authors ascribed the effect of maleimides on foam morphology, to the partial solubility of N-ethylmaleimide in water (5% wt.). The disconnected morphology was indicative of a high emulsifier concentration. Typically, as the emulsifier concentration was increased in the HIPE process, the foam structure began to break down and produced a disconnected polymer system.

Dynamic mechanical analysis allowed the T_g of the series of foams before and after curing to be determined. The T_g's of the foam samples increased directly with N-ethylmaleimide concentration. The post-cure T_g's were 25-40° C above the pre-cured T_g's and this is probably due to reaction occurring during the curing process and as a consequence of the removal of

SPAN 80 which is known to act as a plasticizer in the polymeric foams. For every 10% increase of ethylmaleimide concentration, a corresponding increase of 20° C was observed in the foam T_g. When BMI-70 was used as a crosslinker the T_g's were approximately the same and independent of the BMI-70 concentration in the emulsion.

The thermal stability was examined by thermogravimetry (TGA). The degradation curve of S-DVB consisted of two steps. When the N-ethylmaleimide modifier was added, a decrease in the size of the first degradation step and a shift to the higher T in the overall curve was observed. Therefore, N-ethylmaleimide inhibited the first degradation step and improved the overall thermo-oxidative stability of the foam system. When the thermal stability in nitrogen was examined, a one step degradation was observed with an increase in thermal stability with increasing N-ethylmaleimide concentration. When BMI-70 was used as a crosslinker only one step degradation curve was observed in air. This suggested that the first degradation step in the oxidative degradation in the DVB crosslinked samples was oxidative chain scission on both ends of the DVB crosslinker, which allowed the DVB blocks to volatilize. In the BMI-70 crosslinked systems and as N-ethylmaleimide was incorporated into the DVB crosslinked foams the isolation of the crosslinking molecule was prevented by the higher thermo-oxidative stability of the maleimide-DVB and of the styrene-maleimide bonds at both ends of the crosslinks. Therefore, the first weight loss step was eliminated with the incorporation of maleimide modifier.

The compression moduli of N-ethylmaleimide foams tended to increase slightly with the increase of its concentration. Conversely, the values for foams obtained from BMI-70 decreased a little when the concentration of this crosslinker increased, and this was the result of the effect observed on the foam morphologies, which were less uniform.

As one of the main problems in incorporating large quantities of N-ethylmaleimide was represented by the partial solubility of this monomer in the aqueous phase, the authors in their attempt to incorporate in the emulsion larger quantities of the maleimide monomers and thus improve their thermal and mechanical properties turned to three other N-substituted maleimides (see Sheme 2.1) with lower water solubility than N-ethylmaleimide: N-propylmaleimide, N-butylmaleimide, and N-cyclohexylmaleimide [5]. These monomers have a solubility in water which decreases with the length of the alkyl chain and for the same reason increases in styrene.

In all cases emulsions containing 50% by weight of maleimide monomers crosslinked with DVB could be prepared without water phase separation. The content of cyclohexylmaleimide that could be incorporated depended on the solubility in styrene which is lower than the other

two monomers. When BMI-70 replaced DVB as the crosslinker agent the total quantity of the combined BMI-70 and maleimide monomers that could be incorporated amounts to 50 % by weight.

One advantage presented by these monomers over N-ethylmaleimide was the reduction of the viscosity of the resulting emulsions which represented an advantage in processing.

The morphologies of the foams presented the behavior already met in the previous paper [4], that is, as the amount of maleimide monomers and crosslinker increased the walls of the foams become thinner with some sign of break-up in the cell structure. The cells contained less of a wall and more of a strut configuration. Nevertheless, it seemed that the quality of the cell structure improved as compared with that of the N-ethylmaleimide derived foams and the authors stress the importance of using water insoluble monomers.

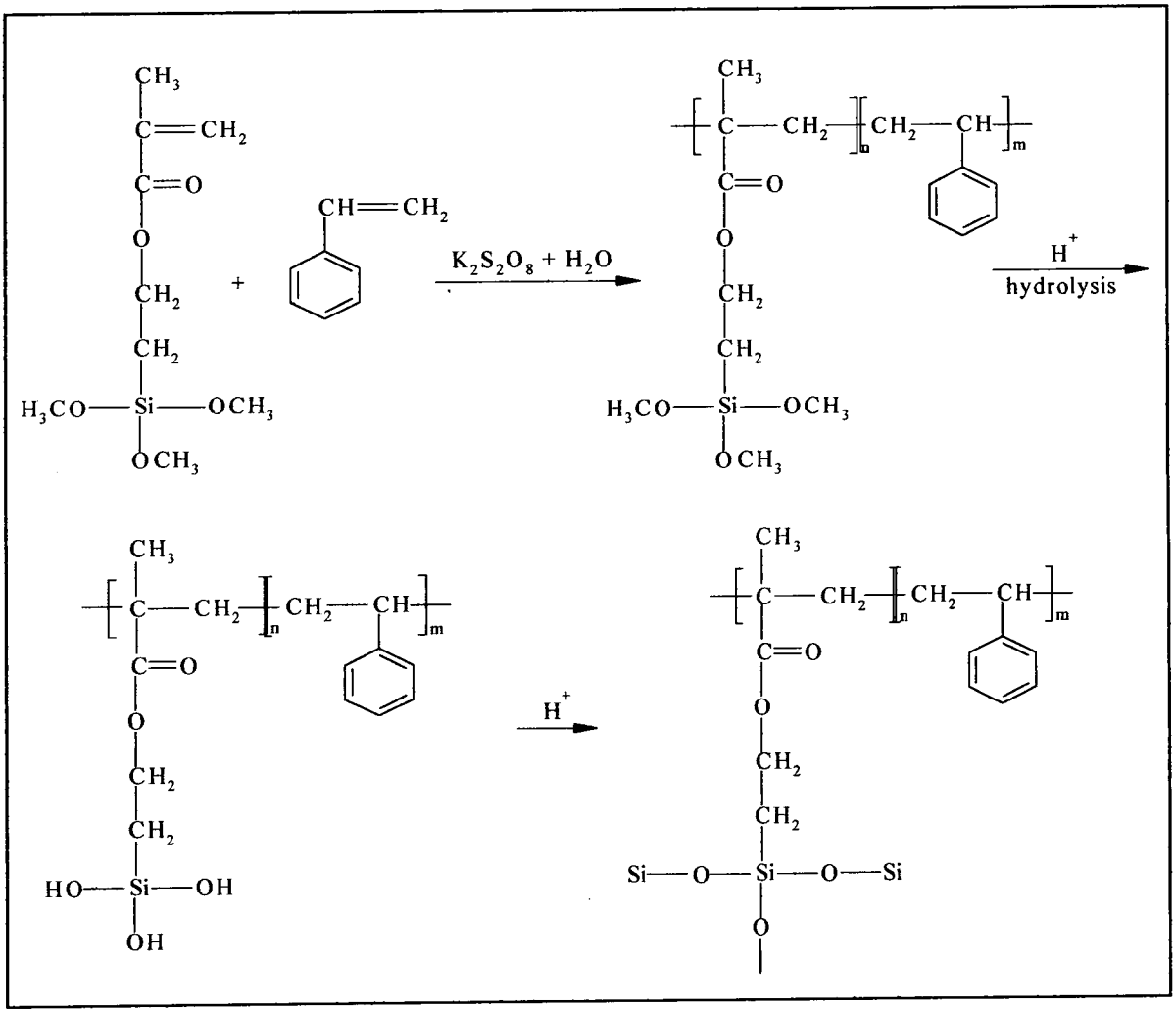

Scheme 2.2. Schematic illustration of the reactions involved in the formation of hybrid foams.

Hybrid PolyHIPE foams which combine an inorganic polysilsesquioxane network with an organic polystyrene network have been synthesized by Sergienko *et al* [6]. The monomer which has been used as a precursor of the polysilsesquioxane network consisted of a methacryloxypropyltrimethoxy silane (MPS). The MPS/styrene copolymerization proceeds via the vinyl group using a typical radical mechanism with a water soluble initiator. The combination of vinyl radical polymerization and condensation in a HIPE yields an organic-inorganic hybrid foam possessing higher thermal stability than a conventional S-DVB polyHIPE.

The reactions are illustrated in Scheme 2.2. The radical copolymerization and hydrolysis are likely to occur simultaneously. The morphology of the foams is heavily influenced by the content of MPS, in the sense that an increase of MPS concentration in the organic phase causes an increasing reduction in size of both cavity and interconnecting windows. The authors argued that this may reflect a reduction in interfacial tension on incorporation of the more hydrophilic MPS. The co-adsorption of MPS at the interface in the emulsion with the highest concentration of MPS increased the viscosity to a point that the shear stress of mixing was not able to break up the large droplets making it difficult to generate a uniform fine dispersion of the aqueous phase, yielding large droplets in the last stage of HIPE synthesis.

Foams produced without the addition of DVB are less stable mechanically, undergoing shrinkage on drying to a degree which is dependent on MPS concentration. Higher concentration of this monomer causes the collapse of the original HIPE yielding an inhomogeneous structure. This effect may again be ascribed to the reduction of interfacial tension to the point that the concomitant reduction of the wall thickness makes the foams prone to collapse. The stability introduced by the formation of a DVB crosslinked network prevents this catastrophic collapse.

Thermal dynamic mechanical measurements show that the T_g increases with the content of MPS. Also, the foams containing higher quantities of MPS are increasingly more rigid and stiff at high temperature. Above the T_g, the organic network is soft and rubbery, while the polysilsesquioxane inorganic network is stiff and rigid.

Studies on thermal degradation showed that when tests were carried out in a N_2 atmosphere the temperature of decomposition (T_d) decreases with an increase of MPS content. The T_d in air is lower than the T_d in N_2, since the presence of oxygen reduces the activation energy for degradation. As opposed to the trend seen for the T_d in N_2, the T_d in air increases with MPS content. The presence of the inorganic polysilsesquioxane network thus increases the stability of the foam in air. The oxygen reacts with the inorganic network to yield silica, imparting

thermal stability.

The preparation of elastomeric PolyHIPE foams have been described and their properties have been studied [7]. The emulsion of 2-ethylhexyl(meth)acrylate in S-DVB foams results in materials whose glass transiton temperatures, as determined by DSC, were found to vary in a non-linear fashion with acrylates content. It was proposed that the (meth)acrylate comonomer units influence T_g in three different ways: first, they introduce significant amounts of free volume due to their bulky side-groups; second, the high flexibility of the side-groups results in increased segmental motion; and third the introduction of EH(M)A units dilutes the concentration of sterically unfavorable styrene-styrene diads. The shape of the individual curves have been explained qualitatively by considering the comonomer unit diad sequencing, which can be predicted by the corresponding reactivity ratios.

Conventional S-DVB PolyHIPE foams are inherently brittle and possess low thermo-oxidative stability. For this reason investigations into the production of more thermally stable materials using suitable monomers and crosslinkers have represented the efforts of many researchers. The preparation and characterization of poly(aryl ether sulfone)(PES) PolyHIPE materials has been described [8]. A maleimide-terminated aryl ether sulfone macromonomer was copolymerized with S-DVB or a bis(4,4'-isopropylidene diphenoxyethyl)vinyl ether (BVE) in the continuous phase of a HIPE in a non-aqueous HIPE system since only dipolar aprotic solvents were able to co-solubilize the polymeric precursor and surfactants. HIPEs of petroleum ether dispersed in a dipolar aprotic solution of maleimide-terminated PES, PEO-PPO-PEO block copolymer surfactants, comonomer, and AIBN, were successfully prepared and polymerized. The open-cell morphology of the PES PolyHIPE materials was confirmed by SEM, which also showed the presence of a porous structure within the polymer walls.

Surface areas of the PES PolyHIPE polymers, as determined by BET treatment of N_2 adsorption were moderate for the materials copolymerized with either S or DVB and higher for the PES/BVE material. Pore size distributions were investigated by mercury porosimetry. The results confirmed the cell sizes observed by SEM, which were in range 10-200 μm, and also the presence of small pores within the polymer walls. The thermo-oxidative properties of the materials were investigated by TGA. The PES-containing porous polymers possessed higher themo-oxidative stabilities than conventional poly(S-DVB) PolyHIPE materials, although somewhat lower than that of poly(aryl ether sulfone) precursor.

S-DVB PolyHIPE foams doped with titania were obtained by Miele-Paiot *et al* [9] by including in the oil phase of a water/oil emulsion titanium alkoxides bearing unsaturated ligands (see Scheme 2.3). These foams were low density microcellular materials and were

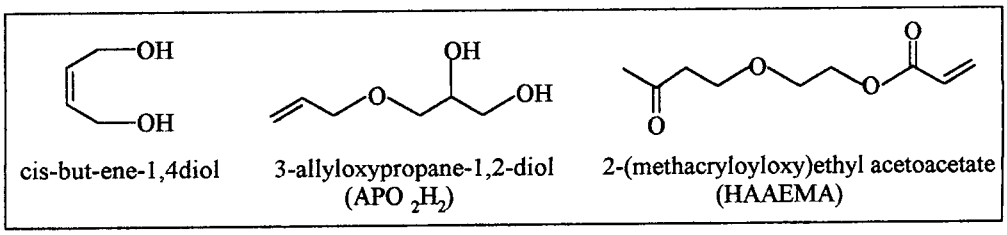

Scheme 2.3. Bidentate O-donor ligands used for the formation of $Ti(OPr^i)_4$.

characterized by SEM, FTIR and compressibility measurements. The presence of a titanium precursor in the organic phase was shown to destabilize the emulsion and required optimization of the experimental conditions by use of the correct amount of surfactant (SPAN 80), the presence or otherwise of an additional solvent such as toluene and the presence of electrolyte (Na_2SO_4) in the aqueous phase. In the latter case more mechanically resistant foams with smaller cells were produced. The best foams (cell size, thickness of the film, homogeneity of the sample, dispersion of the metal) were obtained with $[Ti_4(OPr^i)_8(OCH_2{=}CHCH_2O)_4]$ as the source of titania, probably as a result of the rigidity and limited lability of the bridging diolate ligand.

The foams obtained with $HAPO_2H_2$ and HAAEMA have poor mechanical properties and display irregular porous structures with ill-defined cells despite adjustment of the parameters to obtain stable emulsions. While their unsaturated functionalities are more accessible for homo and co-polymerization reactions, in comparison to n-OC_4H_6O ligands, a drawback is their high flexibility. Alkoxides for which the ligands bear pendant polymerizable functions such as AAEMA or APO_2H_2 are less favorable for the elaboration of foams than those with the unsaturated moiety in a more rigid surrounding as observed for *cis*-but-2-ene-1,4-diol. This flexibility added to a higher lability toward hydrolysis might be responsible for the poor quality of the resulting foams.

The open cellular morphology of PolyHIPE polymers makes them good candidates as damping materials. The effectiveness of PolyHIPEs in such applications depends on their chemical composition. Individual homopolymers are effective damping materials over a limited temperature range. A wider temperature range for damping materials can be obtained using a polymer blend. To this end Sergienko and co-workers [10] produced PolyHIPEs with broad damping peaks through the synthesis of interpenetrating polymer networks (IPN). The technique used involved synthesizing a PolyHIPE foam (polymer I), swelling it with monomer II, crosslinking comonomer and monomer soluble initiator, enhancing diffusion and swelling by imbibing water at elevated temperature and then polymerizing and crosslinking

monomer II. The morphologies, thermal and mechanical properties of the foams were investigated. The damping properties of IPN foams were tailored through changing copolymer composition and monomer composition.

Sergienko prepared a series of copolymer foams from S, EHA, perfluorooctylethyl acrylate (FMA) and DVB and studied their thermal and mechanical properties as a function of foam composition. [11]. They also evaluated the water adsorption performances of the foams and discovered that washing the EHA PolyHIPE in water at 70 °C removed the salt from the PolyHIPE and increased the water adsorption to 500%. Attempts to increase the amount of water adsorbed by coating the internal wall of the foam with polyacrylic acid were unsuccessful because the polyacrylic treatment disrupted the open cell structure and prevented water from penetrating inside the foam.

2.3 PolyHIPE materials as supports for chemical synthesis and separation media.

The morphology of PolyHIPE materials presents some undoubted advantages over more conventional gel and macroporous beads. Gel resins, usually lightly crosslinked S/DVB beads, do not have a permanent porosity and therefore are usable only in solvents effecting a good swelling of their polystyrenic structure, such as toluene and THF. The scale-up for preparative purposes may be problematic as the soft beads used are difficult to manipulate in batches as well as in continuous-flow column devices. The use of macroporous beads with a permanent porosity can be an alternative but is not completely satisfactory. The drawbacks most commonly encountered are: poor reactive site accessibility; some sites may be hidden inside the beads particles; channelling of the reagent solution around the macroporous beads; slow reactions; flow of reagents into beads is limited by the diffusion process [12]. The approach consisting of synthesizing macroporous monoliths in a column shape has been successfully proposed [13]. However, the poor permeability of these materials requires the use of high- pressure column operations and reduces their use for organic synthesis. PolyHIPEs on the contrary are characterized by a high permeability to solvents which makes them usable in low-pressure, continuous flow methods.

Based on these assumptions several attempts have been made to employ polyHIPEs as areactive support media in solid phase synthesis or as separation media.

Monolithic samples of S-DVB PolyHIPE polymers were subjected to a number of electrophilic aromatic substitutions [14]. Reagents and experimental conditions (nature of the

solvents, polarity of the reagents and compatibility between the reagents and the polymeric matrix) were tailored in order to obtain as much quantitative and uniform substitution of the aromatic rings as possible. The particular reactions chosen were sulfonation, nitration and bromination. Sulfonation was carried out with lauryl sulfonic acid in cyclohexane, nitration with tetrabutylammonium nitrate-trifluoroacetic anydride in dichloromethane and bromination with bromine-stannic chloride in dichloromethane. An average degree of sulfonation of 2.4 $mmol \cdot g^{-1}$ was achieved, with a fall in sulfonic acid content of approximately 1 $mmol \cdot g^{-1}$ from monolith surface to center. Nitration occurred to a lesser extent, with similar differences in substitution between surface and center being observed. PolyHIPE monolithic samples were brominated to an extent of 3.6 $mmol \cdot g^{-1}$, and this time bromination was uniform across the entire substrate.

Mercier and co-workers [15], have tried to functionalize S-DVB foams following two routes:

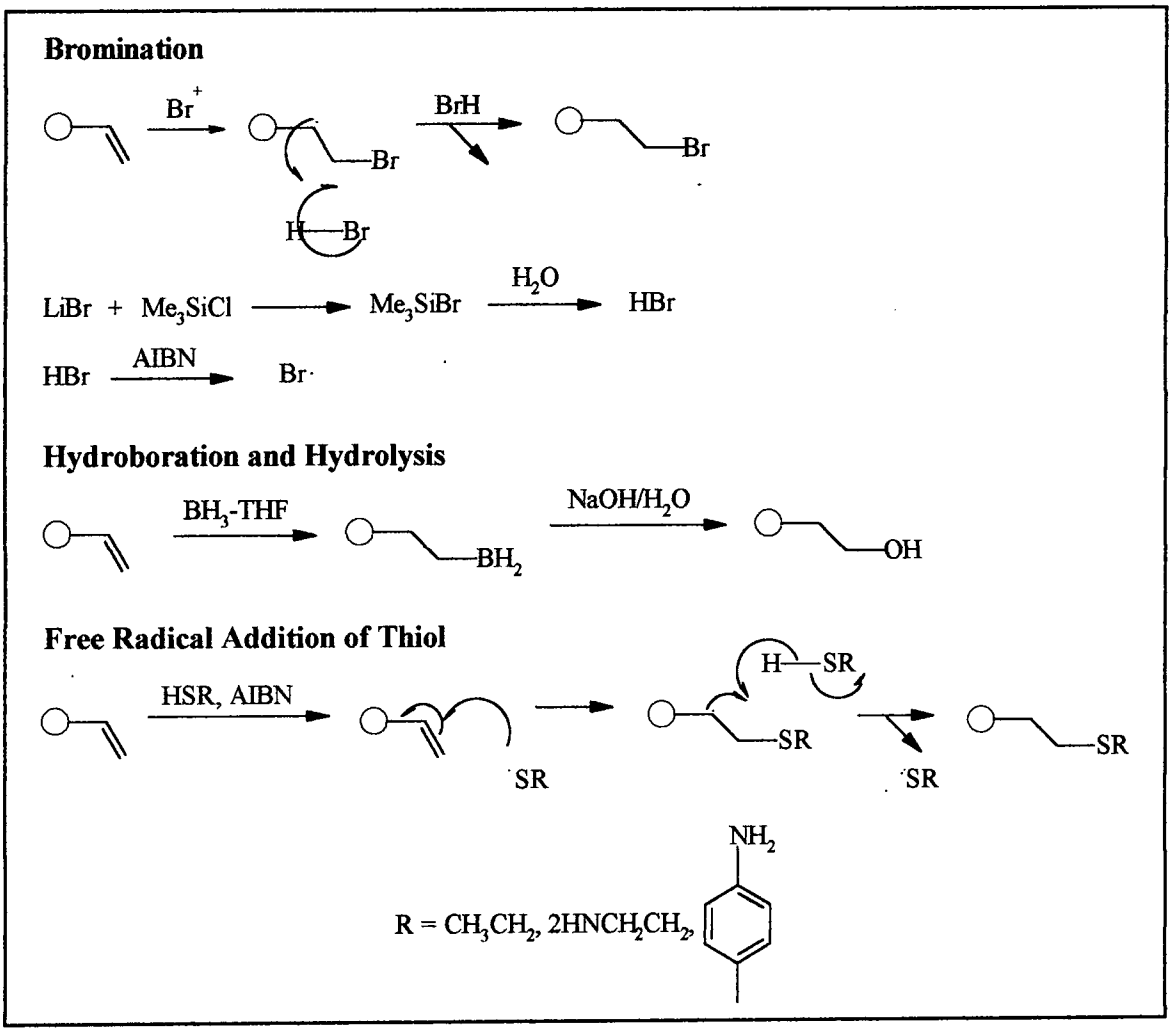

Scheme 2.4. Reactions of functionalization of DVB 80% PolyHIPE supports.

using batch and continuous flow functionalization. In the first method a small cube of PolyHIPE is freeze dried under vacuum to evacuate air followed by impregnation of the PolyHIPE cube with the mixture of solvent and reagents. In the second method the mixture of solvent and reagents is forced through a column filled with a polymeric rod and thus allowed to be impregnated and react in the appropriate conditions. Results in terms of degree of functionalization are in general better for the first method. The functionalization reactions carried out are schematized in Scheme 2.4.

In an attempt to broaden the functional groups incorporated on the polyHIPE resin the same authors [16] have carried out the derivatization of DVB 80% polyHIPE foams with several thiol based reagents. The basic reaction used for such purposes is the regioselective β-addition of RSH to residual vinyl double bonds shown in Scheme 2.4. The PolyHIPE bound thioethers were subsequently chemically modified in order to obtain a wide range of functional PolyHIPEs. Some examples are shown in Scheme 2.4. Degrees of functionalisation between 0.5-2.0 mmol·g^{-1} were obtained.

Free radical reactions such as dehalogenation of alkyl, vinyl or aryl halides, often followed by intra- or intermolecular C-C bond formation are in increasing use in organic synthesis since a large variety of functional groups is tolerated, avoiding laborious protection and de-protection sequences. However the toxicity of tributyltin hydride has limited the development of its use in the synthesis of pharmaceutical derivatives. A possible way around this problem could be

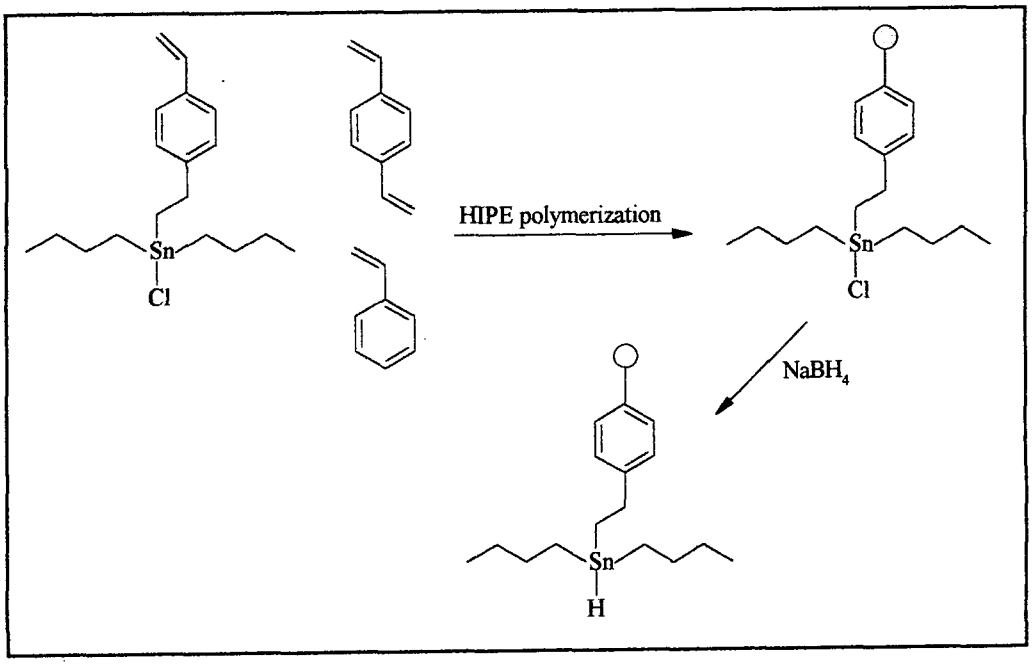

Scheme 2.5. Preparation of PolyHIPE-supported organotin hydride.

the use of polymer-supported organotin hydrides. Mercier *et al* [17] have described the preparation of an emulsion derived foam from 4-ethyl-(2-dibutylchlorostannyl)styrene and DVB (Scheme 2.5).

Another route to foam functionalization [18] involves the addition of thioacetic acid to the pendant vinyl groups, followed by aminolysis, leading to supported SH functionalities (Scheme 2.6). These porous supports showed a good activity towards dehalogenation and

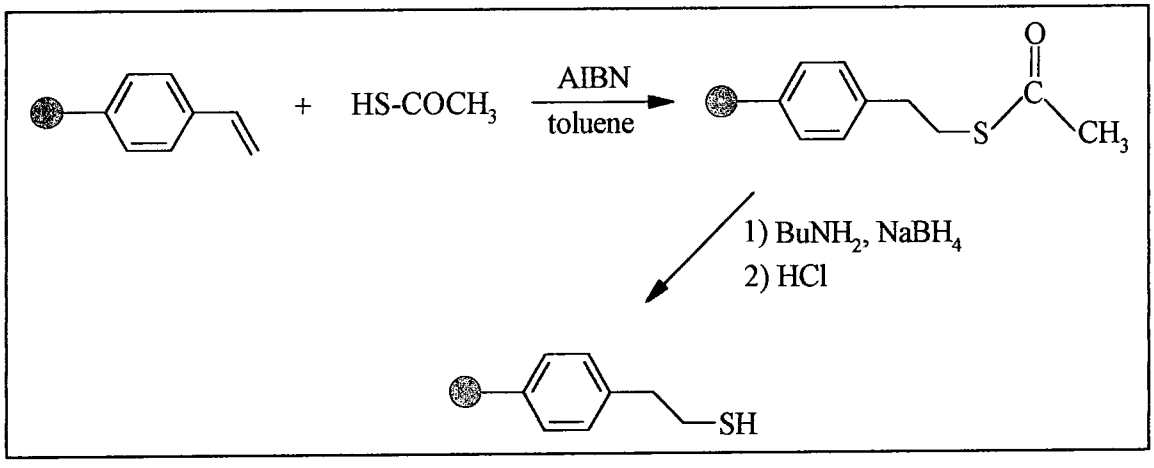

Scheme 2.6. Preparation of PolyHIPE-supported organo thiol.

radical cyclisation.

VBC-DVB PolyHIPE foams were employed as precursors of monolithic polymer supports and scavengers via nucleophilic displacements of chlorine [19]. Reaction of monolithic PolyHIPE with tris(2-aminoethyl)amine, 4-aminoethanol, tris(hydroxymethyl)aminoethane, morpholine and hexamethylenetetramine, led to functionalized polymers with amino and hydroxyl functionalities with high degrees of conversion. The functionalization was carried out both in bulk or flow-through conditions. While the degree of functionalization was comparable in both cases, the flow-through method was significantly faster. 4-chlorobenzoyl chloride was efficiently and rapidly scavenged from solution by the tris(2-aminoethylamine) derivative of poly(4-vinylbenzylchloride-*co*-divinylbenzene) PolyHIPE at ambient temperature. The excellent flow through properties of PolyHIPE were exploited in the hydration of cyclohexene[20]. For this purpose a sulfonated PolyHIPE was prepared following different approaches and its performance was evaluated in different experimental conditions. For the hydration of cyclohexene in a 90 mol % sulfolane-water solution, the results obtained with sulfonated PolyHIPE were an order of magnitude lower than that with ionic-exchange

resin beads. For the hydration of cyclohexene in a separate aqueous phase, sulfonated PolyHIPE appeared to perform comparably to conventional ion-exchange resin beads. In the latter system, mass-transfer limitations between the organic and aqueous phase do not occur. The conversion per m^3 of reactor in the three-phase system is about a factor of 10 smaller than that for the conventional resin beads, mainly because of the low density of the PolyHIPE.

The open cell structure of the foams allows mass transport through a monolith to be mainly convective over the interior surfaces of the cell, minimizing diffusion. In conventional resin beads, most of the surface area available for solute sorption exists in the pores where the liquid medium is essentially stagnant, so here diffusion is the dominant mechanism for mass transport. Diffusion is the slow step that causes elution curves of individual components to broaden and overlap, making separation difficult. Industry's solution to this problem has been to make smaller and more uniform sized resin beads. Smaller resin beads result in higher pressure drops across the column, lower throughput rates and increased chances of channelling. The open cell structure of foams also allows novel functionalization chemistry of the surface with ligands and ion-exchange groups that is not practical in resin beads.

A 4-vinylpyridine functionality has been incorporated into VBC-S copolymer foams by graft-polymerization of vinylpyridine with the aim of rendering it effective in separating heavy metals [21](Scheme 2.7). The performance of these foam columns in removing iron and platinum from aqueous solutions was studied and compared to equally functionalized beads. The open structure of the foam and the flexible graft-polymerized ion-exchange chains result in improved kinetics in metal uptake. Iron uptake kinetics were greatly increased in the grafted foam over resin beads of similar structure. Plutonium uptake kinetics were moderately

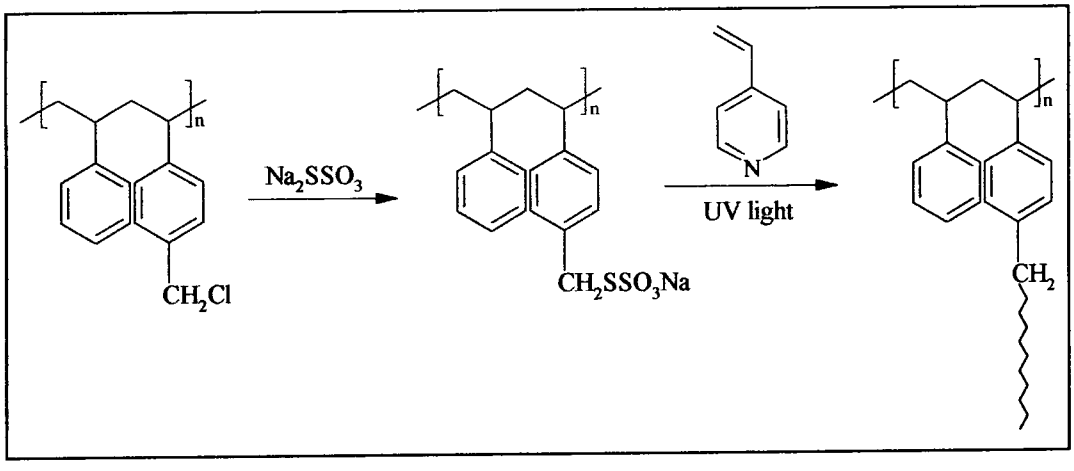

Scheme 2.7. Reaction of functionalization of VBC-S PolyHIPE foams with pendant poly(vinylpyridine) chains.

increased in the foams.

The functionalization of VBC-DVB polyHIPE foam with trialkyl phosphite and tetralkylvinylpyridine diphosphonate allowed to widen the number and type of metals which could be scavenged from aqueous solutions [22]. The performances of the polyHIPE functionalised foams were again compared with those of equivalently functionalised resins and gels in metal ion complexation from dilute solutions. Enhanced complexation kinetics were attributed to the foams greater porosity and water content relative to beads. The foams showed a greater advantage in solutions of high ionic strength, where the decrease in hydration of the ligands caused the collapse of the polymer network in the gels. An increased crosslinking of the foams results in a lower metal ion uptake relative to less crosslinked foams, but the foams still maintain a greater accessibility than beads.

A patent filed by Pharmacia-Biotech [23] describes the use of S-DVB, hexadecafluorodecylmethacrylate/DVB, octadecylmethacrylate/ethylenglycoldimethacrylate monoliths as stationary phases in liquid chromatography. The preparation procedure can be schematized as follows: the emulsion is polymerized in either a Teflon coated mould or HDPE column. The polymerized continuous matrix was taken out of the polymerization container and transferred to a column with rubber tubing along the wall. By applying pressurized air the tubing was inflated and was pressed against the continuous matrix. The matrices in general showed very good flow properties together with high plate number (the height of a plate ranged between 20 to 60 μm). These columns were tested in the separation of peptides and proteins showing moderately good performances.

PolyHIPE foam modules were sulfonated with concentrated sulfonic acid in order to obtain ion exchange resins and their performance were compared to those of a commercial ion exchange resin [24]. The sulfonation was difficult due to a combination of the small sizes of windows that connect larger cells and the high viscosity of concentrated sulfuric acid. The harsh condition of derivatization also caused damage to the foam structure. The extended surface area and high permeability, together with the low mass of adsorbent material that arises as a result of the cellular structure of the media, are properties that make PHP attractive as a potential adsorbent. Although the total capacity of the PHP was rather lower than that for the commercial cation resin the far superior hydrodynamics of the PHP structure ensured better contact between the adsorbent and fluid. This led to PHP being capable of treating larger volumes of liquid before breakthrough of ions at the downstream end of the bead, resulting in higher breakthrough capacities for the PHP even though its degree of sulfonation was much lower.

2.4 PolyHIPE materials in technological applications.

The preparation of blocks of PolyHIPE materials presents some problems:

1. the complete removal of unpolymerized emulsion components is quite difficult to achieve by inexpensive and simple means.

2. the blocks have a skin that forms at the interface between the HIPE and the container (depending on the material the container is made from) used for polymerization. To produce a permeable block , the skin must be removed.

A patent filed by Biopore Corporation [25] describes a new methodology for the preparation of porous polymeric beads whose morphology resembles closely that characteristic of PolyHIPEs. The procedure consists of the preparation of a conventional inverse emulsion of water dispersed in an oil phase comprising a water insoluble monomer (S, VBC), a crosslinker (DVB) and a porogen (dodecane, trichloroethane) stabilized by a surfactant (SPAN 80). Once formed the HIPE is added to an aqueous suspension medium in the presence of a suitable suspension stabilizer (polyvinyl alcohol, acacia gum, gelatin plus colloidal silica, clay) and subjected to a sufficient shear agitation to form a stable suspension. The polyHIPE beads and derivatives obtained by functionalization, are claimed to be suitable for application in the chromatographic separation of proteins, solid phase synthesis, immobilization of antibodies or enzymes and microbial and mammalian cell culture. In a development of the previous patent Kitagawa [26] succeeded to produce hydrophilic PolyHIPE microbeads by polymerizing acrylic acid (pH = 5) with methylen-bis-acrylamide dissolved in water. The discontinuous phase was represented by toluene and the emulsion was stabilized by the surfactant TritonX405. The hydrophilic monomer phase also included a stabilizer that reduces loss of the oil discontinuous phase from the emulsion and helps in preventing coalescence. When producing hydrophilic polymers in microbeads form, a suitable stabilizer is capable of forming a boundary between the oil discontinuous phase of the emulsion and the oil suspension medium when these two media interface in the microdroplet suspension. The stabilizer can be a film forming compound that is soluble in the hydrophilic monomer phase and sufficiently hydrophobic to stabilize the interface with the oil discontinuous phase of the emulsion. Stabilizers used were methylcellulose, acacia or guar gum, ethylcellulose and PVA. The microbeads exhibited an extremely rapid rate of saline adsorption capacity within 20 seconds and half maximal saline adsorption within 5 seconds.

Novel applications of PolyHIPE materials in the field of scaffolds for tissue engineering have been described in both the patent and academic literature. A patent [27] describes the

preparation of PolyHIPE foams based on S, EHA and DVB. The dimension of cavities and interconnecting holes is tailored for specific growth applications. In general, pore size and interconnecting holes are selected according to the type of cell to be grown and the type of growth, i.e. with or without penetration into the bulk of the matrix. Pore sizes in zones intended for growth of the cells should be 2-3 times the diameter of the cells to be grown.

This goal was achieved through four different mechanisms:

1. Basic pores: This is the basic pore structure the size of which is determined at the emulsification stage of the PHP formation. Therefore, the pore size is mainly determined by the deformation (flow) history of the emulsion and on the chemistry of the oil and aqueous phase, phase volume and the polymerization conditions

2. Coalescence pores: This type of pore architecture is obtained through the controlled coalescence of the type 1 pores during polymerization. The dispersed phase droplets in the emulsion of the PHP are coalesced by the addition of water soluble polymers into the aqueous phase, or by adding slightly hydrophilic oils (such as styrene oxide) to the oil phase. The size of the interconnected holes in this case is the same as that of type 1 pore which form a matrix incorporating the coalesced pores.

3. It is possible to obtain a network of microcapillaries within the type 1 or 2 pores. These microcapillaries are formed using a specially constructed mould, in which rods or fine fibers are inserted. The PHP emulsion is pumped into the mould and polymerization is carried out. After polymerization, these inserts are removed either by pulling them out or by dissolving the inserts in acid or suitable solvent. The minimum diameter of these micro capillaries can be as low as 10 μm (using glass, carbon or polymeric fibers). Metallic fibers can be used to obtain microcapillaries in the range 50-1000 μm.

4. The walls of the cavities can be made nano-porous by using a suitable solvent in the oil phase which are usually chosen among good solvents for either the monomer and the polymer. This allows the creation of a very fine porous structure which is comprised within the walls of the cavities.

The uses claimed for the material were the manufacture of contact lenses, dental fillings, cochlear implants, vascular supports including heart valves, cardiac pacemakers and drug delivery skin patches.

The route followed by Busby and Cameron [28] consisted of synthesizing an acryloyl terminated poly(ε-caprolactone) (PCL) macromonomer and its polymerization in the continuous phase of high internal phase emulsions either alone or with a comonomer (S or

methyl methacrylate). Subsequent drying yields low density foams with cell diameters of around 10 μm. Foam morphologies as determined by SEM depends on the type of diluents (S, methyl methacrylate, or toluene) added to the emulsion organic phase and on the PCL content. Increasing the latter increases the continuous phase viscosity to a point where emulsion formation is impeded. Foam swelling in toluene, 2-propanol and water was investigated by solvent imbibition and increased with increasing solvent hydrophobicity. Furthermore, it was found generally to decrease with increasing PCL content, due to increasing cross-linking. Swelling generally increased when higher molar mass PCL macromonomer was used due to the formation of a less tightly cross-linked network.

A foam consisting of a copolymer of PCL and S was used as a support for the growth of human fibroblasts and results indicated that the material is sufficiently biocompatible to support cell function and growth.

PolyHIPE foams obtained from S/DVB/EHA were used as a template for the production of a granular interconnected Ni structure with a specific surface area of about 50 m^2g^{-1} [29]. Two routes were followed to this end. In the first one, named electroless plating, Ni ions in aqueous solutions reacted with a reducing agent also present in solution and were deposited onto catalytic sites of the substrate to be plated. The overall deposition reaction, occurring at

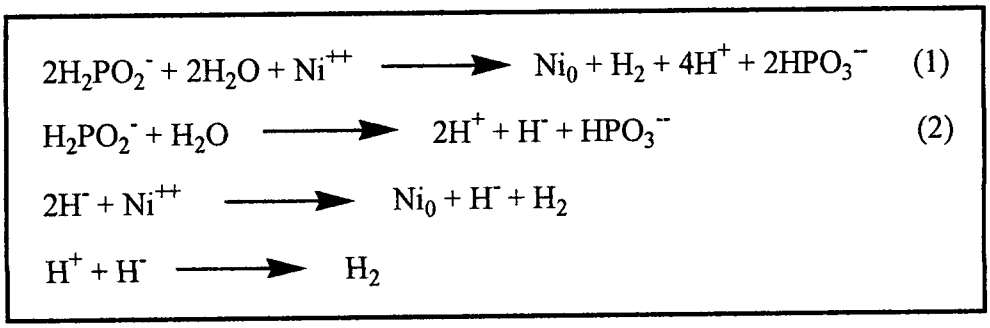

Scheme 2.8. Ni deposition reaction occurring inside PolyHIPE foams.

93°C , is described in Scheme 2.8. A side reaction between protons and hydride ions (Scheme 2.8, reaction (2)) also leads to hydrogen evolution. The evolution of hydrogen gas poses a severe limitation in substantial plating of the interior of the microporous sample since the gas trapped in the pores after the deposition has been initiated prohibits further deposition by blanketing-drying out the interior of the polymer. Photographs of the cross-sections showed that the Ni coating was not uniform throughout the sample: the Ni content fades out as one moves from the outer surface into the core of the sample. SEM micrographs of the interior showed that the foam retained significant porosity, isolated nuclei of Ni being dispersed

randomly. The other route consisted of Ni electrodeposition. A disk of foam was incorporated into an electrolytic devices and immersed in a solution of Ni ions. The SEM micrographs showed a closed, filled-in structure. Still a gradient in Ni concentration is observed from going from the surface toward the interior but this time was much less pronounced than before. The burning out of the polymeric matrix produced a granular structure with some honeycomb features. Overall, the structure is not very regular and this was attributed to uneven current distribution in the pores during electroplating. SEM images taken at higher magnification showed Ni globules of 10-20 μm diameter interconnected by smaller granules of 1-5 μm. This reflects the matrix-metal deposit relationship.

A development of the previous study [30] was aimed at the production of porous Ni coatings onto Ni or stainless steel electrodes. A Ni cathode (together with a Ni anode) is immersed into the precursor emulsion and finally entrapped in the PHP body after polymerization. The Ni-cathode/PHP/Ni-anode composite cell is then used in a Ni electroplating bath, and Ni is deposited through the polymer pores onto the cathode. Burnout of the polymer matrix produced a coating on the cathode represented by a cauliflower structure organized in near spherical interconnect aggregates of 50-150 μm diameter, which consists of smaller spherical deposits. Variation of the electroplating time and current density showed that the structure of the Ni coating is determined by the local distortions of the electric field inside the tortuous microporous body of the insulating polymer.

With the aim of increasing the adsorption capability of PolyHIPEs towards aqueous body fluids researchers of Dow Chemical [31] copolymerized vinyl monomers (EHA, S, DVB) with chemically modified surfactants in which a vinyl moiety was introduced to make them prone to polymerization. The surfactant were either ionic, bearing an ammonium functionality capped with a vinylbenzyl group or non ionic (polybutylenoxide-polyethylenoxide-polybutylenoxide triblock copolymer) capped with an acrylate or methacrylate group. The combination of elastomeric properties due to the employment of the rubbery monomer EHA and of the hydrophilic character due to the surfactant chain bound to the matrix allows the adsorption of relatively large quantities of water.

The preparation, properties and performance of a novel membrane system based on PolyHIPE were described by Bhumgara *et al.* [32, 33] It was shown that a skin/core structure (asymmetric membrane) could be achieved in these polymeric foams through the epitaxial polymerization at the interface with a suitable substrate. The porosity of the skin is controlled by the difference ($\Delta\delta = \delta_s - \delta_m$) between the solubility parameters of the substrate (δ_s) and the

monomer (δ_m) which constitutes the continuous phase of a high internal phase emulsion. The porosity of the skin layer decreases with decreasing $\Delta\delta$. If $\Delta\delta$ is positive and high, the surface porosity is identical to the bulk porosity. The thickness of the skin layer is equal to the wall thickness of the porous polymer which can be controlled through the processing or phase volume of the emulsion. A number of self-supported porous channel (SPC) filtration modules were prepared and used in the cross flow filtration of calcium carbonate (aragonite) and surfactant suspension. Effects of membrane skin porosity and surface modification on the filtration characteristics of SPC modules were evaluated. The solute deposition mechanism during aragonite suspension filtration were deduced.

In the patent *WO 0238657 A2* [34] fibers were included in PolyHIPE foams with the aim of increasing their strength and to confer them specific abilities such as the capability of retaining malodors from air. This goal was reached by the inclusion of carbon fiber possessing very high surface areas.

Another application disclosed in [35] regards PolyHIPE foams suitable in adsorbing and storing body fluids, even when opposed to by significant hydrostatic pressures.

Bibliography

1 N.R. Cameron, D.C. Sherrington, *Adv. Polym. Sci.*, 1996, **126**, 163.

2 N.R. Cameron, D.C. Sherrington, L. Albiston, D.P. Gregory, *Colloid Polym. Sci.*, 1996, **274**, 592.

3 R. Butler, C.M. Davies, A.I. Cooper, *Adv. Mater.*, 2001, **13**,1459.

4 M.A. Hoisington, J.R. Duke, P.G. Apen, *Polymer*, 1997, **38**, 3347.

5 J.R. Duke, M.A. Hoisington, D.A. Langlois, B.C. Benicewicz, *Polymer*, 1998, **18**, 4369.

6 H. Tai, A. Sergienko, M.S. Silverstein, *Polymer*, 2001, **42**, 4473.

7 N.R. Cameron, D.C. Sherrington, *J. Mater. Chem.*, 1997, **11**, 2209.

8 N.R. Cameron, D.C. Sherrington, *Macromolecules*, 1997, **30**, 5860.

9 N. Miele-Paiot, L.G. Hubert-Pfalzgraf, R. Papiernik, J. Vaissermann, R. Collier, *J. Mater. Chem.*, 1999, **9**, 3027.

10 H. Tai, A. Sergienko, M.S. Silverstein. *Polym. Eng. Sci.*, 2001, **41**, 1540.

11 A. Sergienko H. Tai, , M. Narkis, M.S. Silverstein. *J. Appl. Polym, Sci.*, 2002, **84**, 2018.

12 D.C. Sherrington, *Chem. Commun.*, 1998, 2275.

13 F. Svec, J.M.J Frechet, *Science*, 1996, **273**, 205.

14 N.R. Cameron, D.C. Sherrington, I. Ando, H. Kurosu, *J. Mater. Chem.*, 1996, **6**, 719.

15 A. Mercier, H. Deleuze, O. Mondain-Monval, *React. & Funct. Polym.*, 2000, **46**, 67.

16 A. Mercier, H. Deleuze, O. Mondain-Monval, *Macromol. Chem. Phys.*, 2001, **202**, 2672.

17 A. Mercier, H. Deleuze, B. Maillard, O. Mondain-Monval, *Adv. Synth. Catal.*, 2002, **344**, 33.

18 A. Chemim, A. Mercier, H. Deleuze, B. Maillard, O. Mondain-Monval, *J. Chem. Soc., Perkin Trans.* 1, 2001, 366.

19 P. Krajnc, J.F. Brown, N.R. Cameron. *Org. Lett.*, 2002, **4**, 2497.

20 M. Ottens, G. Leene, A.A.C.M. Beenackers, N. Cameron, D.C. Sherrington, *Ind. Eng. Chem. Res.*, 2000, **39**, 259.

21 B.C. Benicewicz, G.D. Jarvinen, D.J. Kathios, B.S. Jorgensen, *J. Radioanalyt. Nucl. Chem.*, 1998, **235**, 31.

22 S.D. Alexandrotos, R. Beauvais, J.R. Duke, B.S. Jorgensen, *J. Applied Polym. Sci.*, 1998, **68**, 1911.

[23] K. Allmer, E. Berggren, E. Ericson, A. Larsson, I. Porrvik, *WO 97/19347* (1997).

[24] R.J. Wakeman, Z.G. Bhumgara, G. Akay, *Chem. Engineer. J.*, 1998, **70**, 133.

[25] H. Li, J.R. Benson, N. Kitagawa, *US576097* (1998).

[26] N. Kitagawa, *US6048908A* (2000).

[27] G. Akay, S. Downes, V.J. Price, *WO 00/34454* (2000).

[28] W. Busby, N.R. Cameron, C.A.B. Jahoda, *Biomacromolecules*, 2001, **2**, 154.

[29] Sotiropoulos, I.J. Brown, G. Akay, E. Lester, *Materials Letters*, 1998, **35**, 383.

[30] .J. Brown, D. Cliff, S. Sotiropoulos, *Mater. Res. Bull.*, 1999, **34**, 1055.

[31] S. Mork, G. Rose, *WO 97/18246* (1996).

[32] Z. Bhumgara, *Filtration and Separation*, 1995, 245.

[33] G. Akay, Z. Bhumgara, R.J. Wakeman, *Trans IchemE*, 1995, **73**, 782.

[34] J.C. Dyer, M.E. Tremblay, R.J. McChain, E.C. Smith, T.A. Desmarias, *WO 02/38657 A2* (2001).

[35] T.A. Desmarais, *WO 99/47183* (1999).

PREPARATION AND CHARACTERIZATION OF POLY(DVB) PolyHIPE FOAMS.

Chapter III

3 PREPARATION AND CHARACTERIZATION OF POLY(DVB) PolyHIPE FOAMS.

3.1 Introduction

Many application of porous materials, such as reverse-phase HPLC and solid-phase extraction, require high surface areas. Moderately porous monolithic polymers with sufficient surface areas for such applications have been prepared and described extensively by Svec, Frechet and coworkers [1]. PHPs have significantly higher porosity but tend to posses low surface areas (around 5 $m^2 \cdot g^{-1}$) due to their relatively large cell size (5-100 μm), which has hampered their performance in such applications. Hainey et al. [2] reported that the surface area of PHPs could be increased up to 350 $m^2 \cdot g^{-1}$ by a combination of three factors: an inert diluent (porogen) added to the monomer phase; a high crosslinker level; and a high surfactant concentration (33 wt% relative to total organic phase). The highest surface areas were obtained when a solvating porogen, such as toluene, was used in conjuction with a crosslinker level of 80%.

As part of our work on the preparation of novel PHPs for materials applications, we required materials of high surface area together with sufficient mechanical strength to allow their use in applications involving, for example, the flow of liquids. An initial investigation of the materials described by Hainey *et al.* indicated that their mechanical properties were insufficient for our needs, and were only improved at the expense of surface area when the surfactant level was dropped. For this reason, we decided to investigate fully the influence of the porogen type on the porous characteristics, morphology and mechanical properties (in a qualitative sense) of the resultant PolyHIPE foams.

3.2 Experimental Section

3.2.1 Materials

Divinylbenzene (Aldrich; 80% vol. *m*- (55 vol.%) and *p*-divinylbenzene (25 vol%), the remainder being *m*- and *p*-ethylstyrene) was purified by passing through a column of basic alumina (Brockmann I) to remove the inhibitor (p-*tert*-butylcatechol). Toluene (T), chlorobenzene (CB), (2-chloroethyl)benzene (CEB), 1,2-dichlorobenzene (C_2B), 1-chloro-3-phenylpropane (CPP) (Aldrich), potassium persulfate (Aldrich) and calcium chloride dihydrate (Avocado) were used as supplied. The surfactants used (all supplied from Aldrich), are listed in Fig. 3.1.

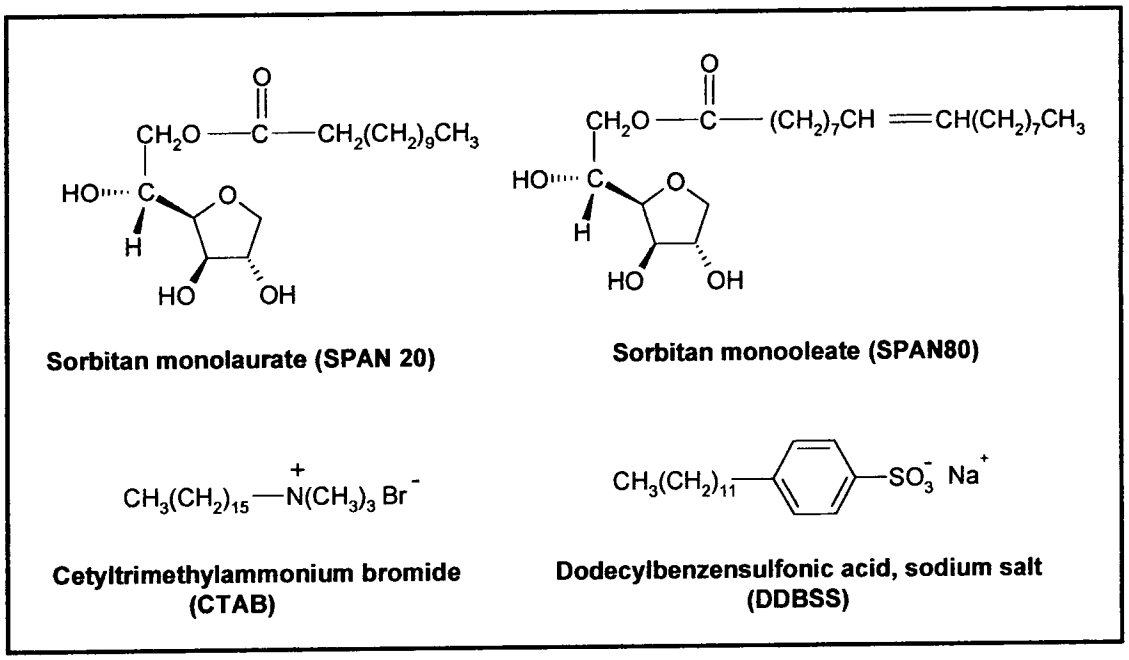

Fig. 3.1. Structures of the surfactants used.

3.2.2 PolyHIPE Preparation

The foams prepared were nominally 75, 85, 90 and 92% porous, based on aqueous phase content.

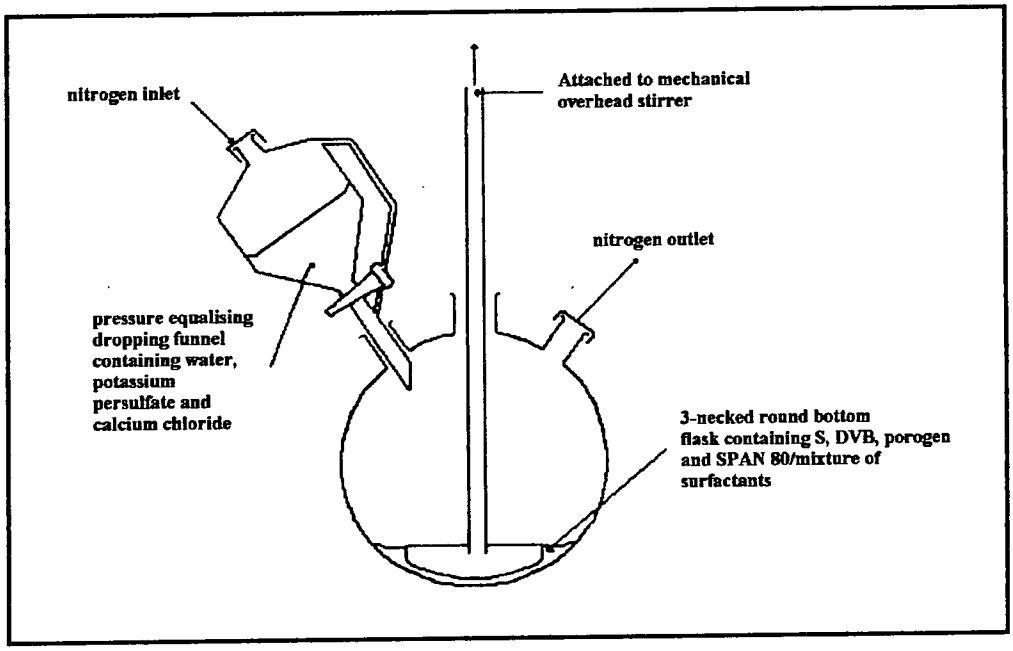

Fig. 3.2. Equipment for foam synthesis.

The emulsions were obtained by adding dropwise an aqueous solution of $CaCl_2$ (1.11% wt.) and potassium persulfate (0.22% wt.) to the organic phase, made of DVB 80% and either SPAN 80 (20% vol. relative to total monomer plus porogen volume) or a mixture of SPAN20,

DDBSS and CTBA (6.3, 0.4 and 0.3% wt., respectively, relative to total monomer plus porogen weight), under stirring (Fig 3.2).

The polymerization was carried out at 60°C in an oven for 48 h. The foams were extracted with water then isopropanol for 24 h each in a Soxhlet apparatus. Foams were dried under vacuum at 50°C.

3.2.3 PolyHIPE Coding System

The PolyHIPE materials are classified by a code which is dependent on the monomers and crosslinker used to prepare the polymer, its crosslink density and pore volume.

The codes for the basic poly(styrene-DVB) systems have the general form *XaPVb(zPor)Surf*, where *X* is the nominal crosslink density which corresponds to the actual concentration of DVB contained in the commercial products used (55 or 80%), *PV* is the pore volume as percentages, *Por* indicates the porogen which is present in the organic phase of the emulsion whose concentration is referred to the volume of the monomer plus crosslinker (*z*) and *Surf* is the surfactant employed in emulsion preparation. Thus X20PV90(1T)S80 would represent a poly(styrene-DVB) PolyHIPE material of approximately 20% crosslinker content, 90% pore volume, containing toluene as the porogen (1:1 vol:vol, monomer plus crosslinker to porogen) and prepared using SPAN80 as the surfactant. The mixture of surfactants will be designed S20AD, where S20 represents SPAN 20, A stands for Adogen which is the commercial name for cetyltrimethylamonium bromide and D is the initial of dodecylbenzensulfonic acid, sodium salt.

3.2.4 Bulk Polymerization

The polymerization of DVB 80% was carried out in the presence of toluene, chlorobenzene, 1,2-dichlorobenzene, (2-chloroethyl)benzene and 1-chloro-3-phenylpropane respectively, as diluents (monomer:porogen, 1:1 (v:v)). The polymerization reactions were carried out at 60 °C in 30 ml glass vials in a temperature-controlled oil bath for 24 h. AIBN was used as initiator (1 % wt. relative to DVB 80%). The prepared bulk samples were crushed into powders and washed in a Soxhlet apparatus for 24 h each with THF and acetone. The polymers were dried in a vacuum oven for 48 h at 50°C. The samples were analyzed by mercury intrusion and N_2 adsorption porosimetry and SEM.

3.2.5 Surface Area/Pore Size Distribution

Nitrogen adsorption/desorption measurements were performed at 77.3 K on a

Micromeritics TriStar 3000 model. Samples were degassed at 100°C overnight under vacuum prior to data collection. Surface area measurements utilized a nine points adsorption isotherm collected over 0.05 to 0.20 P/P_0 and analyzed via the BET method [3]. For each sample a minimum of six determinations were carried out and results are expressed as averages with the associated standard deviations. The average pore size distributions utilized a 53-point adsorption isotherm and were analyzed via the BJH method in accordance to British Standards Institution [4]. Micropore volumes and areas were evaluated with the t-Plot method.

3.2.6 Mercury Porosimetry

Mercury porosimetry analysis was performed by using a Micromeritics AutoPore III 9420. Samples were outgassed under vacuum at room temperature for 30 min. before intrusion. Intrusion and extrusion mercury contact angles of 130° were used; measurements were conducted according to the set-time equilibration mode.

Penetrometers with a stem volume of 1.1310 ml were used. The intrusion volume was always comprised between 50 ÷ 85 % of the stem volume. Intrusion pressures never exceeded 200 psi in order to avoid any specimen compression.

3.2.7 Electron microscopy

A Hitachi S2400 electron microscope operating at 25 kV was used for studies of the morphology of the samples. Prior to analysis, specimens were sputter coated with a thin layer of gold to enhance conductivity.

Samples for TEM were fixed in 1% aqueous OsO_4 solution and dehydrated in a graded series of alcohols, then embedded in Emix (medium) Resin TO28 (TAAB Laboratories Equipment Ltd.). Curing of the resin was carried out for 36 h. at 60 °C. Ultrathin sections (90 nm) of the resulting composite were cut using a Diatome 45 diamond knife (TAAB Laboratories Equipment Ltd.) on a Ventana (RMC) MT-XL Ultramicrotome (Ventana Medical System Inc.). The sections were mounted on uncoated 400 mesh copper Gilder grids G400, of 3.05 mm diameter. The grids were examined using a Philips CM100 (compustage) Transmission Electron Microscope (TEM) operated at 100 kV. Micrographs were recorded at magnifications of 380, 4600 and 10500 ×. Micrographs taken at 380 × were used for the evaluation of the average cavity and interconnecting window diameters. Such a measurements were carried out with a ruler and making reference to the scale bar on a significant number of cavities (typically, at least one hundred) in order to give statistical relevance to the figures produced. Speciments preparation and TEM observations were carried at Electron

Microscopy Unit at the medical School of the University of Newcastle.

3.2.8 Solid-state ^{13}C NMR

Solid-state ^{13}C NMR were recorded on a Varian Unity Inova spectrometer with a 7 mm rotor (Doty Scientific MAS probe). The spectra were obtained using a direct polarisation experiment with proton decoupling during acquisition at a frequency for ^{13}C of 75.43 MHz. A 90° excitation pulse (duration 5 μm) was used with a 30 s recycle delay, at a spin-rate of 7800 Hz. 2200 repetitions were accumulated. The acquisition time was 15ms. Spectral referencing was respect to an external sample of $(CH_3)_4Si$. Data were supplied by the solid state NMR service within the Department of Chemistry of the University of Durham.

3.2.9 Determination of the diffusion coefficient of water in emulsions using ^1H NMR

The self diffusion of water was measured using a 500-MHz Varian Unity Inova 500 narrow bore spectrometer equipped with a Performa II gradient pulse amplifier and an actively shielded 5 mm indirect detection probe capable of producing up to 30 G cm^{-1} z field gradient pulses. Automated z gradient shimming based on deuterium spin echoes was used. The temperature for all measurements was 25 ± 0.1 °C. Water diffusion coefficient were measured using a pulse sequence incorporating pulsed-field gradients such as the *b*ipolar *p*ulse *p*air *s*timulated *e*cho (BPPSTE) pulse sequence. Diffusion coefficients are obtained from BPPSTE spectra by monitoring signal attenuation as a function of the applied magnetic field gradient amplitude and fitting Eq. 1 to the experimental results

$$I = I_0 \exp\left[-D(\gamma\delta G)^2(\Delta - \delta/2 - \tau/3)\right] \quad (1)$$

where I is the resonance intensity measured for a given gradient amplitude, G, I_0 is the intensity in the absence of the gradient pulse, γ is the gyromagnetic ratio, δ is the duration of the bipolar gradient pulse pair, Δ is the diffusion delay time, and τ is a short gradient recovery delay time during which relaxation and spin-spin coupling evolution are not significant. Data were supplied by the solution state NMR service within the Department of Chemistry of the University of Durham.

3.2.10 Surface pressure-area (π-A) curves

Surface pressure *vs.* molecular area were obtained using a Langmuir film balance supplied by NIMA Technologies. Measurements were carried out as follows: 30 ml of a Span 80 solution

(2.33×10^{-3} mol·dm^{-3}) either alone or including porogen (1.17×10^{-2} mol·dm^{-3}) in chloroform was spread on an aqueous solution containing 6.1×10^{-2} mol·dm^{-3} of $CaCl_2 \cdot 2H_2O$. Surface pressure was recorded immediately after the deposition of the organic solution as the porogens show some tendency to dissolve in the aqueous phase. Barrier closing speed was adjusted to 200 cm^2·min^{-1} to minimise the dissolution of porogen in the water phase during measurements.

3.3 Results and Discussion

3.3.1 Foams obtained by using SPAN 80

The surfactant most commonly employed in the production of W/O HIPEs is sorbitan monoleate (SPAN 80, HLB = 4.6), which is insoluble in water (low HLB value surfactants are hydrophobic) so, it was natural to use this surfactant in the production of our foams.

The HIPEs were prepared with 20% (v/v) surfactant concentration relative to the continuous phase (minus surfactant), using procedures described in the experimental section (§ 3.2.2). No difficulties were encountered, and all HIPEs were stable up to the point of gelation. Therefore, the changes in structure discussed in the forthcoming section are not due to emulsion breakdown. A difference in viscosity was noted between emulsions containing T, CB and C_2B and those containing CEB and CPP as a porogens. The former were viscous fluids, the latter had the consistency of toothpaste and as a result flowed only slightly under gravity stress. As the morphology of the materials is quite complex, it is worthwile at this point to define some of the terminology that will be used in the subsequent discussion. The foams are open-cell, therefore the large (on the order of microns) spherical cavities in the materials (see Fig. 3.3) are termed cells. The circular holes connecting adjacent cells are referred to as windows. Finally, the use of inert porogens in the monomer phase results in the formation of pores within the polymer phase. These may be micro-, meso- or macropores, according to their size as defined by IUPAC [5].

3.3.2 Single component porogenic solvent

Examination of SEMs at low magnification (Fig. 3.3) indicates an influence of the porogen type on the foam morphology on a large scale. Changing from T (Fig. 3.3a) to CB (Fig. 3.3b) causes a marked decrease in cell diameter. It is well known that droplet size decreases with increasing emulsion stability since the surface energy per unit area is lower. A decrease in emulsion droplet size leads to a decrease in PolyHIPE cell size since the foam is

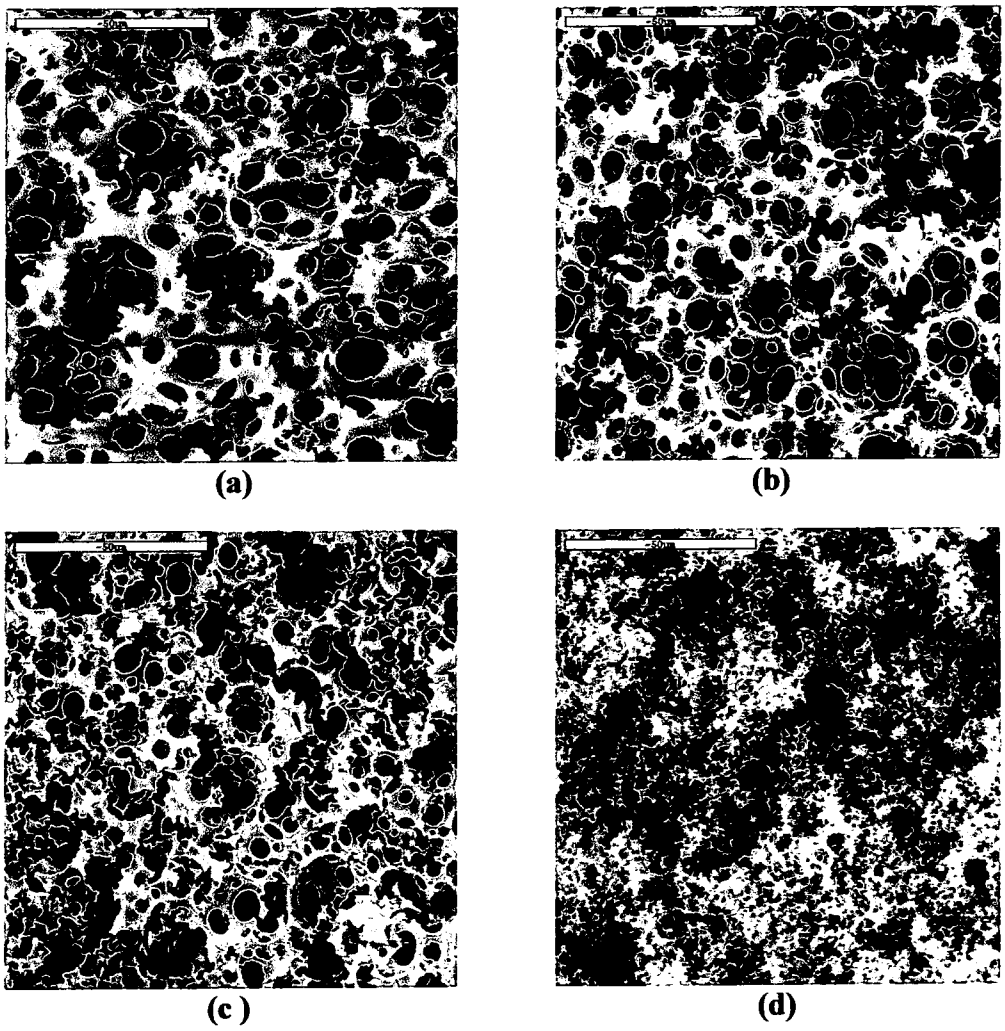

Fig. 3.3. SEMs of PHPs prepared with porogens: (a) T; (b) CB; (c) C_2B; (d) CEB.

effectively a replica of the emulsion structure immediately prior to gel formation. Futher evidence to support this general hypothesis is provided in Fig. 3.4, which shows the results of spreading and compressing solutions that mimic the HIPE continuous phases employed in this work. Again, this clearly demonstrates that the adsorption of solvent with SPAN 80 at the interface increases as the solvent is varied from T to CB to C_2B to CEB (CEB and CPP π-A curves coincide) and implies a decrease in interfacial tension. The data also correlates well with the difference in cell size between foams prepared with T and CB. It is worth pointing out that these π-A curves were all reproducible (six times), and that steps were taken to prevent dissolution of the solvents in the aqueous phase (see experimental § 3.2.9). We believe this has been successful, since the curve of C_2B is shifted to the right of CB, despite the former being less hydrophobic and therefore more likely to be removed from the monolayer by dissolution. Furthermore, the curve for CB is shifted to the right of T. Similarly, with the possible exception of T, we would anticipate that minimal evaporation of each

solvent would occur over the short timescale of each experiment. Fig. 3.3d provides futher information on the influence of porogen on foam morphology, and suggests that the characteristic open-cellular PolyHIPE structure is absent when the porogens are CEB and CPP. The morphology of this material resembles more closely that of monoliths prepared by Svec and Frechet [1], albeit with higher porosity. It is conceivable that the HIPE has collapsed prior to polymer gelation, resulting in a non-cellular structure, however no evidence of

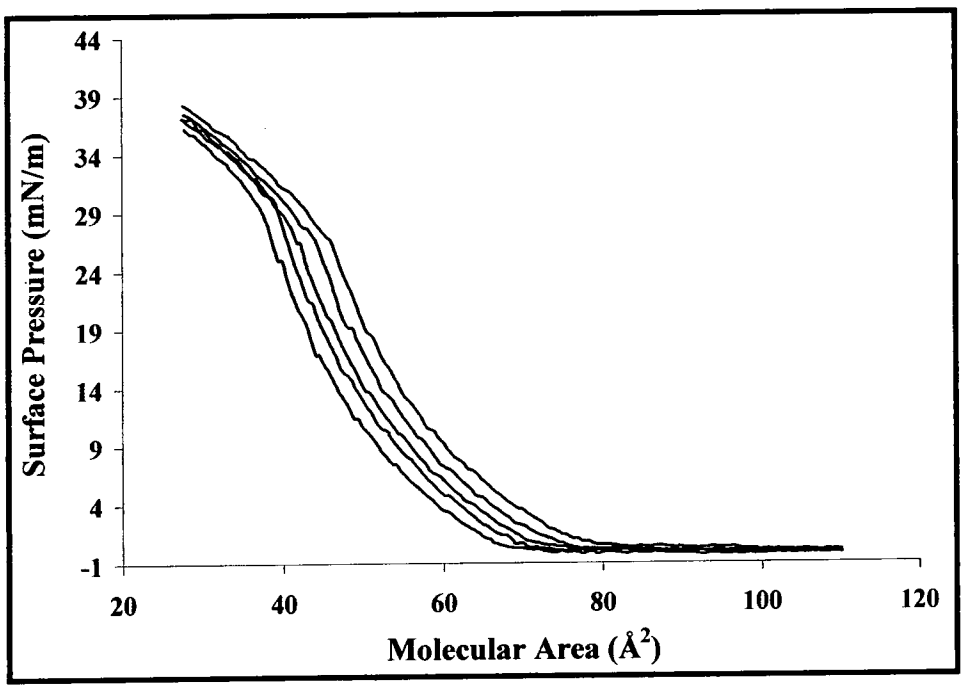

Fig. 3.4. π-A curves of films containing (from left to right) SPAN 80 alone (17 mol% relative to total oil phase) plus T, CB, C_2B and CEB (≡ CPP).

emulsion breakdown such as separated aqueous phase was observed. On the contrary, the trough evidence (Fig. 3.4) seems to suggest the opposite, that CEB and CPP increases emulsion stability (more condensed interfacial layer). We wondered whether this morphology transition could be due to an influence of the porogen on the size of the windows connecting adjacent cells, in addition to an influence on cell size. If the window diameter increased to a sufficient high extent, only polymer struts would remain giving the impression of a loss of cellular structure. This hypothesis is supported also by Fig. 3.3c, referring to a PHP prepared by including C_2B in the organic phase. Its morphology represents a transition between those of X80PV90(1CB)S80 and X80PV90(1CEB)S80. The typical PolyHIPE open cellular morphology is still evident but the walls have lost some of their structural integrity resulting in the appearance of some strut structure.

Williams and coworkers [6] observed a loss of cellular structure at very high surfactant levels (75% relative to total oil phase including surfactant) for poly(S-DVB) PHPs, although this was not rationalised fully. Also reported in that work, and separately by workers at Unilever [7], was an increase in window size as the concentration of electrolyte in the aqueous phase was increased. Both these observations imply that window size increases as the interfacial tension decreases. The explanation is that as the interfacial tension decreases, the films separating adjacent emulsion droplets become thinner. Previously, using cryo-SEM experiments [8] it was shown that the point at which the windows appear coincides with the polymerisation gel point, implying that shrinkage due to the conversion of monomer to higher density polymer is the probable cause of window formation. Thinner film undergoing shrinkage would result in a larger window, and one can imagine that if the windows were very large the cellular structure would not be obvious. The lowering of interfacial tension inferred from the π-A curves shown in Fig. 3.4 is indeed greatest with the solvent CEB and CPP, which seems to support our hypothesis. Further evidence is provided by TEM at low

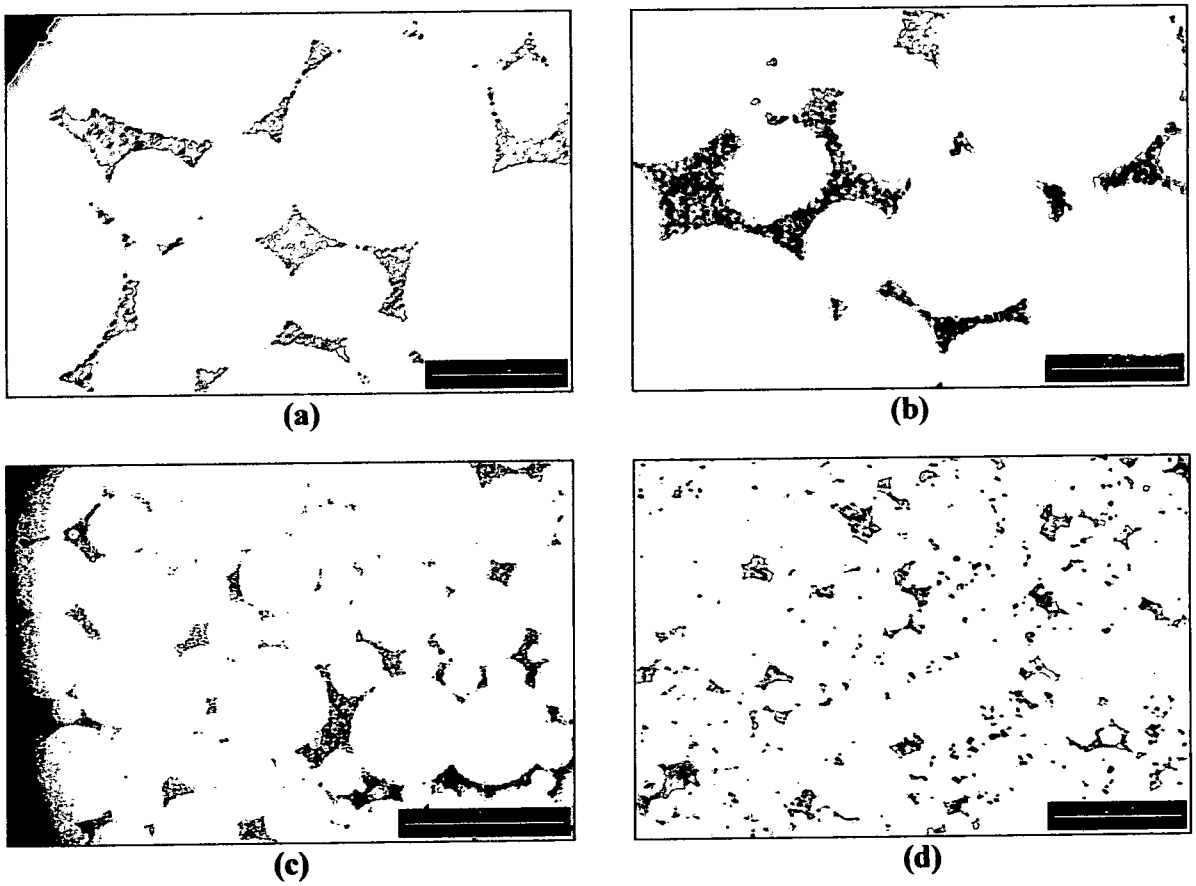

Figure 3.5. Transmission electron micrographs of PolyHIPE materials, scale bar 10 or 20 μm: (a) X80PV90(1T)S80; (b) X80PV90(1CB)S80; (c) X80PV90(1C$_2$B)S80; (d) X80PV90(1CEB)S80.

magnification of the foams prepared with C_2B, CEB and CPP (Fig. 3.5c and d), which indicates that the cellular morphology has indeed been retained, and that the original spherical droplets merge to a greater extent when the solvent is C_2B, CEB or CPP.

This TEM shows much more clearly the retention of the cellular structure than the corresponding SEM (Fig. 3.3d), and proves that the HIPE has been stable up to the gel-point. Therefore, these data seem to confirm the suggestion that the apparent loss of cellular structure is due to extremely large interconnecting holes appearing due to excessive thinning of surfactant films between adjacent emulsion droplets, as a result of a progressive lowering of interfacial tension as the solvent become a better cosurfactant. The high levels of surfactant required by Williams *et al.* [6] to achieve a similar effect rules out the possibility that the results here reported are due to small changes in SPAN 80 concentration due to experimental technique.

TEM micrographs taken at a low magnification (× 380) are useful in providing quantitative information regarding the average dimension of cavities (*D*) and interconnecting windows (*d*). In Table 3.I these data are reported together with the values of their ratio (*d/D*). By changing the porogen from T to CB, *D* decreases by about 15 %, while *d* increases by 10%. When C_2B replaces CB, *D* and *d* decreases by about 25% and 9%, respectively. The value of the *d/D* ratio increases constantly along the first three foams listed in Table 3.I indicating that cavities tend to overlap to a larger and larger extent. It was not possible to evaluate *D* and *d* for foams prepared with CEB and CPP porogens because of the extensive overlapping (Fig. 3.5d)

Table 3.I. Characterisation of PolyHIPE foams.

	SAMPLE	*D* (μm) [1]	*d* (μm) [2]	*d/D*	Sample characteristics
	SINGLE POROGEN				
1	**X80PV90(1T)S80**	10.0	3.5	0.35	chalky; moderately tough
2	**X80PV90(1CB)S80**	8.5	3.9	0.46	chalky; moderately tough
3	**X80PV90(1C_2B)S80**	6.4	3.2	0.50	chalky; less tough than entry 2
4	**X80PV90(1CEB)S80**		not determinable		crumbles easily into fine powder
5	**X80PV90(1CPP)S80**		not determinable		crumbles easily into fine powder
	MIXED POROGEN				
6	**X80PV90(0.5CB+0.5CEB)S80**	6.4	3.0	0.47	chalky; moderately tough
7	**X80PV90(0.5CB+0.5CPP)S80**	6.5	3.0	0.45	chalky; moderately tough
8	**X80PV90(0.5T+0.5CEB)S80**	5.0	2.6	0.51	chalky; moderately tough
9	**X80PV90(0.5T+0.5CPP)S80**	5.2	2.7	0.53	chalky; moderately tough

[1] average cavity diameter

[2] average interconnecting window diameter

among cavities which rendered difficult reliable measurements. These data offer further support to the hypothesis outlined above, regarding the progressive thinning of the film of the continuous phase surrounding the droplets when the porogen is changed from T to CB, C_2B and, presumably, CEB and CPP.

In Table 3.I is also given a qualitative assessment of macroscopic foams visual and mechanical characteristics. All materials were chalky under shear stress. While the consistency of the first two foams was reasonably good to allow their manipulation without causing them any damage, foams prepared with CEB and CPP were very fragile and crumbled easily under the application of small compressions and this is clearly the result of poor wall connectivity as evident from SEM (Fig. 3.4c) and TEM (Fig 3.5c) micrographs. Mechanical characteristics of X80PV90(1C_2B)S80 were somewhat midway those of foams of entries 2 and 3 (Table 3.I).

The surface areas and porosity data (plus associated errors in their measurement) for the first five foams listed, are reported in Table 3.II. In Fig. 3.6a a representation of the N_2 sorption isotherm and hysteresis loop encountered with these foams is displayed. All foams exhibit a type II isotherm and type H3 hysteresis loop. Pore size distribution curves are shown in Fig. 3.6b. All distributions are quite broad, spanning a range in pore diameter of two orders of magnitude, and all exhibit a significant proportion of macropores (> 50 nm). Differences between foams prepared with T and CB consist mainly of the relative proportion of macro and mesopores (2-50 nm). The distribution of the former rises above that of CB in the lower side

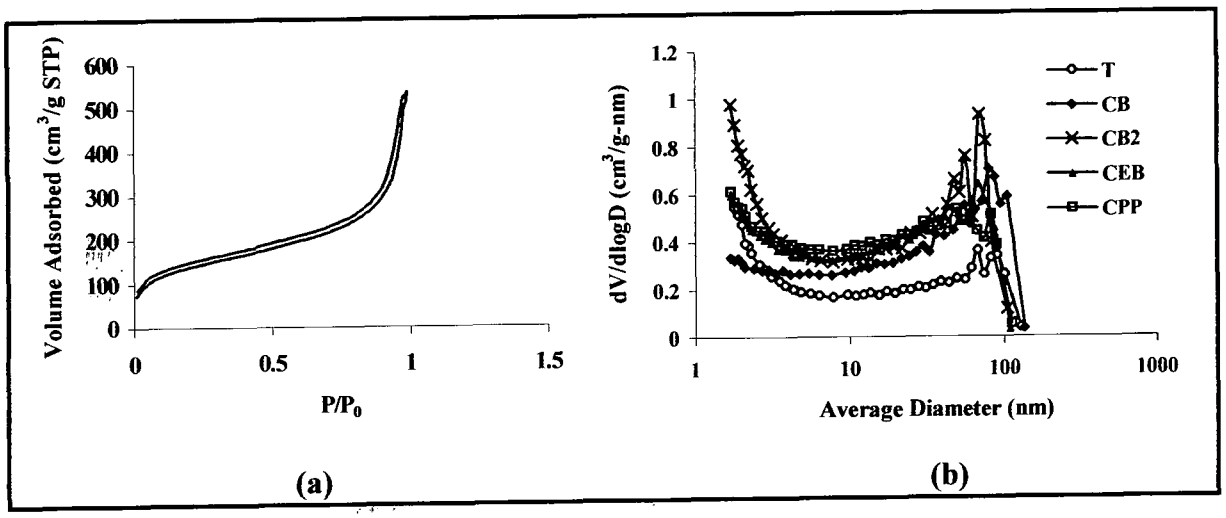

Fig. 3.6. (a) example of N_2 isotherm and hysteresis loop encountered with foams listed in Table 3.II and (b) pore size distributions (BJH) of X80PV90(1Por)S80 PolyHIPE foams calculated from the adsorption branch of the isotherms.

Table 3.II. Surface areas, cumulative pore volume, average pore diameter, micropore volume, micropore areas of DVB 80% PolyHIPE foams. Porogens used: T, CB, CEB, CPP and 1:1 vol:vol of CB/CEB, CB/CPP, T/CEB and T/CPP. Surfactant employed: SPAN 80. Polymerization temperature: 60 °C. Data obtained by nitrogen adsorption.

	SAMPLE	Surface Area (m^2/g)[a]	Pore Volume (cm^3/g)[b]	Average Pore Diameter (nm)[c]	Micropore Volume (cm^3/g)[d]	Micropore Area (cm^2/g)[d]
1	**X80PV90(1T)S80**	359 ± 10	0.44 ± 0.02	6.4 ± 0.1	0.022 ± 0.001	59 ± 3
2	**X80PV90(1CB)S80**	346 ± 46	0.68 ± 0.05	8.4 ± 0.6	0	0
3	**X80PV90(1C_2B)S80**	499 ± 18	0.85 ± 0.02	6.7 ± 0.2	0.019 ± 0.003	59 ± 7
4	**X80PV90(1CEB)S80**	432 ± 19	0.72 ± 0.04	7.0 ± 0.3	0	0
5	**X80PV90(1CPP)S80**	435 ± 20	0.74 ± 0.04	7.0 ± 0.2	0	0
6	**X80PV90(0.5CB+0.5CEB)S80**	579 ± 5	0.88 ± 0.01	5.85 ± 0.08	0.026 ± 0.001	75 ± 2
7	**X80PV90(0.5CB+0.5CPP)S80**	161 ± 7	0.52 ± 0.01	12.0 ± 0.1	0	0
8	**X80PV90(0.5T+0.5CEB)S80**	248 ± 34	0.60 ± 0.01	9.6 ± 0.9	0	0
9	**X80PV90(0.5T+0.5CPP)S80**	429 ± 32	0.74 ± 0.02	0.74 ± 0.01	0	0

[a] from BET; [b] from BJH adsorption;

[c] from BJH adsorption

[d] from t-Plot

of the mesopore region and 17% of its surface area is due to the presence of micropores, while the latter is characterised by a higher amount of macropores and as a result possess a higher pore volume (Table 3.II). Foams prepared with CEB and CPP are each other superimposable and characterised by pore volumes similar to that of X80PV90(1CB)S80.

The pore size distribution of the foam prepared with C_2B, is characterized by a higher content of both macro and mesopores as compared to the previous foams and as a result its surface area and pore volume are the highest. The combination of a narrow hysteresis loop and broadpore size distributions is indicative of good pore connectivity [9].

This is further supported by TEM micrographs taken at higher magnifications (Fig. 3.7, right column).

The solubility parameters (δ) values of the five solvents are also given in Table 3.III. Comparison of the values with that of the polymer gives an idea of the extent of interaction between the two; the smaller the difference, the greater the interaction and so the better is that solvent at solvating the polymer chains. This is expressed quantitatively in eqns. (2) and (3), known as the Hildebrand solubility parameter approach:

$$\frac{\Delta H_m}{V} = (\delta_1 - \delta_2)^2 \phi_1 \phi_2 \tag{2}$$

$$\Delta G_m = \Delta H_m - T\Delta S_m \tag{3}$$

where ΔH_m, ΔG_m and ΔS_m are the enthalpy, free energy and entropy of mixing, respectively, V is the molar volume of the solvent, and δ and ϕ are the solubility parameter and volume fraction, respectively, of the solvent (1) and polymer (2). Thus, when δ_1 and δ_2 are similar, ΔH_m is small and ΔG_m is negative.

Polymer resins are generally divided into two classes; gel-type and macroporous [10]. The former are lightly crosslinked (<2%), are prepared without added diluents and have a porosity only in the swollen state, whereas the latter are more highly crosslinked (>5%), are prepared in the presence of porogenic solvents and possess permanent porosity in the dry state. The class of resins obtained is a function of several factors, including crosslinker content, nature and concentration of diluent and temperature. The morphology and surface area of macroporous resins is profoundly influenced by the nature of the porogen. If a thermodynamically good solvent is employed, phase separation of the polymer gel phase is delayed until late in the polymerisation. This produces a large number of small microparticles, which remain discrete until complete conversion since the residual monomer level is low, and results in a material of high surface area (if the polymer is sufficiently crosslinked).

Table 3.III. Solubility parameters of the solvents used as a porogens in the preparation of PolyHIPEs and in the bulk polymerization of DVB 80%.

Porogen	δ(MPa)$^{1/2}$	δ_d(MPa)$^{1/2}$	δ_p(MPa)$^{1/2}$	δ_h(MPa)$^{1/2}$	d_0
T[1]	18.2	18	1.4	2	8.3
CB[1]	19.4	19	4.3	2	6.5
C_2B[1]	20.5	19.2	6.3	3.3	5.6
CEB[2]	20.3	18	7.7	3.9	3.8
CPP[2]	20.0	18.1	6.8	3.5	4.3
T-CEB	19.4	18.0	4.8	3.0	5.4
T-CPP	19.2	18.1	4.5	2.9	5.7
CB-CEB	19.9	18.4	6.2	3.1	5.0
CB-CPP	19.8	18.5	5.8	2.9	5.4
PolyDVB(80%)[3]	20.5	17.5	7.5	7.6	

[1] J. Brandrup, E.H. Immergut, E.A. Grulke, *Polymer Handbook*, Wiley, New York, 1999.
[2]values calculated by the method of Hoftyzer-Van Krevelen and Hoy, and average taken (D.V. Kevrelan, *Properties of Polymers*, Elsevier, Amsterdam, 1991).
[3]values calculated by the method of Hoy.

A thermodynamically poor solvent, however, causes precipitation of polymer microparticles at an earlier stage when monomer levels are higher. The residual monomer will be partitioned between the porogen and polymer gel phases and cause "filling in" of the gaps between microparticles as it polymerises. The result is a lower surface area material. Poly(styrene-divinylbenzene) (PDVB) macroporous resins have been prepared using a wide range of porogens, including swelling and non-swelling solvents (as individual components or mixtures) [11-13] and linear polymers [14]. The value of solubility parameter (δ) for PSDVB quoted in the literature [15] is 18.6 (MPa)$^{1/2}$; comparison of this value with those in Table 3.III where the three dimensional solubility parameters for the various solvents are reported, indicates that there is not a good correlation between differences in δ and polymer surface areas. All solvents are very good solvents, their solubility parameters being between 18.2 and 20.5 (MPa)$^{1/2}$. According to the values of δ, T should be the best solvent and as a consequence when used in preparing foams produce materials with the highest surface area. Surface area results, on the contrary, indicate that the highest surface area is obtained in conjunction with C_2B whose solubility parameter (Table 3.III) is the most distant from that of PSDVB. In practice the level of crosslinker employed also influences the onset of phase separation and for some commercially produced S-DVB resins, the DVB level is adjusted upwards such that even with toluene, a thermodynamically good solvent for polystyrene as a porogen, phase separation occurs eventually, since pure poly(DVB) is less compatible with toluene than is

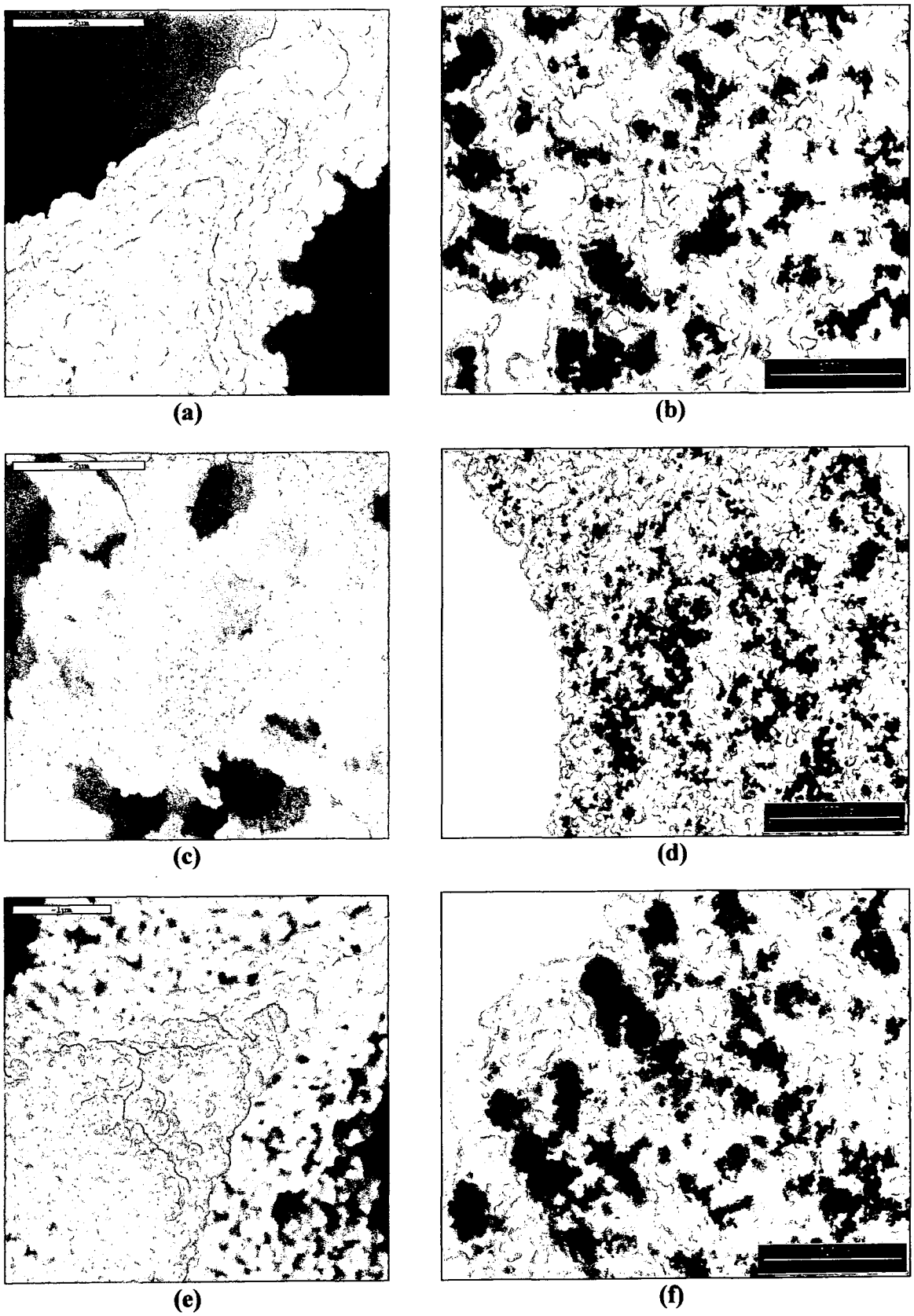

Fig. 3.7. SEMs (left column, scale bars = 2 and 1 μm) and TEMs (right column, scale bars = 1 and 0.8 μm) of PHPs prepared with porogens: (a) and (b)T; (c) and (d) CEB; (e) and (f) C_2B.

polystyrene itself. Thus, it is to be expected that the real value of δ for Poly(DVB 80%) to be higher than 18.6 $(MPa)^{1/2}$ quoted for polystyrene. This point will be further illustrated and commented in a later section of this chapter. The values of the three dimensional cohesion parameters and of its constituents, dispersive δ_d, dipolar δ_p and hydrogen bonding δ_h, interactions of T, CB and C_2B were taken from the literature [15], those of CEB and CPP were caculated by applying a group contribution method according to Hoftyzer-Van Krevelen and Hoy [16]. Both methods are of the same accuracy, and it has been suggested that these should be averaged [16]. As can be seen from the data reported in Table 3.III δ reaches its maximum value with C_2B. Furthermore, δ_p as well as δ_h increase steadily from T to CEB and CPP.

The increase in polarity and hydrogen bond forming ability maches well with the interfacial behaviour of the solutions containing these molecules as evidenced by π-A measurements. In the literature [17] it has been reported that aromatic molecules have the capability of penetrating the surfactant monolayer at the interface and that this property is enhanced by the polarity and hydrogen bond formation ability of these molecules [18].

Further evidence to suggest that C_2B and CEB are better porogens than T is provided by high magnification SEMs and TEMs of the various foams (Fig. 3.7). It can be seen quite clearly that the size of the microparticles comprising the foam decreases as the solvent is changed from T (Fig. 3.7a) to CEB (Fig. 3.7b) to C_2B (Fig. 3.7c) (there was not discernable difference in microparticle size between PHPs prepared with CEB and CPP). This indicates that C_2B and CEB are solvating the polymer network until late in the polymerisation, resulting in small microparticles. This trend is more evident from high magnification TEM pictures (Fig. 3.7. right column). The decrease in both microparticle size (dark regions) and interstitial voids (light/white regions) as the solvent is changed from T to C_2B (Fig. 3.7a and b) is indeed marked. These findings are in direct agreement with pore size distributions reported in Fig.3.6b.

One of our initial goals was to increase surface area without compromising mechanical stability. Table 3.I gives an indication of the mechanical stability of the various foams and, unfortunately, a few among those with the higher surface areas prepared with single porogens (CEB or CPP) are extremely fragile and so unlikely to be of much practical use. However, the foam pepared with C_2B has a surface area 30% higher than that prepared with T, together with similar handling properties. This is due mainly to the presence in the former of smaller polymer microparticles and, to a lesser extent, a smaller cell size.

3.3.3 Mixed porogenic solvents

The results from foams prepared with single porogens indicate that varying the solvent can increase the surface area, arguably as δ of the solvent approaches that of the polymer. However, there is also an influence of foam morphology on a larger scale; the cell size decreases and the relative window size increases. In two cases, this latter parameter increases to such an extent that the cellular morphology is apparently lost and poor mechanical properties result. We wondered if it could be possible to strike a balance between these factors

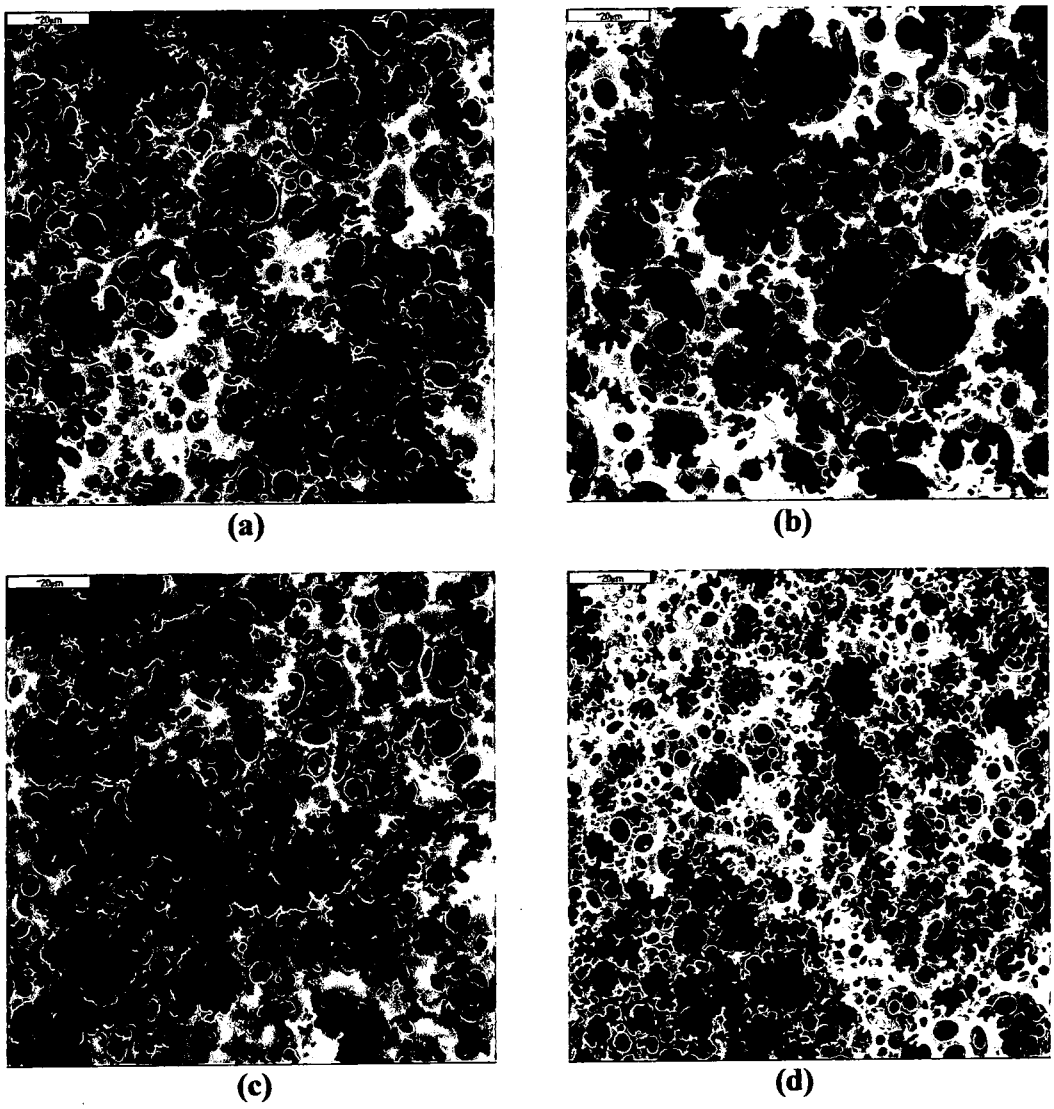

Fig. 3.8. SEMs of PHPs prepared with a 1:1 (volume ratio) mixture of porogens: (a) CB-CEB; (b) CB-CPP; (c) T-CEB; (d) T-CPP. Scale bar = 20 μm.

(porosity and cellular structure), by using mixed porogenic solvents to prepare PHPs. In particular, it was hoped that we could prepare foams of very high surface area but that retained a PolyHIPE morphology. SEMs at low magnification demonstrate clearly that each

foam prepared from mixed solvents has a recognisable PolyHIPE cellular structure (Fig. 3.8). This suggests that the mixed porogens have a different effect on HIPE interfacial behaviour than the single components. The π-A curves of films of the various mixed solvents, shown in Fig. 3.9, appear to confirm this. Curves for all mixed solvents are shifted to the right of the curve of SPAN 80 alone and are more or less coincident, indicating that each solvent pair produces a monolayer packed to a similar extent. In addition a comparison of Figs. 3.4 and 3.9 indicates that the mixed porogens do not have a great cosurfactant effect as CEB and CPP alone. This correlates well with the differences in morphologies of the various materials; CEB and CPP have the greatest influence on π and also produce the non-cellular morphology, whereas the mixed solvent have less of an influence on π and retain the PHP structure.

Further differences compared to foams prepared from single components can also be observed in Fig. 3.8. For example, there appears to be an influence on interconnects size, as shown by the presence of regions where the foam structure is more closed-cell (Fig. 3.8c). In addition, the cell size distribution is more polydisperse with mixed porogens. These observation are confirmed by the analysis of TEM micrographs taken at low magnification (Fig. 3.10a and c) of foams prepared with the mixture CB-CEB and T-CPP (similar considerations apply for foams prepared with CB-CPP and T-CEB mixture of porogens). The porogen mixture

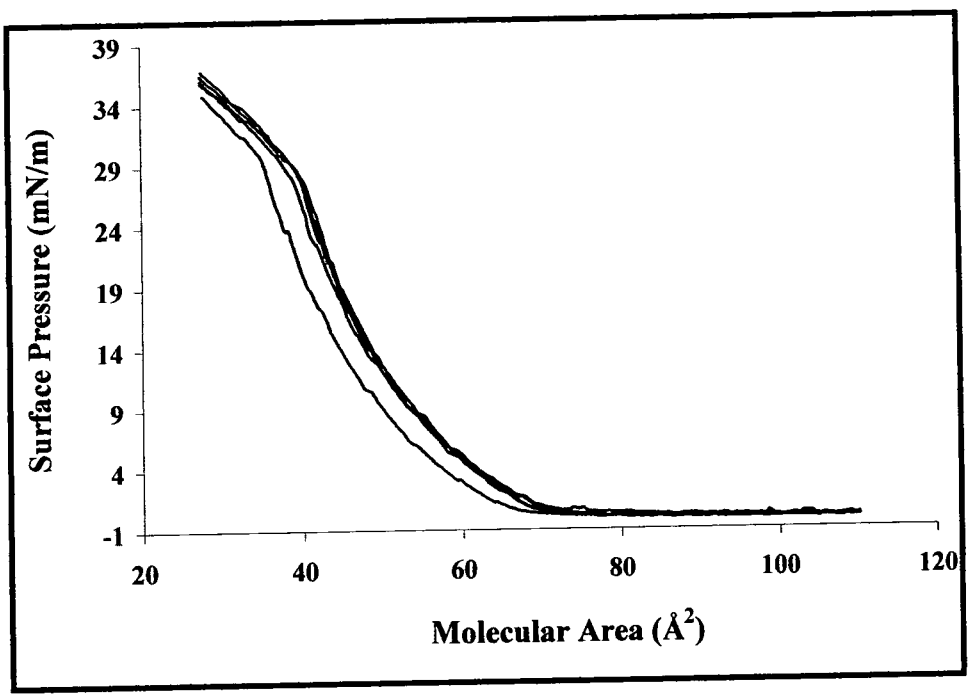

Fig. 3.9. π-A curves of films containing (from left to right) SPAN 80 alone (17 mol% relative to total oil phase) plus mixed porogens (50:50 volume ratio): T-CEB, T-CPP, CB-CEB and CB-CPP.

produce a foam with an higher average diameter (D) than the couple T-CPP (Table 3.I). The respective interconnecting windows average diameters (d), on the other hand, are very similar, independently of the mixture of porogens employed. A direct consequence of this imbalance between D and d is that the ratio d/D is higher for the latter foams. This implies that the film of continuous phase surrounding the droplets in the precursor emulsion is thinner when T is used in conjuction with CEB/CPP in the porogen mixture. TEM images (Fig. 3.10) confirm also the observation made by the examination of SEM micrographs (Fig. 3.8): the cavity size distributions for the foams prepared by using the porogen mixture CB-CEB/CPP tend to be more polydisperse than foams were T replaced CB as the co-porogen. These are all indications that HIPEs prepared with mixed porogens are less stable, *i.e.* the solvent mixtures do not lower the interfacial tension to the same extent as single solvents such as CEB and CPP. These conclusion are supported by surface pressure experiments (Fig. 3.9).

The influence of the cellular structure on foam mechanical properties is evident from Table 3.I, in a qualitative sense. All of the foam samples prepared with mixed porogens were much tougher and less brittle than those prepared with either CEB or CPP single solvents.

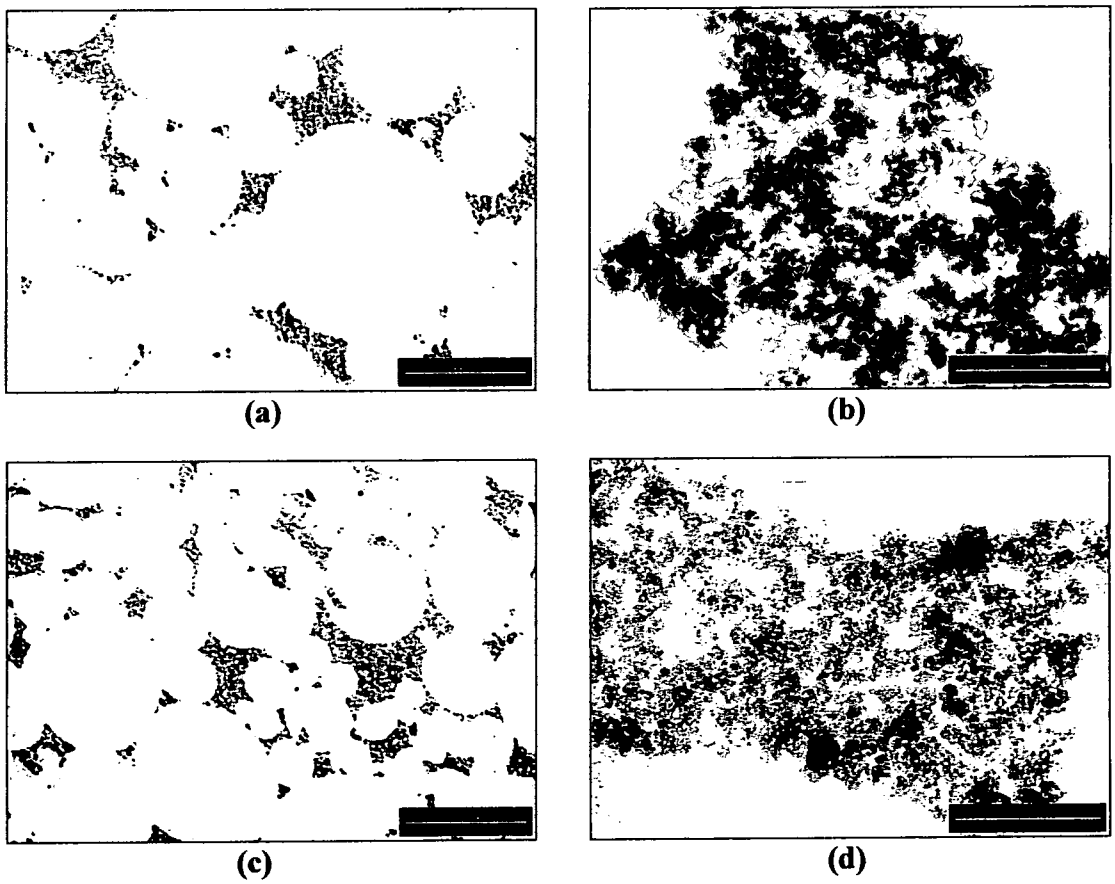

Fig. 3.10. TEMs of PHP at two magnifications prepared with (a, b) CB-CEB and (c, d) T-CEB (50:50 volume ratio) mixture of porogens. Scale bars: 10 and 1 μm.

We ascribe this to the retention of the PolyHIPE cellular morphology with these mixed porogns, which undoubtedly leads to materials with greater mechanical strength [19].

The surface area values of foams prepared from mixed porogens (Table 3.II) are also rather interesting: T with CEB produces a material whose surface area is below those of both the individual components; whereas T with CPP gives a surface area similar to CPP alone; CB with CEB results in a very high surface area, the highest one among foams prepared with

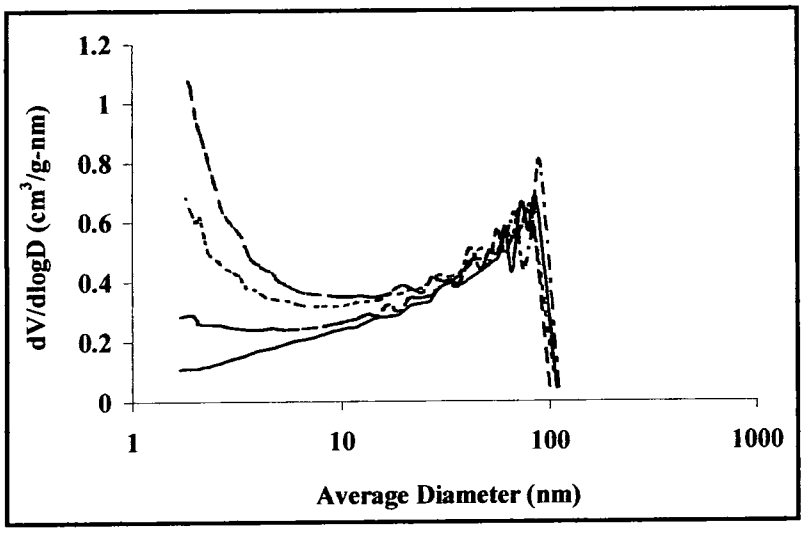

Fig. 3.11. N_2 BJH adsorption pore size distribution of PolyHIPE foams (PV 90) prepared using SPAN 80 as a 1:1 mixture of solvents as porogens. (----) 0.5CB+0.5CEB; (——) 0.5T+0.5CPP; (----) 0.5T+0.5CEB; (——) 0.5CB+0.5CPP.

SPAN80 as a surfactant; and CB with CPP leads to a value lower than that of either component. In Fig. 3.11 the pore size distributions of foams obtained by using the mixture of porogens are reported. It can be seen that all distributions are coincident in the macropore region but differ considerably in the mesopore one. Differences in surface areas and in the average pore diameters (Table 3.I) are a direct consequence of this feature. The distribution relative to X80PV90(0.5CB+0.5CEB)S80 is extending to some extent in the micropore region as evidenced by the contribution (13%) to its total surface area due to micropore (Table 3.II, entry 6).

The δ values of the mixed solvents (δ_{mix}) were calculated according to Eq. 4 [20],where x_i and V_i are the mole fraction and molar volume of component i, respectively; these are also reported in Table 3.III.

$$\delta_{mix} = \frac{x_1 V_1 \delta_1 + x_2 V_2 \delta_2}{x_1 V_1 + x_2 V_2} \qquad (4)$$

For entry 9, in Table 3.II, there is a good correlation between δ and the surface area obtained as both parameters lie between the values of the individual components. However, the surface areas of entries 6-8 do not relate simply to the calculated δ values of the mixed solvents. It would appear that in these cases either the solubility parameter of the mixture is not a simple function of the values of the individual components, or the surface area is influenced by some other unforeseen parameters. A further possibility is the presence of errors in the calculation of δ of CEB and CPP (±10%). However, TEM (Fig. 3.10b and d) clearly demonstrates the presence of pores within the PHP walls, which are responsible for the high surface areas (the micrographs shown are representative of the foams prepared). Examination of the δ values reported in Table III reveals a close similarity between the solubility parameters and of its components between C_2B and CB-CEB with which foams with the highest surface areas were prepared (Table 3.3, entires 3 and 8). This observation allows the inference that the tridimensional solubility parameter of polyDVB 80% should be close to those of these porogenic solvents. Another important observation is that values of δ_d for the various solvents and mixture of solvents are comprised in a narrow range, variations being less than 6%. Coversely, δ_h and particularly δ_p vary to a much larger extent and this may indicate that polarity could play a fundamental role in the solvation of the polymeric network.

It should be pointed out that all of the materials prepared in this study were derived from HIPEs containing 20% surfactant, as opposed to 33% used by previous workers [2]. The high surfactant content of materials in the latter case reduces their mechanical stability. By varying the porogen type and maintaining surfactant level at 20%, we have achieved an increase in surface area of almost 100% without compromising mechanical stability

3.3.4 Influence of Pore Volume on foams characteristics

The effect of pore volume (PV) on the morphology (cell size, interconnecting windows size and degree of cell packing) of PolyHIPE foams obtained from DVB 80% and with CB as a porogen (monomer: porogen = 1:1) is illustrated by SEM and TEM micrographs in Figs. 3.12 and 3.13, respectively. It is evident that thickness of the cavities walls depends strongly on PV and as a result the size of the interconnecting windows vary inversely with PV. This is the consequence of the layer of continuous phase surrounding the droplets, in the precursor emulsion, being thicker. As a consequence, the monomer phase shrinkage, which vinyl monomers undergo during polymerisation, [8] will produce a smaller window size. Both SEM and TEM micrographs show that at a 75 and 85% PV (Fig. 3.12, and 3.13, a and b), the

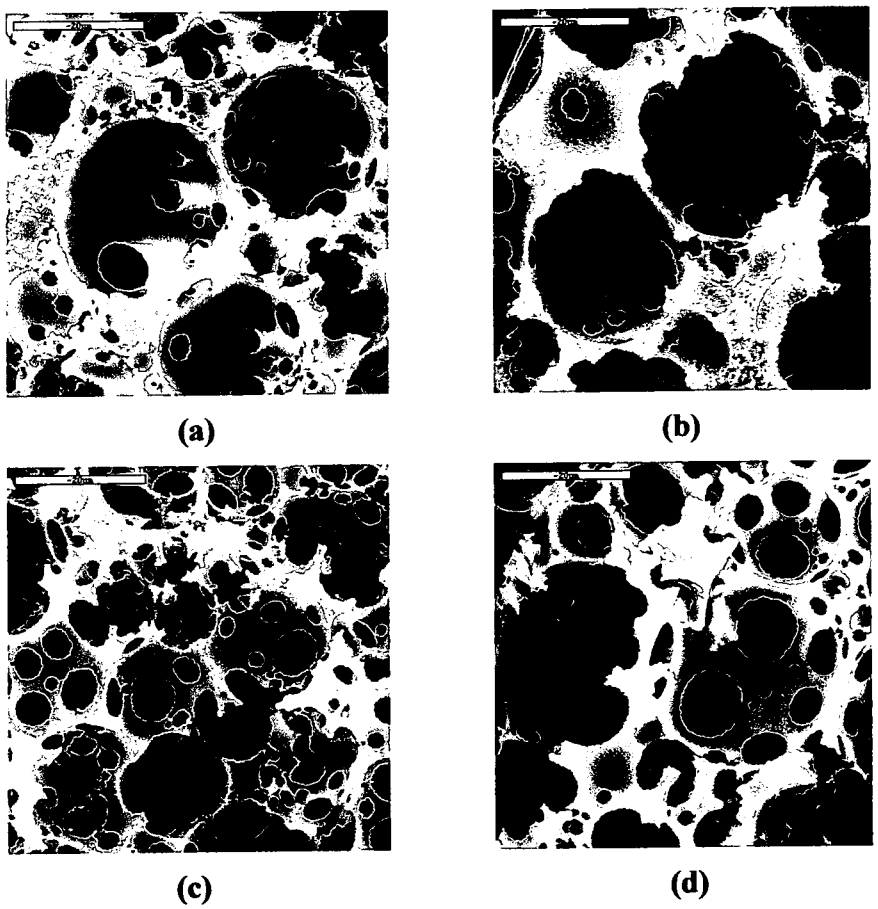

Fig. 3.12. Scanning electron micrographs of PolyHIPE foams characterised by increasing pore volume (a) X80PV75(1CB)S80, (b) X80PV85(1CB)S80; (c) X80PV90(1CB)S80; (d) X80PV92(1CB)S80. Scale bar = 20 μm.

average cell size is relatively large. Due to the high organic/aqueous phase ratio the degree of overlapping among cavities is limited (Fig. 3.13a and b) and the size of the interconnecting windows, especially in X80PV75(1CB)S80 is relatively small (Fig. 3.12 a). In the case of X80PV85(1CB)S80, windows size distribution seems to be more polydisperse (Fig. 3.12b). When the PV is 90 (X80PV90(1CB)S80, (Fig. 3.12c) the size of the cells is smaller than in the other members of the series and as a result the cell packing is denser. X80PV92(1CB)S80 morphology (Fig 3.12 and 3.13, d) is characterised by both large cells and windows. The increase in PV is accompanied by the thinning of the interfacial film separating emulsion droplets. On polymerisation, shrinkage is more significant causing larger windows to appear. Examination of TEM micrographs (Fig. 3.13) confirms the observations made on SEM micrographs and reveals some interesting additional features. For instance, the comparison between foams characterised by PV 75 and 85 shows that cavities in the latter are on the average more separated than in X80PV75(1CB)S80 and tend to be grouped in clusters,

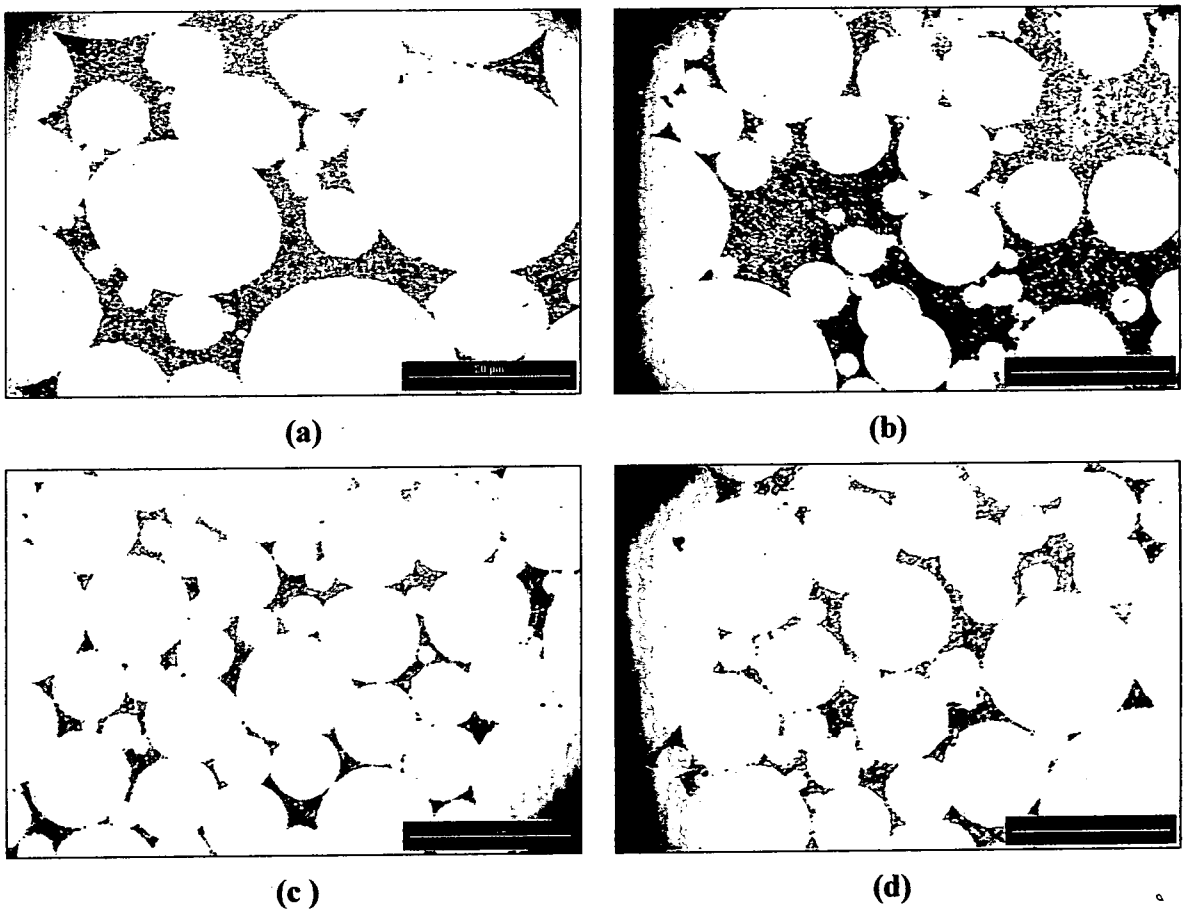

Fig. 3.13. Transmission electron micrographs of PolyHIPE foams characterised by increasing pore volume (a) X80PV75(1CB)S80, (b) X80PV85(1CB)S80, (c) X80PV90(1CB)S80, (d) X80PV92(1CB)S80. Scale bar = 20 μm.

leaving zones of the foam free of cavities. This will turn out to be an important observation.

TEM micrographs were used for the evaluation of the average cavities (*D*) and interconnecting holes (*d*) diameters. Results are reported in Table 3.IV. With exception of X80PV75(1CB)S80 both *D* and *d* increase with PV. Values of the ratio *d/D* increase steadily along the series of foams indicating that overlapping is occurring to a greater and greater extent as PV is increased. Pore size distributions were measured by intrusion mercury porosimetry and data of the relative average diameters (indicated with Δ in order to distinguish it from the analogous data determined by TEM, *D*) are also shown in Table 3.IV. Comparison with the values determined from TEM micrographs shows that the agreement between the two series of values, with the exception of entry 1, is very good. The disagreement regarding X80PV75(1CB)S80 is judged to be due to an overstimation of *D* in the method based on TEM micrographs caused by the shape of larger cavities that (Fig 3.13a) tend to be more ellipsoidal than spherical. In this particular case the main axes of the

ellipsoids were measured and averaged. This process implies that spheres of radii equivalent to this average were considered. This approximation is considered to be the source of the discrepancy between values of the cavity average diameters provided by the two techniques. For the other two foams were such a comparison can be made (Table 3.IV, entry 2 and 3) that is X80PV85(1CB)S80 and X80PV90(1CB)S80, it can be seen that values of Δ are consistenlly smaller than D. This difference is negligible in the former case but larger in the latter. This difference is probably due to compression suffered by these two foams when analysed by intrusion mercury porosimetry. This compression is more consistent when the PV is 90 than 85 because of the thinner walls of the former. For this reason intrusion mercury porosimetry results were judged not reliable in the case of X80PV92(1CB)S80. Pore size distributions determined by intrusion mercury porosimeter of the first three foams listed in

Table 3.IV. Characterisation of PolyHIPE foams.

	SAMPLE	D (μm) [1]	d (μm) [2]	d/D	Δ (μm) [3]	Polydispersity
1	**X80PV75(1CB)S80**	7.1	2.5	0.34	5.2	0.95
2	**X80PV85(1CB)S80**	6.3	2.5	0.40	6.2	2.60
3	**X80PV90(1CB)S80**	8.5	3.9	0.46	8.1	11.1
4	**X80PV92(1CB)S80**	9.1	4.6	0.51	—	—
6	**X80PV75(1CB)S20AD**	3.4	1.1	0.32	3.3	2.0
7	**X80PV85(1CB)S20AD**	2.3	1.0	0.43	2.4	3.6
8	**X80PV90(1CB)S20AD**	3.8	2.0	0.53	4.1	2.4
9	**X80PV92(1CB)S20AD**	6.0	3.7	0.62	—	—
10	**X80PV90(1T)S20AD**	4.1	2.5	0.60	—	—
11	**X80PV90(1C_2B)S20AD**	5.7	3.1	0.54	—	—

[1] average cavity diameter (determined by TEM);

[2] average hole diameter (determined by TEM)

[3] relative average pore diameter (determined by intrusion Hg porosimetry)

Table 3.IV, are shown in Fig. 3.20. All distribution curves span over a diameter range of about one order of magnitude and their polydispersities are expressed as the 10 – 90% size distribution width divided by the median pore diameter. All foams analysed are characterized by a long tail extending towards the low diameter side. PV 90 foam differentiates from the others by the presence of such a tail also in the high diameter side. For this reason polydispersity of X80PV90(1CB)S80 is much larger than the other two foams with lower PV. The increase in polydispersity may reflect, expecially for the foam of entry 3 of Table 3.IV, the occurrence of coalescence phenomena in the precursor emulsion prior to reachment of the

gel point. In fact as the PV increases, droplets are more densely packed and the layer of the continuous phase surrounding them becomes thinner enhancing the probability of the occurrence of coalescence phenomena. Aronson and Petko [21] showed that emulsions deterioration starts immediately after their preparation and that this phenomena manifests itself on the droplet size distribution which begins tailing towards larger droplet sizes.

Data obtained by N_2 adsorption about surface areas, pore volumes and average pore diameters in the range between 1.7 and 200 nm (Table 3.V, entries 1 and 2), show that for the first two foams characterised by a lower PV, (75 and 85%) these quantities are constant within experimental error. About 10% of the surface area is due to the presence of micropores (diameter < 2nm). All isotherms are of type II and exhibit type H3 hysteresis loop. BJH adsorption *dV/dlogD* pore size distributions, where *D* is the pore diameter (Fig. 3.14), are quite broad spanning over two order of magnitude in diameters and show that the proportion of mesopores increase progressively with the decrease of PV. Accordingly, the surface areas increase in the same fashion and the average pore diameter decrease (Table 3.V). As it can be seen in Fig. 3.15, which relates surface areas to PV, when the PV is increased beyond 85%, a transition takes place: the surface area tends to decrease progressively (Fig 3.15, filled line and Table 3.V). As the composition of the organic phase in the precursor is exactly the same for the first four foams shown in Table 3.V, the physical variables responsible for the transition described above must be related to PV. The variables on which the volume of the

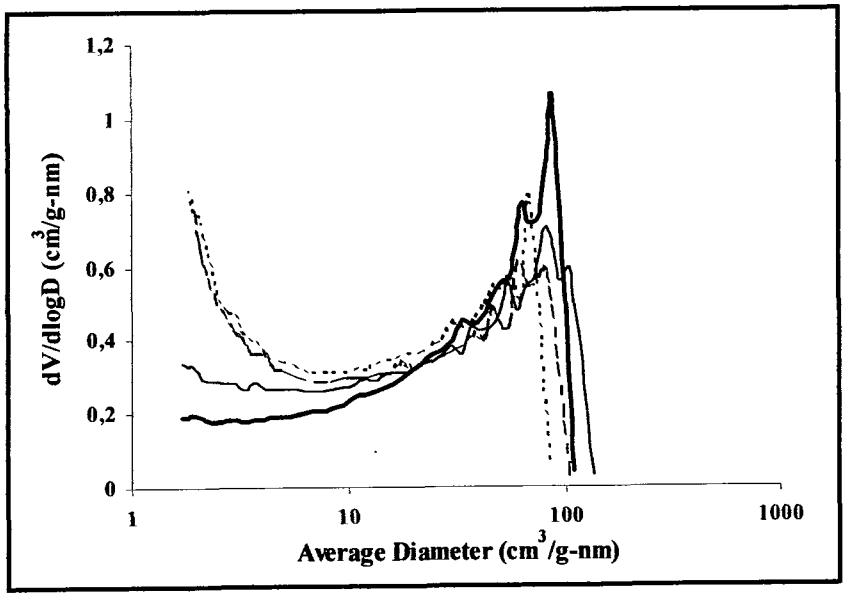

Fig. 3.14. N_2 BJH adsorption pore size distribution of PolyHIPE foams prepared by using SPAN 80 as a surfactant and CB as a porogen and characterised increasing pore volume. (——) PV92; (——) PV90; (——) PV85; (– – –) PV75.

Table 3.V. Surface areas, cumulative pore volume, average diameter, micropore pore volume and micropore areas of DVB 80% PolyHIPE foams. Porogens used: CB, and CEB. Monomer:porogen = 1:0.5 or 1:1 vol:vol. Surfactant used: SPAN 80. Data obtained by nitrogen adsorption. Polymerisation temperature: 60 °C.

	SAMPLE	BET Surface Area (m^2/g)[a]	Cumulative Pore Volume (cm^3/g)[b]	Average Pore Diameter (nm)[c]	Micropore Volume (cm^3/g)[d]	Micropore Area (cm^3/g)[d]
1	X80PV75(1CB)S80	457 ± 28	0.66 ± 0.05	6.0 ± 0.2	0.0076 ± 0.0002	55 ± 6
2	X80PV85(1CB)S80	472 ± 3	0.77 ± 0.03	6.2 ± 0.2	0.015 ± 0.002	48 ± 5
3	X80PV90(1CB)S80	346 ± 46	0.68 ± 0.05	8.4 ± 0.6	0	0
4	X80PV92(1CB)S80	236 ± 11	0.65 ± 0.03	11.2 ± 0.2	0	0
5	X80PV90(0.5CB)S80	375 ± 28	0.52 ± 0.04	6.3 ± 0.5	0.25 ± 0.007	65 ± 15
6	X80PV90(0.5CEB)S80	157 ± 24	0.33 ± 0.03	8.7 ± 0.6	0	0
7	X80PV90(1CEB)S80	432 ± 19	0.72 ± 0.04	7.0 ± 0.3	0	0
8	X80PV75(1CEB)S80	367 ± 6	0.54 ± 0.01	6.2 ± 0.2	0	0

[a] from BET; [b] from BJH adsorption;

[c] from BJH adsorption;

[d] from t-Plot.

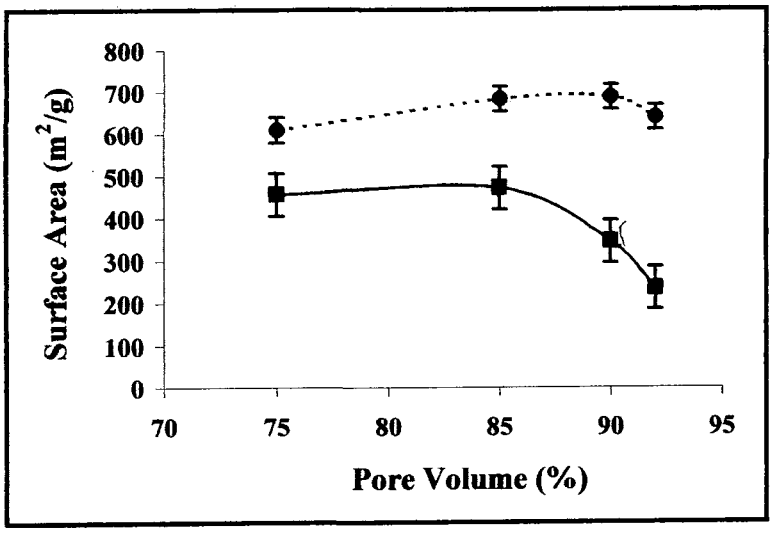

Fig. 3.15. Effect of the pore volume on the surface areas of PolyHIPE foams characterised by increasing PV. (■) symbol refers to foams belonging to the series X80PVN(1CB)S80. Error bar: 20 m^2/g; (●) to foams belonging to the series X80PVN(1CB)S20AD. Error bar: 40 m^2/g.

dispersed phase exerts an influence are the droplets dimensions, degree of packing (Fig. 3.13 and Table 3.IV) and presumably the surfactant interface excess.

High internal phase emulsions consist of two isotropic liquid phases: one is a submicellar surfactant solution in water, and the other is a swollen reversed solution or water-in-oil (w/o) microemulsion [22-25]. Since the surfactant aggregates formed are microemulsions, the critical concentration of surfactant required for their formation is referred to as critical microemulsion concentration (c.μ.c.). For non ionic surfactants the c.μ.c. in oil is typically of the order of 0.1 M whereas the value in the corresponding aqueous phase is of the order of 10^{-5} M. The oil-water interface tension (γ) reaches a virtually constant value above the c.μ.c.

The surfactant molecules present in the organic phase are distributed between the interface and reverse micelles. As the aqueous/oil phase ratio increases, the water-oil interface area increases and some of the surfactant molecules present in the bulk of the organic phase will be adsorbed at the interface to cover the newly created interface area. As a consequence, the number of reverse micelles decreases with increasing water content and as the water fraction approaches 1 no reverse micelles are present in the continuous phase. Also, the absolute amount of surfactant present in the dispersed phase in the form of sub micelles will increase with the PV. O. Foyeke *et al.* [26] showed that the effect of SPAN 80 bulk concentration above C.M.C. on the interfacial tension at the mineral oil/water interface seem to indicate the

occurrence of multilayer adsorption/association. Their study also indicated that excess surfactant may be advantageous for emulsion stability as the interfacial elasticity and hence film strength increase with surfactant concentration. This effect has also been observed in different systems, for instance asphaltene dissolved in heptol [27]. Binks *et al.* [28] showed that when the polarity of the medium in which the surfactant is dissolved is changed from apolar, such as heptane, to more polar, such as a 1:1 vol:vol mixture of heptane and medium chain length triglyceride, the surfactant c.μ.c. increased from 3.0 to 10.3 wt. %. They have also discovered a strong dependence of post c.μ.c. tension (γ_c) on temperature, a variation of about 10 °C, causing a two-fold increase of γ_c.

In the light of the findings exposed above it is possible to make a reasonable hypothesis about the mechanism through which the PV affects foam microstructure. The concentration of SPAN80 in the oil phase is close to 0.5 M (20 wt. % based on monomer plus porogen used). Because of the presence of a high level of CB (a relatively polar molecule, see Table 3.III), the polarity of the organic medium is expected to be high and as a consequence SPAN80 c.μ.c. might be of the same order of magnitude as the actual concentration of SPAN80 in the organic phase. The constancy of surface area and porosity data between X80PV75(1CB)S80 and X80PV85(1CB)S80 might indicate that the surfactant concentration is, at the temperature of polymerisation (60 °C), at or above c.μ.c. In such a situation the interface is completely coated by a mono/multilayer film of surfactant and the interface tension is at its minimum. When PV is increased to 90 and 92 % it can be envisaged that because of the larger surface over which the surfactant has to spread and taking into account that the amount of surfactant, dissolved in the aqueous phase increases with PV, the surfactant concentration in the oil phase at 60 °C is below c.μ.c. In this situation the interface is not completely saturated with surfactant molecules and the interface tension is above its minimum value.

We tried to measure the interfacial tension between the pre-equilibrated aqueous and organic phases by using the spinning drop method [29] to provide experimental support to the hypothesis of a change of interface excess with PV. It turned out that the densities of the aqueous and organic phases were very close to each other differing less than 1% and this prevented the successful application of this technique.

Further insight into the behaviour outlined above regarding the influence of PV on the morphology and microstructure of foams can be obtained by examining the nitrogen adsorption results for a foam in which the porogen(CB)/monomer ratio has been reduced to 0.5. Results are reported in Table 3.V (entry 5). Surprisingly, the surface area of

X80PV90(0.5CB)S80 is, within experimental error, the same as X80PV90(1CB)S80 (Table 3.V, entry 3). The values of surface areas of this two foams are very similar to that (~ 350 m^2/g) found for X80PV90(1T)S80 (Table 3.II), where toluene (T) is the porogen used [2]. T and CB are very good swelling liquid for macroporous resins obtained from DVB 80% [30]. Surface areas in excess of 500 m^2/g with a narrow distribution of very small pores (10 nm) are obtained by employing such solvents as porogens. When the monomer to porogen ratio is 1:1 the surface area is expected to be higher than when this ratio is 1:0.5, because the growing polymeric network is better solvated and phase separation occurs at later stages of polymerisation. When phase separation occurs, most of the monomer has already reacted and the fine (in the mesopore, 2÷50 nm and micropore < 2 nm, regions) porous structure is preserved. On the contrary when the porogen induces polymer network phase separation at much lower monomer conversion, macroporous resins characterised by lower surface areas and broad pore size distributions are obtained [31]. The experimental evidence reported, concerning the effect of PV and monomer to porogen ratio on DVB 80% PolyHIPE microstructure, shows that the actual composition of the organic medium in the corresponding emulsions has changed from the initially prepared organic phase solution. Nitrogen adsorption data (Table 3.V) show that the surface areas are relatively low in spite of the good quality of the porogenic solvents employed and the pore size distribution is broad (Fig. 3.14), which indicates that the organic medium has poor solvating properties toward the polymeric matrix (Table 3.V and Fig. 3.13). When CB [30] is used as a porogen in the bulk polymerisation of DVB 80%, a resin with a surface area as high as 850 m^2/g and a narrow pore size distribution can be produced. It is reasonable to assume that the effect exerted by variation of PV and monomer/porogen ratio on foam microstructure has a common origin.

In Table 3.V are reported nitrogen adsorption results for foams containing CEB as a porogen, at a monomer to porogen ratio of 1:0.5 and 1:1 vol:vol (entry 6 and 7, respectively) and at two different nominal PVs, 75 and 90% (entry 7 and 8). The comparison of surface area data between these foams with the corresponding ones prepared by employing CB as a porogen, reveal a completely different behaviour. When CEB is used, the surface areas of the foams characterised by a constant PV (90%) but at different monomer to porogen ratios, 1:1 and 1:0.5, X80PV90(1CEB)S80 and X80PV90(0.5CEB)S80, are approximately in a 1:0.35 ratio as opposed to the approximately 1:1 ratio exhibited by the same kind of foams prepared by using CB. At constant monomer to porogen ratio but at two different PVs, 75 and 90%, X80PV75(1CEB)S80 and X80PV90(1CEB)S80, the relative surface areas are close to each other, the surface area of the latter being slightly higher. The influence of the PV on surface

area is just opposite to that occurring in the series X80PVN(1CB)S80. These results allow the inference that it is the nature of the porogen, which is responsible for the dependence of foam microstructure on PV and on monomer to porogen ratio. In § 3.3.2 we have provided some evidence that CEB has the tendency to be co-adsorbed at the interface together with the primary surfactant SPAN 80 increasing the interface excess and reducing the interfacial tension. This effect might be responsible for the preparation of a PolyHIPE foam possessing a high surface area, X80PV90(0.5CB+0.5CEB)S80 (Table 3.II, entry 6), from an emulsion containing a porogenic mixture of CB and CEB in a 1:1 vol:vol ratio.

The set of results detailed so far is coherent in indicating that the phenomenon mainly responsible for the dependence of foam microstructure on PV and on monomer to porogen ratio is Ostwald ripening. Ostwald ripening is the process by which large droplets grow at the expense of smaller ones due to the difference in their chemical potential. In Ostwald ripening the growth occurs by diffusion of the dispersed through the continuous phase. The kinetics of Ostwald ripening is most often described in terms of the LSW theory [32-34]:

$$\omega = \frac{da_c^3}{dt} = \frac{8c(\infty)\gamma V_m D}{9RT} f(\phi) \qquad (5)$$

where a_c is the critical radius of a drop which at a given time is neither growing nor decreasing in size, $c(\infty)$ is the solubility of the dispersed phase in an infinite sized drop, i.e. at a planar interface, γ is the interface tension, V_m is the molar volume of the dispersed phase, D is the diffusion coefficient of the dispersed phase in the continuous phase, and $f(\phi)$ reflects the dependence of the rate of ripening, ω, on the dispersed phase volume fraction ϕ.

Analysis of Eq. (5) is of help in the interpretation of the results obtained in the series of PolyHIPEs so far presented. For instance, as stated above, it is expected that the surface area of X80PV90(1CB)S80 would be higher than that of X80PV90(0.5CB)S80, because a higher level of porogen is more effective in solvating the growing polymeric network during polymerisation. The results obtained (Table 3.V, entry 3 and 5) contradict this expectation. A reasonable explanation is a correlation with the term $c(\infty)$ in Eq. (5). A higher concentration of CB in the organic phase should favour the dissolution of a higher amount of water, because the affinity of the continuous phase towards the dispersed phase should increase. As shown in Table 3.III, CB as a solvent combines a relatively high polarity (δ_p) with some hydrogen bonding capability (δ_h). For this reason the value of $c(\infty)$ should be higher for the emulsion characterised by a 1:1 than a 1:0.5 monomer to porogen ratio. Hence the rate of ripening should be faster for the former ratio [32-34]. Because of water diffusion, there is a balancing

effect between the amount of porogen which favours the creation of high surface area foams and the amount of water dissolved in organic phase which tends to turn the porogenic medium into a poor one for the polymer. As a result, X80PV90(1CB)S80 and X80PV90(0.5CB)S80 have comparable surface areas.

The rate of ripening depends also on the interfacial tension, γ. The presence of a surfactant has itself a stabilising effect towards Ostwald ripening because of the reduction of interfacial tension and the creation of a barrier which opposes to diffusion. If a co-surfactant capable of inserting among the primary surfactant molecules adsorbed at the interface is present, an additional stabilising force results. This is the case of the emulsion containing the mixture of CB and CEB. The further lowering of interface tension thanks to the co-adsorption of CEB molecules at the interface, slows down the diffusion of water through the continuous phase and a PolyHIPE with a much higher surface area is obtained, X80PV90(0.5CB+0.5CEB)S80 (entry 6 of Table 3.II).

The same kind of phenomenon is probably occurring when the PV is changed in the series X80PVN(1CB)S80. At low PV, 75 and 85% and at 60 °C, the surfactant interface excess might be higher than at 90 and 92% PV and as a consequence, the interfacial tension could be lower and the density of the interfacial film less penetrable by water molecules. Another possibility is represented by the influence of PV on $f(\phi)$. Interdroplet diffusional interactions will affects the dynamics of Ostwald ripening to an extent which is dependant on PV.

The discussion so far presented shows that a porogenic solvent may play multiple roles in determining the final foam microstructure. These are:

(1) The compatibility (with a solubility parameter similar to that of the polymer) of the porogenic solvent with polyDVB 80%.

(2) The surface activity of the porogenic solvent used. It is well known that shorter chain and polar molecules tend to penetrate to a larger degree between the chains of a surfactant monolayer, creating a wedge effect on the oil side of the monolayer and increasing the spontaneous curvature [18]. As argued above the lowering of interfacial tension and possibly the creation of a more coherent film, reduced the rate of diffusion of the dispersed through the continuous phase, thus preserving the swelling property of the porogen towards the polymer.

(3) The polarity of the porogen. Arguably, the higher the polarity of the solvent and the greater its ability to form hydrogen bonds with water, the higher will be its ability to incorporate larger and larger quantities of water. In other words, the weight of the term, $c(\infty)$, in Eq. (5) becomes more and more pronounced. In a similar fashion the amount of porogen

which partitions with the aqueous phase should increase with porogen polarity. This property also affects the surfactant c.μ.c. and consequently the degree of covering of the oil/water interface. In this respect the polarity of the porogen influences surfactant c.μ.c also through an indirect mechanism: the diffusion of water (whose magnitude depends on porogen polarity) confers an even higher polarity to the organic phase contributing in this way to shift c.μ.c to higher values.

3.3.5 Macroporous monoliths from DVB 80%

The superimposition of all the effects described above makes it difficult to establish, for a given porogen, their relative contribution in determining the final macro and micro morphology of a foam. With the aim of establishing an order of solvent quality towards polyDVB 80%, we carried out the bulk polymerisation of DVB 80% in the presence of the five porogenic solvents listed in Table 3.VI and investigated the structure of the obtained resins by SEM, nitrogen adsorption and intrusion mercury porosimetry. The values of surface

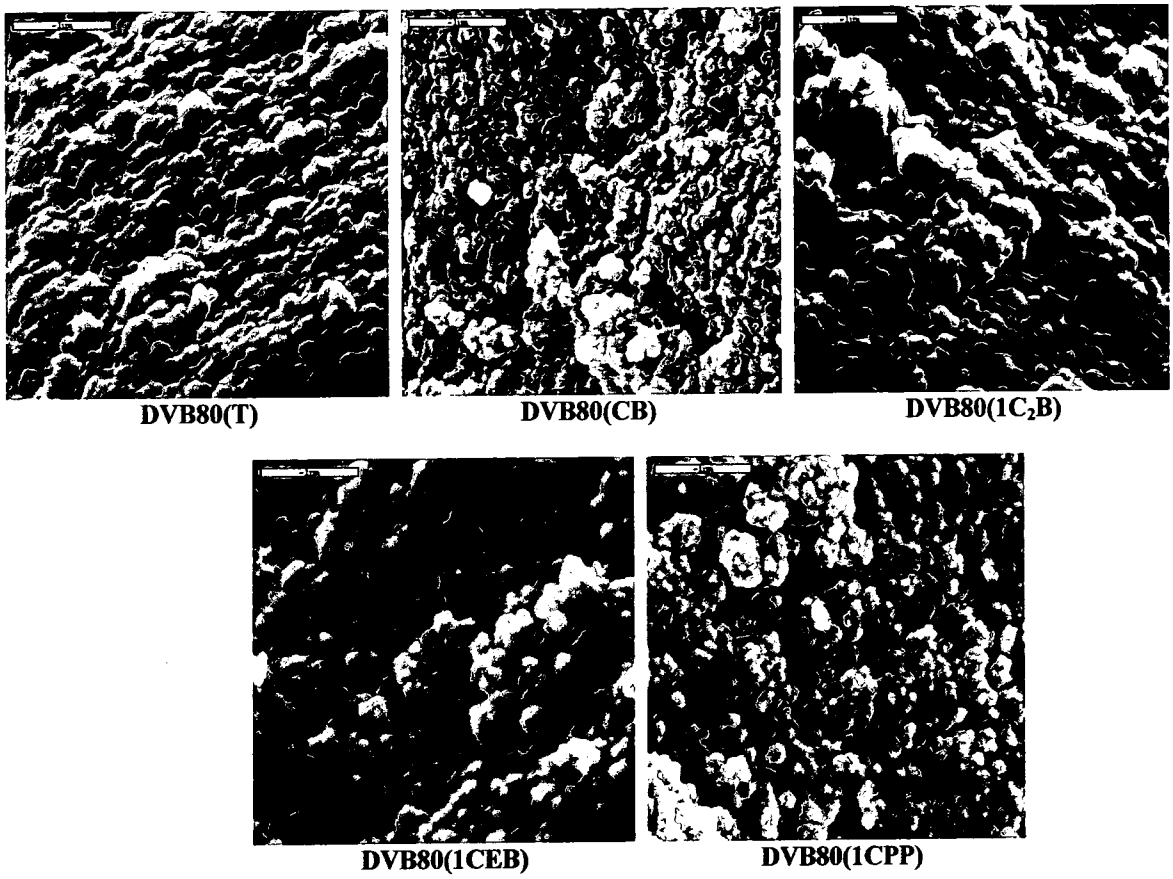

Fig. 3.16. SEMs of DVB 80% macroporous resins obtained by bulk polymerisation and using different porogens. Scale bar 1 μm.

Table 3.VI. Nitrogen adsorption results for DVB80% macroporous monoliths obtained in the presence of different porogenic solvents. Monomer to porogen ratio = 1:1. Polymerisation temperature: 60 C.

	SAMPLE	Surface Area (m^2/g)[a]	Pore Volume (cm^3/g)[b]	Average Pore Diameter (nm)[b]	Micropore Volume (cm^3/g)[c]	Micropore Area (cm^3/g)[c]
1	DVB80(T)	760 ± 8	0.891 ± 0.008	4.515 ± 0.008	0.0057 ± 0.0004	40 ± 1
2	DVB80(CB)	781 ± 9	0.982 ± 0.009	4.92 ± 0.02	0.0173 ± 0.0006	64.0 ± 0.4
3	DVB80(C_2B)	829 ± 7	1.09 ± 0.01	5.08 ± 0.01	0.0118 ± 0.0003	54.6 ± 0.7
4	DVB80(CEB)	799 ± 0.5	1.159 ± 0.003	5.66 ± 0.01	0.0126 ± 0.0007	55 ± 1
5	DVB80(CPP)	783 ± 2	1.219 ± 0.008	6.07 ± 0.05	0.0123 ± 0.0004	54 ± 1

[a] from BET;
[b] from BJH adsorption;
[c] from t-Plot.

areas of the macroporous resins are also useful in another respect: they allow us to establish an upper limit in PolyHIPEs surface area values reachable with a porogen when it enters as a constituent in an emulsion. The comparison between surface areas of a resin and that of the corresponding polyHIPE foam, both obtained using the same porogen, can give an indication of the extent of the cumulative effects exerted by partitioning and diffusion occurring in the latter.

SEM images (Fig. 3.16) of the bulk polymers show clearly the particle structure of the materials.

For the first two resins reported in Table 3.VI, polyDVB(T) and polyDVB(CB), there are already data available in the literature (9). Our values of surface areas are within less than 10 % of the published ones. Regarding the influence of the other three chlorinated solvents, C_2B, CEB and CPP, on the microstructure of polyDVB as far as we know, no data have been published so far. As can be seen, all solvents represent very good porogens for polyDVB

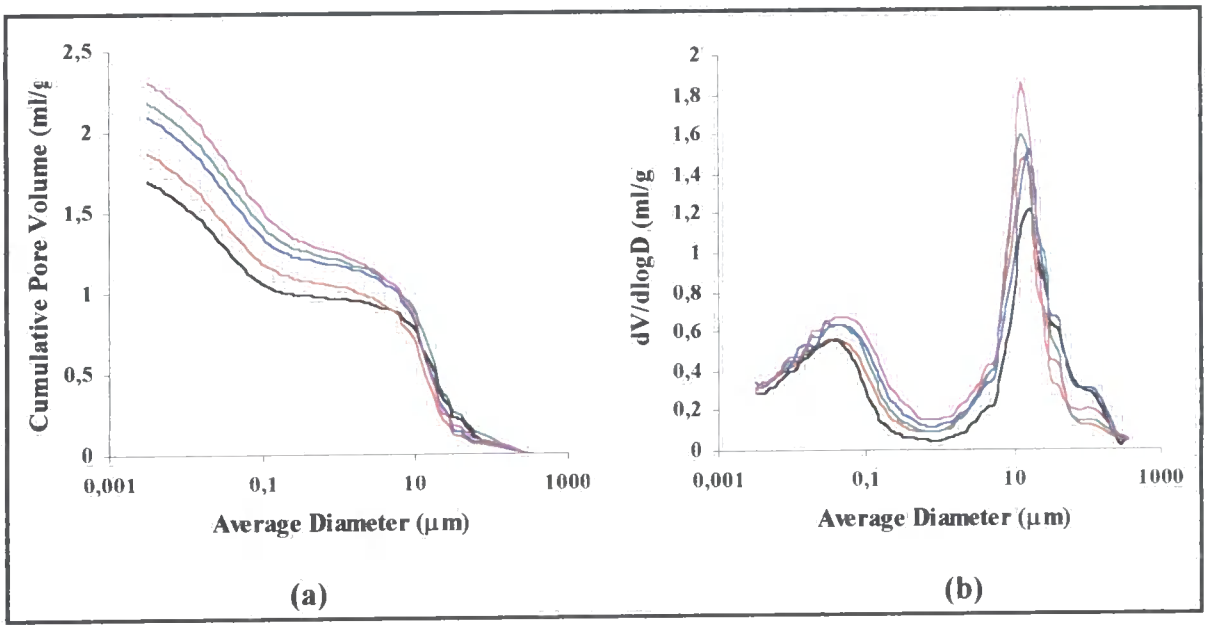

Fig. 3.17. Cumulative pore volume and pore size distributions determined by intrusion mercury porosimetry of DVB 80% resins obtained by bulk polymerisation in the presence of different porogenic solvents. (——) DVB(T); (——) DVB(CB); (——) DVB(CB_2); (——) DVB(CEB); (——) DVB(CPP).

80 %, porous resins with surface areas exceeding 700 m^2/g being produced. It is evident from the data reported in Table 3.VI that surface areas pass through a maximum in the case of polyDVB(C_2B). This indicates that C_2B is the best porogen. Pore volume increases steadily

along the series of macroporous resins reported in Table 3.VI, and reaches its maximum value in correspondence of polyDVB(CPP). This resin possesses the same surface area of polyDVB(CB) but its pore volume is about 25% higher. The pore volume behaviour of the resins prepared is illustrated by both intrusion mercury porosimetry and N_2 adsorption results, (Fig. 3.17a and Fig 3.18a, respectively). The amount of mercury intruded or of N_2 adsorbed by the resin, which is given by the differences of the extremes of the ordinates of the cumulative pore volume increases in the following order: T <CB < C_2B < CEB < CPP. Pore volumes follow the same trend.

The N_2 sorption isotherm are complete and are of type IV [5] with a type H2 hysteresis loop[9]. The adsorption and desorption branches get closer when the porogen employed in resin preparation is changed from T to CPP and this is clearly an indication that the adsorption and evaporation processes take place in pores of increasing diameters as evident in Fig.3.18a.

In Fig. 3.18b, BJH adsorption *dV/dlogD* pore size distributions and isotherms are reported. The pore size distributions of resins obtained by using as porogens T, CB and C_2B cover the

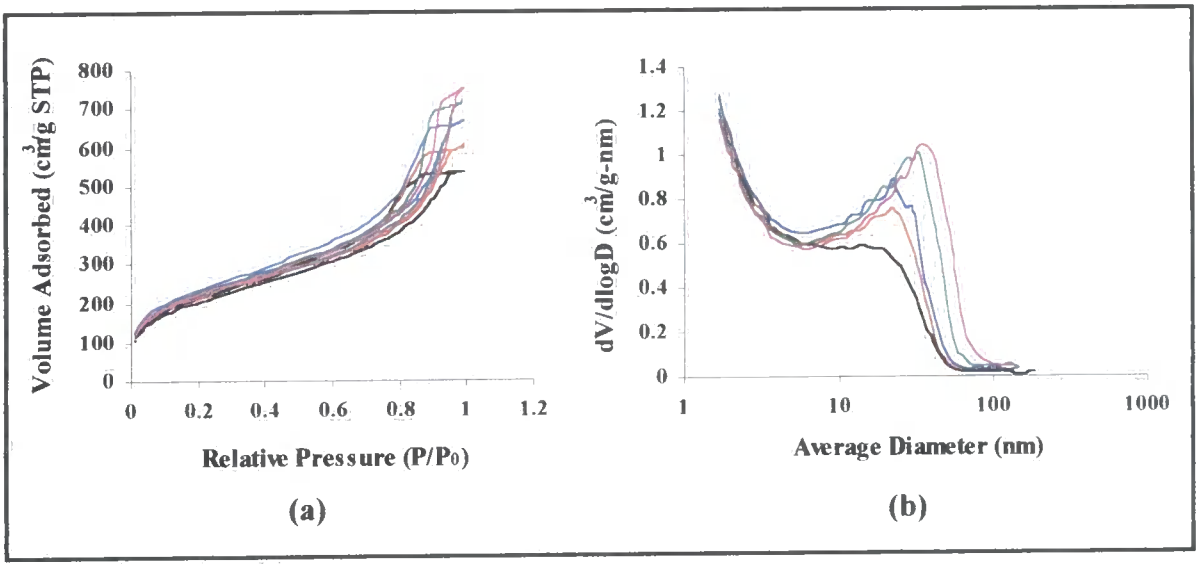

Fig. 3.18. N_2 adsorption (a) and BJH pore size distributions of DVB 80% resins obtained by bulk polymerisation in the presence of different porogenic solvents. (——) DVB(T); (——) DVB(CB); (——) DVB(C_2B); (——) DVB(CEB); (——) DVB(CPP).

same diameter range. As can be seen, the position of the peaks is the same, the differences consisting of the relative heights in each case. In the case of resins obtained by using CEB and CPP as porogens, the pore size distributions become increasingly broader and as a result, the position of the peaks shifts towards higher diameter values, the proportion of lager pores

increases while that of the mesopores remains at level comparable to that of polyDVB(CB). The set of N_2 adsorption results shown, indicate that C_2B is, among the solvents studied here the one with the best swelling properties towards polyDVB 80%.

The correlation between δ and surface area data indicates that the solubility parameter of polyDVB(C_2B) should be very close to 20.5 $(MPa)^{1/2}$.

N_2 adsorption results for macroporous resins indicate that solvent quality is not responsible for the differences encountered among the polyHIPE foams obtained by using the same porogens. In fact in the former samples, surface areas differ less than 10% from each other while in the latter variations are much more pronounced.

The large differences between surface area values and porosity data of the macroporous DVB 80% resins reported in Table 3.VI and the corresponding PolyHIPE foams obtained from emulsions containing CB, C_2B and CEB as porogens, seem to indicate that diffusion of the dispersed phase through the continuous one and possibly partitioning of the porogen between the two phases are the dominant processes in determining the microstructure of foams.

In terms of the extent to which these phenomena occur, the nature of the surfactant should play a fundamental role. SPAN80 as a surfactant presents some drawbacks: the oleic tail is in the *cis* conformation and this prevents to some extent an efficient packing of surfactant molecules in the interfacial film [35-38].

In order to prepare more stable emulsions and to exploit as much as possible the porogenic properties of T, CB and C_2B, we searched in the literature for a surfactant system more efficient than SPAN 80.

The effectiveness of a mixture of an anionic, or cationic, surfactant with an amphiphilic compound for emulsion stabilisation has been known for a long time [39]. The interfacial film made by this mixture of surfactants shows an increased ability to withstand the pressure of droplet contacts (to prevent coalescence) and to act as a barrier to the passage of the dispersed phase into the continuous phase (to limit Ostwald ripening). It has been discovered that the two surfactants together reduced the interfacial tension to very low values (~ 0.1 mNm^{-1}), much lower than each of them separately [40]. Emulsions containing this surfactant and co-surfactant system remain mobile at low total concentration of the surfactants, but become semi-solid at higher concentration (~ 10% or less of the total weight of the emulsion). The surfactants, in fact, associate into a mixed bilayer and form a lamellar phase, which co-exist with oil and water in a three-phase equilibrium. This process, whereby the agent, which stabilises the emulsion also controls the consistency over a wide range of values, is referred to

as self-bodying action. The essential feature of this self-bodying action is the introduction of a significant viscoelastic component into the reological behaviour [41].

Hallworth et al. [42], as early as 1972, recognised that long paraffin chain may be associated with the hydrocarbon chain of alkyl sulfates and thus be held in the interface. Due to this association the film will be very coherent and will prevent coalescence of oil droplets

The patent literature [43] describes the use of a mixture of non-ionic, anionic and cationic surfactants: sorbitan monolaureate (SPAN 20), dodecylbenzenesulfonic acid sodium salt (DDBSS) and cetyltrimethylammonium bromide (CTBA). This mixture of surfactants is claimed to stabilise emulsions more effectively than SPAN 80. For instance, using a surfactant concentration of less than 10% it is possible to prepare HIPEs at elevated temperatures (≥ 100 °C) without inducing any water phase separation.

3.3.6 PolyHIPE foams prepared with a mixture of surfactants

In order to compare the effectiveness of this surfactant system with SPAN80 the same set of foams illustrated above was prepared again, this time employing the mixture of surfactants, and characterization was carried out as previously. In Fig. 3.19 SEM micrographs of X80PVN(1CB)S20AD foams are reported. They exhibit the same overall features already met with X80PVN(1CB)S80 foams. One notable difference between the two sets of foams is that in the former case both cell and window sizes are, on the average, smaller than in the latter. This observation is confirmed on a quantitative basis by intrusion mercury pore size distributions in the macropore region (> 2μm) for the two sets of foams, Fig. 3.20. Again, the distribution curves referring to X80PV92(1CB)S20AD foam has been omitted on purpose because the materials was not sufficiently tough to survive the analysis and did not produce any reproducible results. All distributions referring to members of X80PVN(1CB)S80 series are positioned to the right of those of X80PVN(1CB)S20AD. Values of the average pore diameters together with the relative polydispersities are reported in Table 3.IV. It can be seen that the average diameters of the X80PVN(1CB)S20AD foams type are about one half those of the corresponding foams prepared with SPAN 80. Polydispersities do not exhibit any major differences and any trend on variation of PV and the lack of the tail extending towards the high diameter side may be an indication that coalescence has been suppressed or greatly reduced. This may be a consequence of a more rigid interfacial film formed at the interface by the mixture of surfactants as compared to that formed by SPAN 80. Quantitative data provided by TEM about average diameter *D* and the size of interconnecting windows *d* (Table

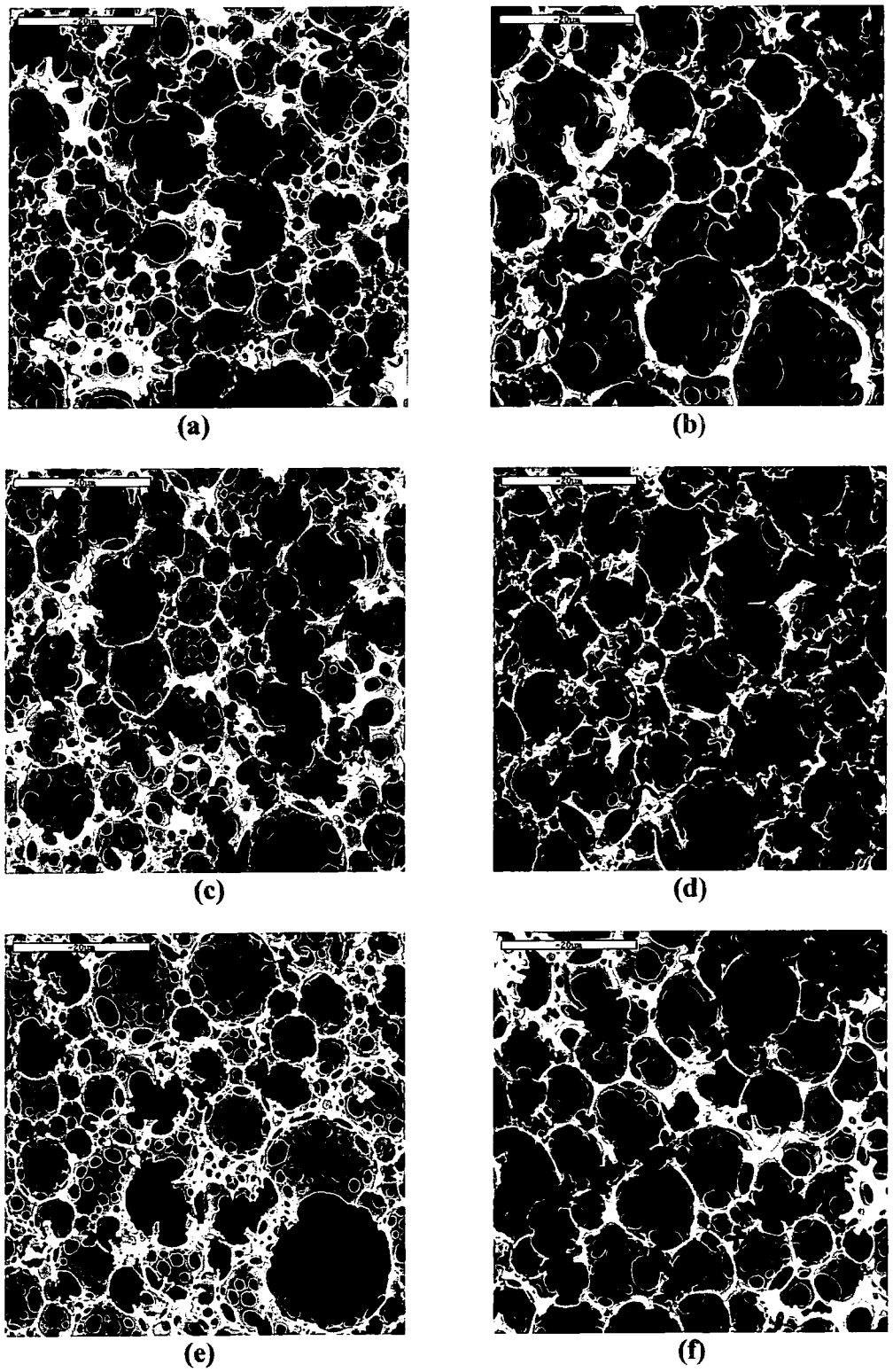

Fig. 3.19. Scanning electron micrographs of PolyHIPE foams characterised by increasing PV (a) X80PV75(1CB)S20AD; (b) X80PV85(1CB)S20AD; (c) X80PV90(1CB)S20AD; (d) X80PV92(1CB)S20AD; (e) X80PV90(1T)S20AD; (f) X80PV90(1C$_2$B)S20AD. Surfactants used: SPAN 20 plus DDBSS and CTABr. Scale bar = 20 μm.

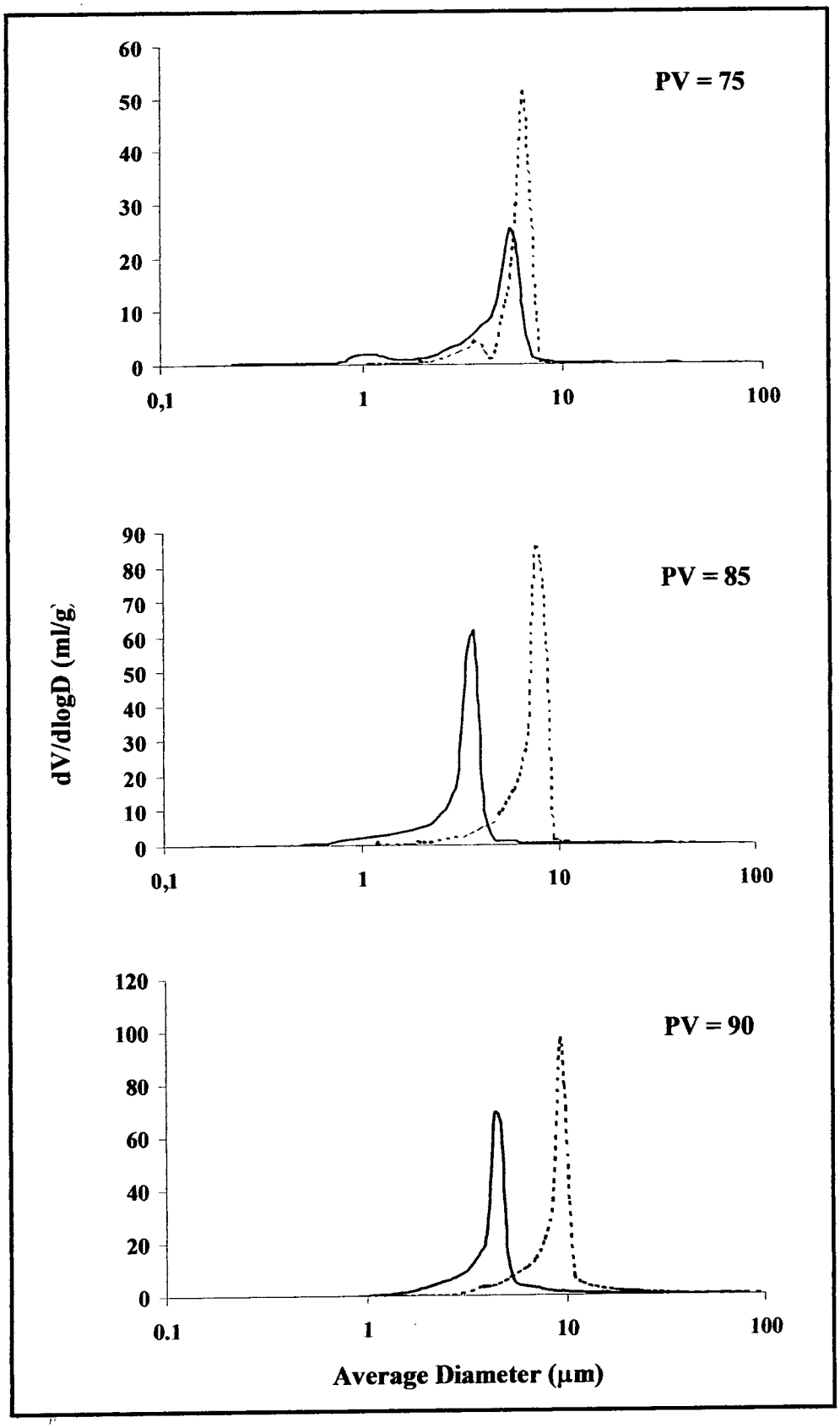

Fig. 3.20. Intrusion mercury porosimetry of DVB 80% PolyHIPE foams prepared using CB as a porogen, SPAN 80 (dashed lines) or the a mixture of SPAN 20, CTABr and DDBSS (solid line) as surfactants and characterised by increasing pore volume.

3.IV) confirm the excellent agreement with the values obtained by intrusion mercury porosimetry, Δ. Furthermore, comparison with the d values referring to foams belonging to X80PVN(1CB)S80 series, shows that the size of the interconnecting windows are proportionally larger relative to cell size and the degree of overlapping as expressed by the ratio d/D indicate that the film of continuous phase surrounding droplets in the precursor emulsions is thinner. All this observations point to a more pronounced reduction of the interfacial tension caused by the mixture of surfactants than that promoted by SPAN 80.

N_2 adsorption results for the series of foams characterised by an increasing PV are reported in Table 3.VII. Two features are immediately evident: the values of surface areas are twice as high as those of X80PVN(1CB)S80 foams and are subject only to minor differences as the PV is changed (Fig. 3.15). For instance, surface area decreases only slightly when PV exceeds 90% and those referring to 85 and 90 PV are the same. That corrsponding to PV 75% is about 10 % lower than PV.

The difference between the surface areas of X80PV90(1CB)S20AD with that of poly DVB(CB) (Table 3.VI) is about 12%. In Table 3.VII the surface area for a foam characterised by a monomer to porogen ratio of 1:0.5 (X80PV90(0.5CB)S20AD, entry 5) is also included.

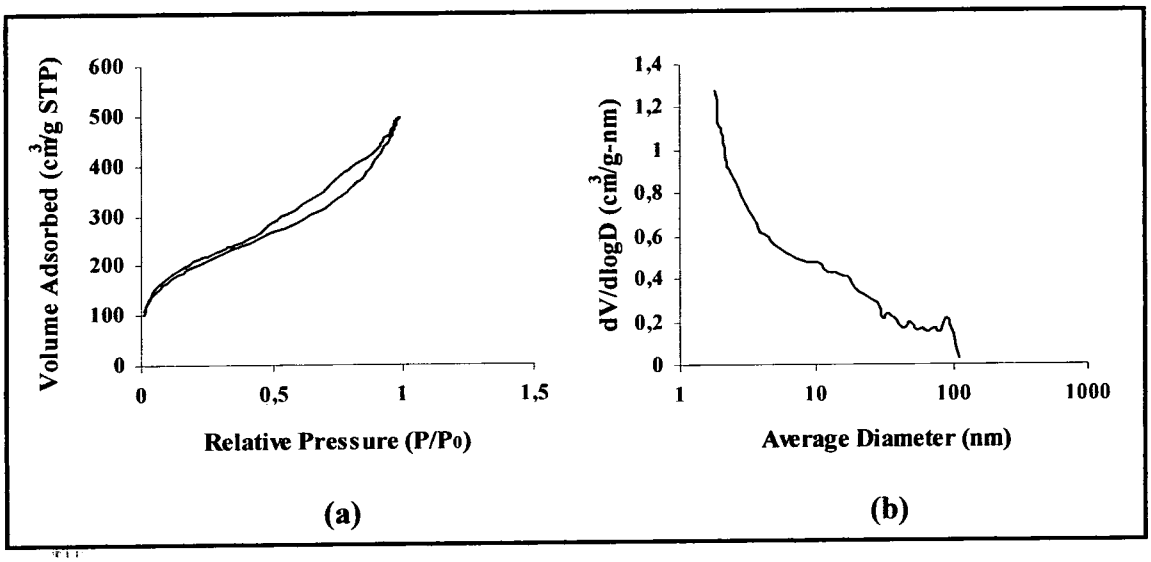

Fig. 3.21. N_2 adsorption and desorption isotherm (a) and BJH adsorption pore size distribution (b) of X80PV90(1CB)S20AD.

Its surface area is about half that of X80PV90(1CB)S20AD (monomer to porogen ratio of 1:1) (entry 3). These results indicate that diffusion of water has been drastically reduced and that the interfacial film made of the mixture of surfactants effectively screens the organic

Table 3.VII. Surface areas, cumulative pore volumes, average pore diameters, micropore pore volumes and micropore areas of DVB 80% PolyHIPE foams. Porogens used: CB, CEB, C_2B and T. Monomer:porogen = 1:0.5 or 1:1 vol:vol. Surfactants used: SPAN 20, DDBSS, CTABr. Data obtained by nitrogen adsorption. Polymerisation temperature: 60 °C.

	SAMPLE	Surface Area (m^2/g)	Cumulative Pore Volume (cm^3/g)	Average Pore Diameter (nm)	Micropore Volume (cm^3/g)	Micropore Area (cm^3/g)
1	X80PV75(1CB)S20AD	610 ± 18	0.73 ± 0.04	4.62 ± 0.04	0.016 ± 0.003	56 ± 7
2	X80PV85(1CB)S20AD	684 ± 5	0.770 ± 0.007	4.26 ± 0.08	0.018 ± 0.003	62 ± 6
3	X80PV90(1CB)S20AD	689 ± 15	0.80 ± 0.03	4.36 ± 0.08	0.018 ± 0.003	64 ± 6
4	X80PV92(1CB)S20AD	640 ± 7	0.710 ± 0.004	4.19 ± 0.04	0.018 ± 0.003	61 ± 5
5	X80PV90(0.5CB)S20AD	351 ± 38	0.35 ± 0.05	3.90 ± 0.07	0.008 ± 0.002	31 ± 8
6	X55PV90(1CB)S20AD	446 ± 31	0.58 ± 0.03	5.2 ± 0.2	0.0011 ± 0.0009	20 ± 3
7	X80PV90(0.5CB+0.5CEB)S20AD	634 ± 21	0.67 ± 0.02	4.61 ± 0.08	0.0020 ± 0.0005	28 ± 9
8	X80PV90(1T)S20AD	721 ± 12	0.81 ± 0.02	4.39 ± 0.05	0.019 ± 0.006	66 ± 11
9	X80PV90(1C_2B)S20AD	435 ± 38	0.56 ± 0.03	5.4 ± 0.2	0	0
10	X80PV90(1CEB)S20AD	665 ± 31	0.81 ± 0.04	4.70 ± 0.04	0.014 ± 0.004	53 ± 9
11	X80PV90(1CPP)S20AD	660 ± 7	0.79 ± 0.01	4.60 ± 0.02	0.006 ± 0.001	37 ± 2

[a] from BET; [b] from BJH adsorption;

[c] from BJH adsorption;

[d] from t-Plot.

medium from the aqueous phase, independently of the polarity of the former.

Table 3.VII includes the surface area data of a foam (entry 6) obtained by using DVB 55%. The comparison of the surface areas between X80PV90(1CB)S80 (Table 3.II, entry 2) and X55PV90(1CB)S20AD shows how influent are partitioning of the porogen and in particular water diffusion through the continuous phase, in altering the quality of the organic medium in which polymerisation is taking place. In spite of a lower crosslinking density, the surface area of X55PV90(1CB)S20AD is 20% higher than that of X80PV90(1CB)S80.

An example of isotherm type and of pore size distribution encountered with X80PVN(1CB)S20AD foams are displayed in Fig. 3.21a and b. All said distributions are very close to each other which is indicative of uniformity of microstructure. Isotherms are all of type IV and exhibit a H2 hysteresis loop type as opposed to the type 2 isotherm and H3 loop exhibited by foams belonging to the X80PVN(1CB)S80 series (Fig. 3.6a). In that case, the adsorption and desorption curves are parallel over almost all range of gas uptake whereas in the case of X80PVN(1CB)S20AD foams the isotherms show a wider hysteresis loop instead of nearly retracing the adsorption curve. The occurrence of a wider, more-pronounced hysteresis loop indicates that evaporation from a pore is a distinctly different process from condensation within it. When gas condenses in a pore, the condensate builds from the wall inwards towards a central core of decreasing diameter. However, it must evaporate from a liquid surface with a quite different curvature. This inhibits the evaporation and causes the decreasing portion of the loop to lag behind until all pores have emptied [44]. Thus, the width of the hysteresis loop is related to the size of pores: the smaller the pores the higher is the radius of curvature of the liquid/gas interface and the higher is the difference of pressure across the interface. The wide hysteresis loops exhibited by X80PVN(1CB)S20AD foams are in accordance with the size distributions being shifted more towards a lower pore size than those of X80PVN(1CB)S80 foams. In Table 3.VII are also reported the surface area data regarding foams prepared with T, C_2B, CEB and CPP porogens. The surface area of X80PV90(1T)S20AD (entry 8, Table 3.VII) is the highest and this is a striking result, expecially if this data is compared with the surface area of the resin obtained by bulk polymerisation of DVB 80% in the presence of T. The difference in their surface areas is 5% only. The same comparison for the other foams and corresponding resins shows that this difference increases in the following order: CB(12%) < CEB ≅ CPP (16%) < C_2B (48%). In the case of the 1:1 mixture of CB and CEB porogens, the inclusion of the mixture of surfactants (Table 3.IV, entry 7) improves only to a little extent the surface area (~ 50 m^2g^{-1}) over X80PV90(0.5CB+0.5CEB)S80 (Table 3.II, entry 6) proving that CEB is itself a good

co-surfactant.

SEM micrographs of X80PV90(1T)S20AD (Fig. 3.19e) show that cavities tend to be more polydisperse and interconnected by larger holes than X80PV90(1CB)S20AD (Fig. 3.19c). X80PV90(1C_2B)S20AD morphology (Fig. 3.19f) is better textured than that of X80PV90(1C_2B)S80 (Fig. 3.3c), the continuity of the walls of the former foam being retained without any significant sign of walls break up. This is remarkable because the value of the *d/D* ratio is, for this foam, the highest among the PV 90 foams listed in Table 3.IV. This implies that droplets in the precursor emulsion are relatively more compressed but the film of continuous phase surrounding them retains its structural integrity. The observations made with SEM are confirmed by TEM microscopy. Micrographs shown in Fig. 3.22 are representative. Clearly, cavities are, on the average, separated by a thinner layer of polymeric material than in X80PV90(1T/CB)S80 (Fig. 3.5a and b) and quantitative estimation of the ratio *d/D* confirm this observation (compare values of entries 8, 10 11 of Table 3.IV with those of entries 1, 2, 3 of Table 3.I). Also cavity, *D*, and interconnecting window, *d*, average diameters are systematically lower than those of the corresponding foams obtained with SPAN 80.

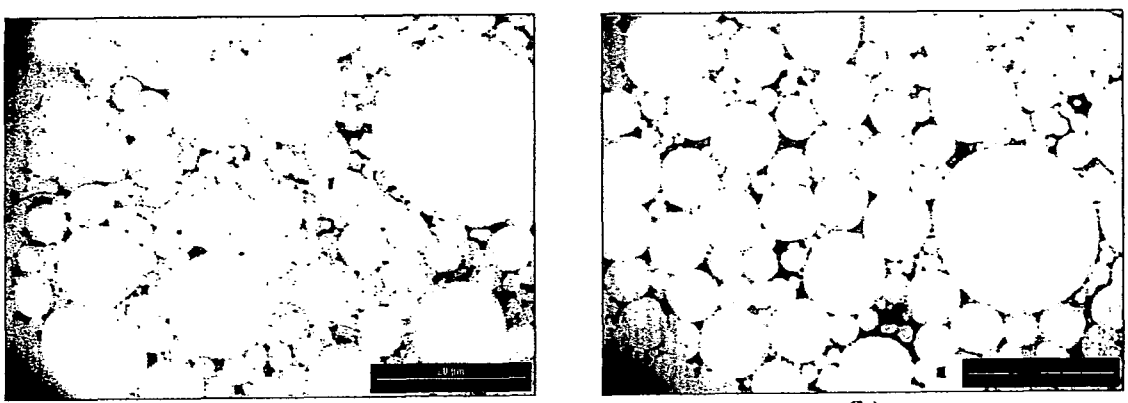

(a) (b)

Fig. 3.22. TEMs of PolyHIPE foams obtained from emulsions prepared with the mixture of surfactants and with different porogens. (a) X80PV90(1T)S20AD (b) X80PV90(1CB)S20AD. Scale bar: 20 μm.

The combined evidence of smaller droplet sizes and of a thinner layer of polymeric material separating adjacent droplets in foams prepared by using the mixture of surfactants indicate that the interfacial tension in the precursor emulsions is lower than in the corresponding ones prepared using SPAN80. The decrease in droplet size is not as dramatic as that caused by the addition to the organic phase of CEB or CPP in X80PV90(1CEB/CPP)S80 emulsions. From

this we can infer that it is not the lowering of interfacial tension which is mainly responsible for the attenuation of Ostwald ripening. It sounds more reasonable to attribute this behaviour to the creation, by the mixture of surfactants, of a compact barrier which opposes the exchange of molecules (water and porogen) between the two phases. In the literature [45, 46] it has been reported that the presence of an adsorbed gelatin layer reduces the rate of transfer of diethylphthalate across the hexadecane/water interface by a factor of approximately 10^4 compared to the diffusion controlled rate. Kabalnov and Shchuckin [47] have given equations describing the retardation effect of a membrane at the interface. We have observed experimentally that if an aqueous layer is deposited carefully on top of an organic one containing the mixture of surfactants, a solid membrane develops at the interface, while in the case of SPAN80 the interfacial film of surfactant remains fluid.

Because the mixture of surfactants has proved to be effective in isolating the organic phase from the aqueous one we would expect, simply from a consideration of the solvating power of the porogens used, that the surface areas of X80PV90(0.5CB+0.5CEB)S20AD and X80PV90(1C_2B)S20AD would be higher or at least equal to that of X80PV90(1CB)S20AD. As can be seen, the surface area of the X80PV90(0.5CB+0.5CEB)S20AD deviates slightly from that of X80PV90(1CB)S20AD while that of X80PV90(1C_2B)S20AD is much lower (Table 3.VII, entries 3, 7 and 9). Also, the difference in surface area between X80PV90(1C_2B)S20AD and DVB(C_2B) (Table 3.VI, entry 3) is particularly marked (about 50 %) which indicates that in the presence of this porogen the mixture of surfactants fails to prevent, with the same effectiveness, both diffusion and partitioning. This hypothesis finds some support from the result concerning the use of T as a porogen. In this case a foam, X80PV90(1T)S20AD (Table 3.VII, entry 8), with the highest surface area is obtained. From these results we infer that the nature of porogen and its interaction with the surfactants is again determinant as far as the final foam microstructure is concerned.

In Fig. 3.23 the microstructures as determined by electron microscopy of X80PV90(1CB)S80, X55PV90(1CB)S20AD and X80PV90(1CB)S20AD are reported. SEM micrographs (left column of Fig. 3.23 A-C) at 30000 × magnification clearly show that the average dimension of the microgel particles composing the walls of the above foams decreases markedly down the series. In particular, X55PV90(1CB)S20AD particles are significantly smaller than those of X80PV90(1CB)S80. TEM micrographs taken at a 10500 × magnification (right column of Fig. 3.23, D-F) provide a direct image of the porosity inside the materials. In accordance with SEM picture (Fig. 3.23 A) and with *dV/dlogD* nitrogen adsorption results of Fig. 3.21, the porous structure in X80PV90(1CB)S80 (voids among particles agglomerates) is rather

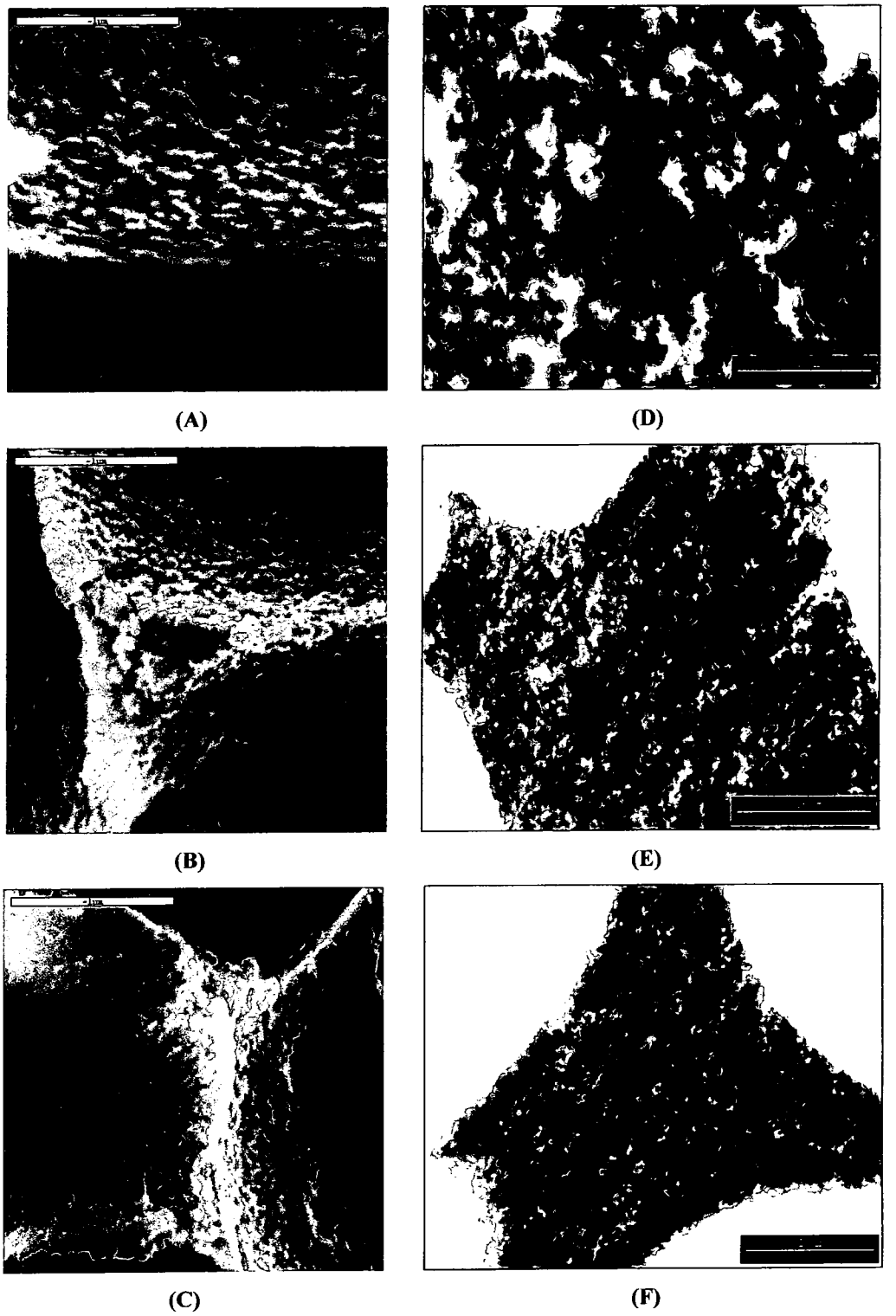

Fig. 3.23. Scanning (A, B, C) and transmission (D, E, F) electron micrographs of PolyHIPE foams. (A, D) X80PV90(1CB)S80; (B, E) X55PV90(1CB)S20AD; (C, F) X80PV90(1CB)S20AD. Scale bars are 1 and 0.8 μm, respectively.

heterogeneous, pores diameters being comprised in a wide range. The micromorphology as evidenced by electron microscopy of X80PV90(1CB)S80 is compatible with a polymerisation

taking place in a less thermodynamically favourable porogen.

When the polymerisation in the emulsion starts in the presence of a poor solvent for the polymer, the porous texture formation follows a three-stage mechanism [48]. The agglomeration of polymer chains to give nuclei (5-20 nm) takes place at first followed by the formation of microspheres (60-500 nm), and finally agglomerates (10,000-100,000 nm). Very small pores (50-150 Å) are located in between the nuclei, and these pores are mainly responsible for the high surface area. In between the micropores, there is a second family of intermediate pores (200-500 Å). A third family of large pores is located between the agglomerates. The resulting porous structure is characterised by a large pore volume with a relatively large-pore diameter. During the polymerisation, the solvating power of the liquid medium is continuously decreasing because the monomer is consumed, and at a certain point the solvent medium does not solvate the polymer formed which precipitates. The separated nuclei preferentially "extract" the monomer from the surrounding liquid polymerisation mixture containing the less compatible solvent because the monomer favours the more thermodynamically favourable enviroment within the nuclei. The enlarged nuclei can also attract and coalesce with the newly precipitated chains and further increase their size. As a result, both large microglobules and large pores are formed.

In the case of X55PV90(1CB)S20AD and X80PV90(1CB)S20AD (Fig. 3.23 B and C), the microgel particles are quite small, especially in the latter where they are at the edge of the resolution limit of the SEM used and are hardly discernable. Their porous structures are therefore much more homogeneous and uniform across the materials. These features are consistent with polymerisation in the precursor emulsions occurring in an organic medium which is a good solvent for the polymeric network. In fact, when the polymerisation is run in the presence of an inert diluent that is a good solvent for the polymer, two levels of particle substructure instead of three, as discussed previously, are formed. The polymer texture is built up of rather large nuclei (20-50 nm) and agglomerates but not microspheres. The quality of the solvent medium does not change much during the course of polymerisation. Because the polarity within the separated nuclei is not very different from that of the surrounding solution, monomers are not forced to adsorb preferentially into the nuclei and the polymerisation proceeds with formation of nuclei that remains individualised. As a result, a larger number of individual nuclei compete for the remaining monomers. This leads to a large number of small microglobules that aggregate thus forming the macroporous structures with fine individual microglobules. This leads to an increased microporosity that enhances the internal surface area. The employment of an increasing fraction of crosslinking monomer generally leads to

porous structures with larger surface areas and smaller pore sizes. The phase separation takes place at a lower monomer conversion for systems with a high fraction of crosslinker. Both the adsorption of monomers and the coalescence of nuclei are limited as a result of their crosslinking. Thereby, the number of smaller individual nuclei remains large and smaller microspheres persist.

Since the real level of cross-linking is known to be an important parameter in the generation of the porous morphology of resins, [49, 50] contributing substantially to controlling the point of phase separation of the growing polymer matrix from the porogen, it was thought important to assess the level of unreacted C=C bonds in the foams. We have already pointed out how the swelling properties of the reaction medium in the continuous phase depended on the nature of the surfactant system employed. When the mixture of surfactant was employed Ostwald ripening was successfully hampered as compared to the situation in which SPAN 80 was used as a surfactant. We wondered if the quality of the solvent medium had an effect on the degree of conversion of DVB double bonds, which would then influence the gel point and hence contribute to the differences in surface areas observed in pairs of foams differing only in the surfactant system used (for instance X80PV90(1T)S80 and X80PV90(1T)S20AD) and similars). To this end, quantitative ^{13}C solid state NMR was employed in order to obtain an estimation of the level of unreacted double bonds. An example of the spectra obtained is shown in Fig. 3.24a and b. In (a) is reported the experimental spectrum showing the ppm position of peaks. In (b) the deconvoluted peaks and the calculated spectra are reported. The peak assignements are illustrated together with the chemical structure in Fig. 3.25. The degree of unreacted double bonds resulted to be about 30% independently of surfactant system and nature of porogen used. This means that the quality of the solvent medium determines pore structure directly through the point of gelation and not via the degree of conversion of double bonds. Quantitative estimation of the degree of crosslinking in polyHIPE foams made from DVB 80%, allowed the calculation of its cohesion solubility parameter and of its components by employing the Hoy approach [16] and Eq. 6

$$\overline{\delta}_i = \phi_1\delta_{1i} + \phi_2\delta_{2i} + ...\phi_n\delta_{ni} \qquad (6)$$

where ϕ represents the volume fractions, and the index i, the type of dispersive interaction (d, p and h) [12]. The solubility parameter δ resulted to be 20.5 $(MPa)^{1/2}$. Even if this data must be considered with caution because of the uncertainty inherent in the method of calculation it is striking the match of this value with that referring to the solubility parameter of C_2B (Table 3.III). A much better correlation may be provided by three dimensional cohesion parameter δ_t,

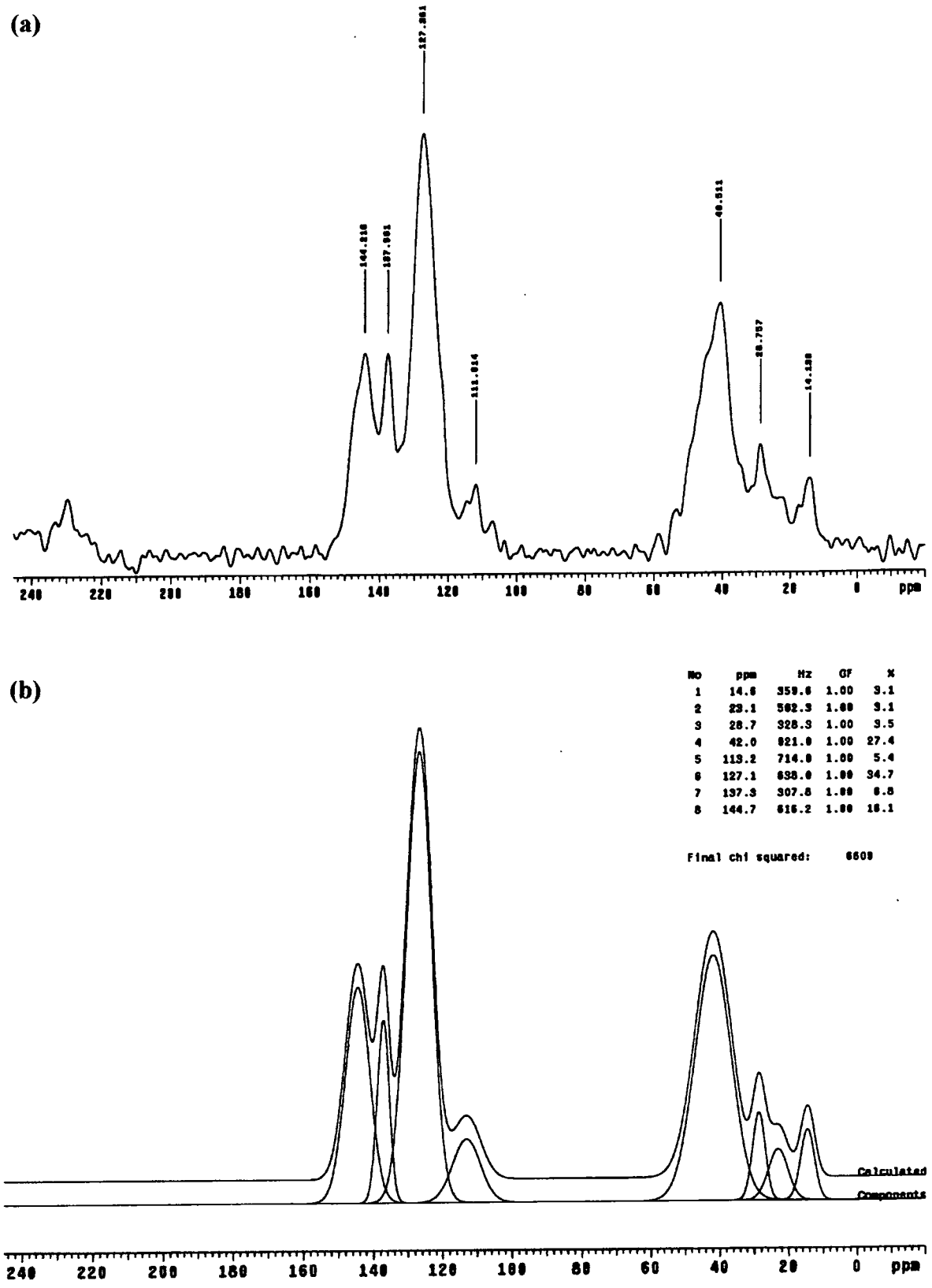

Fig. 3.24. Solid state ^{13}C SPE NMR of dry poly(DVB 80%)HIPE. In (a) is shown the experimental spectrum; in (b) the deconvoluted (calculated) and calculated spectra are shown.

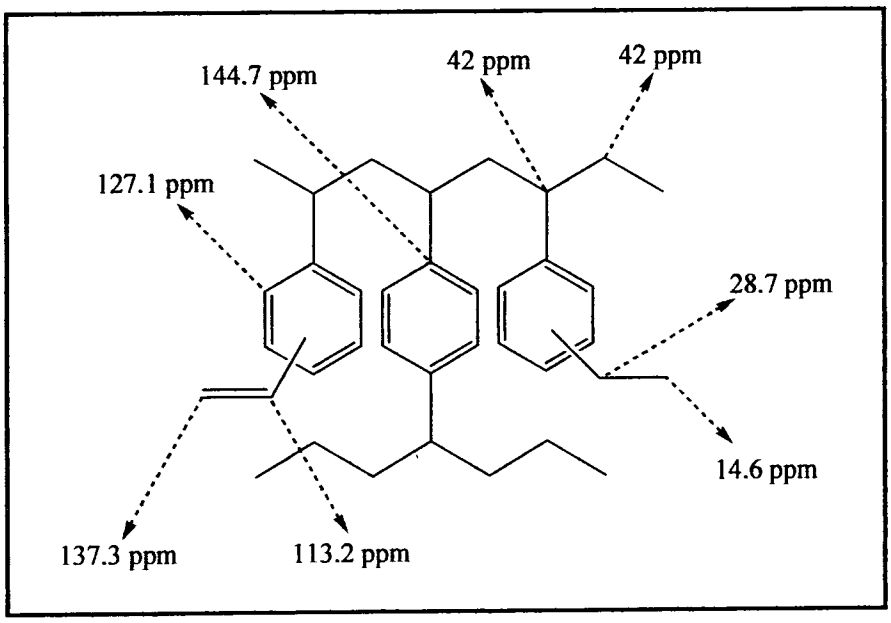

Fig. 3.25. Peak assignements of the ^{13}C solid state NMR spectra of poly(DVB 80%).

which considers the contributions from from dispersive, δ_d, dipolar, δ_p, and hydrogen bonding, δ_h, interactions:

$$\delta_t^2 = \delta_d^2 + \delta_p^2 + \delta_h^2 \tag{7}$$

In a three dimensional diagram the porogen and polymer can be represented by two points, and the polymer-porogen affinity can be described by the distance d_0 between the two points:

$$d_0^2 = 4(\delta_{d1} - \delta_{d2})^2 + (\delta_{p1} - \delta_{p2})^2 + (\delta_{h1} - \delta_{h2})^2 \tag{8}$$

The indices 1 and 2 represent the polymer and porogen, respectively.

The calculated polymer (poly(DVB))-porogen affinity are reported in Table 3.III. The correlation between d_0 and surface areas is strictily applicable only to the resins obtained by bulk polymerisation because as it has been pointed out in the case of foams other factors are intervening in determining their porous structures. For the resins the correlation with surface areas results show that d_0 decreases when the progen is changed fron T to CB and C_2B indicating that quality of these solvent improve towards poly(DVB) in the same order. From d_0 values regarding CEB and CPP, it seems that these solvents are even better porogens than the previous ones but this forecast is contradicted by surface area results which indicate that these solvents are slightly worse than C_2B. The origin of this discrepancy is probably due to the approximation inherent in the calculation of the solubility parameters of CEB and CPP and of poly(DVB) which are presumably higher than differences in the surface areas of the corresponding resins. This finding confirms that this porogen is the best for poly(DVB 80%)

and that the solubility parameter of this polymer is very close to20.5 $(MPa)^{1/2}$.

TEM micrographs, Fig. 3.26, at a magnification of 4600 ×, provide a direct evidence that the porous structure of the walls of the foams is determined mainly (partitioning of the porogen between aqueous and organic phases can also, to some extent, play a role) by diffusion of water through the continuous phase.

In a a finite volume fraction systems, the detail of the spatial distribution of the particles plays a role in determining the ripening behaviour of the system. This is seen by considering the difference in interfacial concentration between two particles of different size, as expressed by the Gibbs-Thomson equation (chapter 1, §1.4, Eq. 16), and the distance between these two particles. For example, if a small particle is located near a large particle, it will have a larger dissolution rate than when it is located at the same distance from a particle of nearly of the same size, since in the former case the interfacial concentrations of the particles are quite different, whereas in the latter case the interfacial concentrations of both particles are nearly the same. In a finite volume fraction system, particles of the same size will coarsen at different rates depending on the local distribution of the other particles in the system. Interparticle diffusional interactions can also influence the morphologies of the coarsening domains. Even under the assumption of isotropic interfacial energy, the particles may not possess the spherically symmetric morphology assumed in the LSW theory [32, 33], but rather a shape that is related to the strength of the local interparticle diffusional interactions.

In the present case it must be remembered that the morphology of the foams is a replica of the emulsion structure at the gel point and its features result from processes taking place in it. Hence, small droplets undergoing the ripening process are surrounded by a diffusion layer characterised by a concentration gradient fading out as the distance from the droplet surface increases. As the concentration of water is higher in the layers of continuous phase adjacent to the droplets surface, the porosity of the foam near the surface of cavities should be locally coarser than in the bulk because there, the quality of the solvent is worse.

From TEM micrographs reported in Fig. 3.26a and b it is evident that the symmetry of the small droplets shown (diameters of about 1 μm) deviate remarkably from a spherical one, showing the presence of branches protruding out from the cavity surface. On the contrary, much larger droplets have much smoother surfaces. The rate at which Ostwald ripening occurs, is affected by the distance between the droplets since the dispersed material must be transported between them. Hence, this process will be accelerated when droplets are more densely packed [51]. The volume fraction dependence is included in LSW theory simply as a

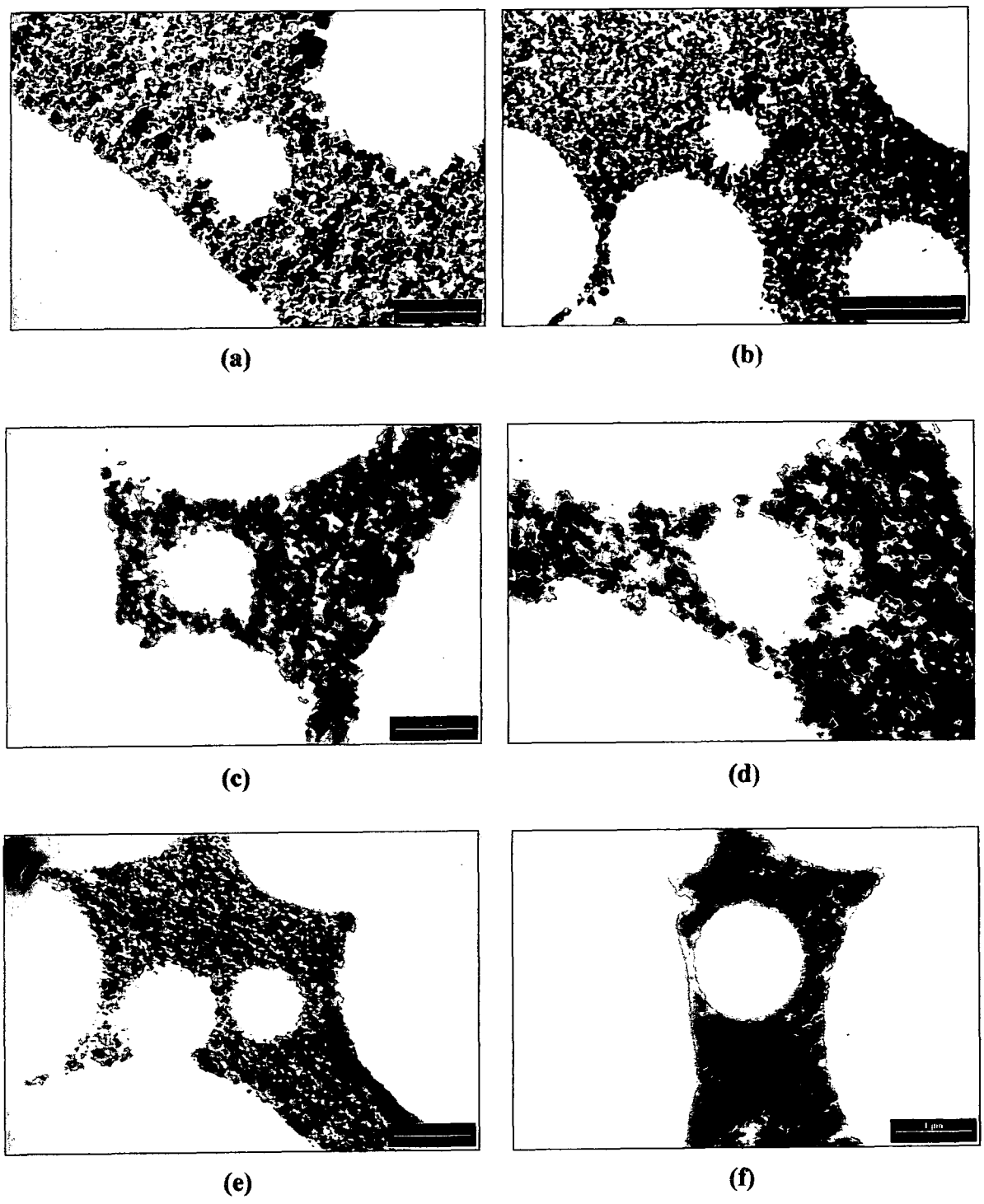

Fig. 3.26. Transmission electron micrographs showing details of droplets morphology of polyHIPE foams: (a) X80PV75(1CB)S80; (b) X80PV85(1CB)S80; (c) X80PV90(1CB)S80;(d) X80PV92(1CB)S80; (e) X80PV90(1CB)S20AD; (f) X80PV90(1T)S20AD. Scale bar 1 and 5 μm.

multiplication factor $f(\phi)$. A number of theoretical studies have examined $f(\phi)$ [52-57]. Analytical solutions are not availaible, hence only numerical solutions have been proposed.

The most discussed of these has been the theory of Enamoto *et al* [52]. The rate is predicted to increase by a factor of 2.5 in the range of $\phi = 0.01$ to 0.3.

The difference in surface areas encountered in the series X80PVN(1CB)S80 may reflect the dependance of diffusion rates on $f(\phi)$. To what extent this phenomenon is responsible for the differences in surface areas is difficult to evaluate. In the literature there are neither theoretical studies nor experimental results concerning the influence of the volume fraction of the dispersed phase on Ostwald ripening rates in the range of the high values of ϕ characteristic of concentrated emulsions ($\phi \geq 0.74$). Anyway, the comparison of the details in the morphology of small droplets and of the porous structure in the portion of the foam surrounding small cavities between foams characterised by 75 or 85% PV and those at 90 and 92% PV allows some differences to be discerned. For instance in the case of X80PV90(1CB)S80 (Fig. 3.26c) and particularly in X80PV92(1CB)S80 (Fig. 3.26d) the porosity of the foams in the proximity of the surface of small cavities tends to be coarser and to span longer distances when compared to those of X80PV75/85(1CB)S80 (Fig. 3.26a and b). This is likely to be the result of an increased interaction between diffusion spheres of neighbouring droplets. When the mixture of surfactants is used, as in the case of X80PV90(1CB)S20AD, (Fig. 3.26e) which is characterised by a very high surface area, cavities of about 1 μm appear spherically symmetrical and the diffusion layer across the droplet boundary is much thinner. This is unequivocally the result of much less intense diffusional fluxes originating from smaller droplets. When T is used as the porogen in connection with the mixture of surfactant, no sign of diffusion is discernable around small droplets (Fig. 3.26f)). The surface area of X80PV90(1T)S20AD is slightly higher than that of X80PV90(1CB)S20AD and considering that it differs from that of polyDVB(T) by about 5% only, it can be concluded that diffusion is almost completely stopped.

In order to test the possibility that temperature of polymerisation exerts an influence on the surfactant c.μ.c., the polymerisation of a few foams was carried out at 100 °C and the values of their surface areas as determined by nitrogen adsorption were compared with those of foams of the same composition but obtained at 60 °C. Results are reported in Table 3.VIII. As can be seen, for both X80PV90(1CB)S80 and X80PV90(1CB)S20AD (entries 1 and 2) foams the values of surfaces areas obtained either at 60 (Table 3.II and 3.6, entry 3) or 100 °C are the same within experimental error. This is not a surprising result considering the chemical structure of the surfactants used in the present study. Usually, a strong dependance of c.μ.c. on temperature is expected for those surfactants containing a poly(ethylene oxide) moiety in

Table 3.VIII. Nitrogen adsorption results for PolyHIPE foams obtained at a polymerisation temperature of 100 °C. PV = 90 %. The porogens used are either CB, or a 1:1 vol:vol mixture of CB and CEB. Monomer to porogen ratio = 1:1. The surfactants employed are either SPAN 80 or a mixture of SPAN 20, DDBSS and CTABr.

	SAMPLE	Surface Area (m^2/g)[a]	Pore Volume (cm^3/g)[b]	Average Pore Diameter (nm)[c]	Micropore Volume (cm^3/g)[d]	Micropore Area (cm^2/g)[d]
1	**X80PV90(1CB)S80**	334 ± 25	0.91 ± 0.09	11.0 ± 0.6	0	0
2	**X80PV90(1CB)S20AD**	703 ± 24	0.91 ± 0.08	5.1 ± 0.08	0.12 ± 0.009	47 ± 8
3	**X80PV90(0.5CB+0.5CEB)S20AD**	693 ± 31	0.88 ± 0.05	5.2 ± 0.2	0.005 ± 0.003	26 ± 12

[a] from BET; [b] from BJH adsorption;

[c] from BJH adsorption;

[d] from t-Plot.

their structure capable of undergoing chain contraction or expansion (a phenomenon accompanied, in appropriate conditions, by phase inversion) with temperature variation. The surface area of X80PV90(0.5CB+0.5CEB)S20AD seems to exhibit a slight dependance on temperature (compare entry 3 of Table 3.VIII with entry 7 of Table 3.IV). From results obtained for X80PV90(1CB)S20AD, the nature of the primary surfactants can be ruled out as the cause of this small temperature effect. Therefore, it seems more reasonable to ascribe it to the composition of the porogenic mixture and in particular to the presence of CEB. It is impossible at this stage of the investigation to assess whether this temperature dependance is a consequence of a variation in the interfacial surfactant/co- surfactant structure or reflects the influence of temperature on the partition coefficient of CEB In any case the effect of temperature is modest.

As has already been pointed out, when C_2B is used as a porogen together with the mixture of surfactants, a foam, X80PV90(1C_2B)S20AD, with the lowest surface area (among foams prepared with the mixture of surfactants) is obtained in spite of the fact that it is the best porogenic solvent for DVB 80% (Table 3.VI, entry 3). On the contrary when C_2B is used together with SPAN 80 the foam produced has, among single porogen foams, the highest surface area (Table 3.II, entry 3). The set of data presented indicate that the interaction between surfactants and porogens is the major factor in determining the final foam characteristics. Another important factor is represented by the intrinsic physical properties of the porogens, in particular we believe that their polarity and hydrogen bonding capabilities play a fundamental role. Data reported in Table 3.I show that when surface areas of foams of the X80PV90(1P)S80 type are arranged according to porogen polarity a maximum is reached in correspondence of C_2B which is characterised by a value of δ_p and δ_h (see Table 3.III) midway those of CB and CEB. This may means that C_2B presents the best compromise between a few effects working in opposition with each other:

1. its ability to be adsorbed at the interface thus reducing Ostwald ripening through its contribution in lowering the interfacial tension,
2. its polarity and hydrogen bonding formation capability, on the contrary, promote water dissolution in the organic phase and the extent of its partitioning between the two phases;
3. its influence on surfactant c.μ.c. and as a consequence on the degree of covering of the interfacial layer by the surfactant molecules.

CB has (similar considerations apply for T), among the porogens examined here, a relatively low polarity and shows limited interfacial activity. This means that because its ability of penetrating the surfactant layer is limited, the reduction of the interfacial tension is also

relatively low. At the same time it is a sufficiently polar molecule to confer to the organic phase the capability of dissolving a relatively large amount of water. This balance is clearly shifted towards the latter contribution because as shown by N_2 adsorption data (Table 3.II, entry 2) and images of microstructure (Fig. 3.23, panels A and D), the organic medium in the precursor emulsion is a relatively thermodynamically poor solvent for polyDVB 80%.

At the other end of the polarity scale there are CEB and CPP which as has been shown previously, exhibit a good ability to penetrate the surfactant monolayer and reduce the interfacial tension. At the same time their values of δ_p and δ_h are high enough so that the equilibrium concentration of water dissolved in the organic phase ($c(\infty)$) and its aqueous/organic phase partition coefficient are the highest. This argument is coherent with values of surface areas of the two foams X80PV90(0.5CEB)S80 and X80PV90(1CEB)S80 (entries 5 of Table 3.V and 4 of Table 3.II, respectively). The lower surface area of the former could be attributed to the relevant tendency of CEB molecules of being adsorbed at the interface, depleting the bulk of the organic phase of porogen and thus explaining why the surface area is less than half that of X80PV90(1CEB)S80. The action of CEB molecules adsorbed at the interface seems to be only to lower the interfacial tension and not to contribute in forming a physical barrier against the transfer of molecules through the interface. The difference in values of surface areas between DVB(CEB) (Table 3.V, entry 4) and X80PV90(1CEB)S80 is relevant and can be explained only by assuming that diffusion and partitioning of CEB molecules are still taking place extensively.

When the 1:1 mixture of CB and CEB is used, the polarity of the organic medium (Table 3.III, entry 8) is lower than the case in which the porogenic solvent is composed completely by CEB. The aqueous phase is probably saturated by the more soluble CEB, which is also being adsorbed at the interface partially preventing Ostwald ripening. In this condition, CB and the fraction of CEB left in the bulk of the organic phase produce the expected porogenic activity of such solvents. C_2B is a molecule which in terms of polarity and hydrogen bond capability is midway between CB and CEB. Its behaviour resembles closely that of the mixture of CB and CEB. The morphology of the foam obtained by employing C_2B as a porogen slightly resembles that of X80PV90(1CEB)S80 (Fig. 3.3d). In fact it is characterised by a partially collapsed structure as evidenced by SEM (Fig. 3.3c) and the TEM micrograph (Fig. 3.5c) shows that the degree of overlapping is higher than in X80PV90(1CB)S80 but less than those of X80PV90(1CEB/CPP)S80. In other words, the drop in interfacial tension caused by the adsorption of C_2B molecules at the interface is high enough to provoke a substantial

thinning of the interfacial layer which is responsible for the partially collapsed structure that characterises this foam.

We can conclude that when SPAN 80 is used as a surfactant the structure of the final foams is dictated by the physical properties of the porogens employed. The polarity of porogens shown in Table 3.III increases steadily from T to CPP, while the interfacial tension due to the adsorption at the interface decreases. As a consequence, it can be inferred that a situation of best compromise will be reached for that porogen which is polar enough to exhibit good interfacial activity, thus limiting diffusion of water through the organic phase, but at the same not too polar to greatly increase the solubility of water in the organic phase. When C_2B or the 1:1 mixture of CB and CEB are used, the combined influence of γ and $c(\infty)$ on $\omega(t)$ is at its minimum and the foams prepared from such porogens are characterised by the highest surface areas.

When the mixture of surfactants is used, a completely different behaviour is observed in connection to the nature of the porogens used. When the surface areas are considered as a function of the values of δ_p and δ_h of the porogens used (Table 3.III) no clear trend is discernible. Conversely, when differences between the surface areas of the resins and foams prepared with the same porogen are arranged according to the polarity of the porogen employed, it can be seen that with the exception of C_2B, as the polarity of the porogen increases, the said difference in surface areas increases, indicating that the solvent quality decreases in the same fashion. When the 1:1 mixture of CB and CEB is used the surface area of the corresponding foam is slightly lower than that of X80PV90(1CB)S20AD but significantly higher than X80PV90(1C_2B)S20AD. This effect can again be explained in term of insertion of polar additives molecules between adjacent surfactant molecules. Clearly a high polarity of the porogen corresponds to a decreased interaction between ionic surfactants molecules. This effect was described a long time ago by Winsor [58] and is responsible for the dramatic variation of the CMC of ionic surfactants when present in polar solvents. As a result of this "spacing" of the ionic groups, attractive interactions among head groups, which are probably responsible for the formation of a compact interfacial film, are subdued and contact between the aqueous and exposed organic phase is enhanced. As a result of these openings through the interfacial surfactant film, water and porogen molecule can diffuse worsening substantially the quality of the reaction medium. There is no simple explanation about the peculiar behaviour exhibited by C_2B which deviates dramatically to the trend described above. Clearly, the effect of this porogen on the surfactant interfacial layer is somewhat disruptive as evidenced indirectly by the large difference in surface areas between

polyDVB(C_2B) and X80PV90(1C_2B)S20AD. A possible explanation may be related to the chemical structure of this molecule which in comparison to the other porogens employed is sterically bulkier and its insertion in the interfacial surfactant layer may partially break down the continuity of the surfactant film. It was shown that the orientation of substituents on the aromatic ring is important [59, 60] in affecting the geometry of surfactants aggregates and the value of surfactants CMC.

The evidence offered by TEM images (Fig. 3.26) which seem to point to a more efficient barrier effect exerted by the mixture of surfactant as compared to SPAN 80 alone, is further supported by measurements of the NMR self-diffusion coefficient of water in the emulsions ($\phi = 0.9$) containing SPAN 80 or the mixture of surfactants (Fig. 3.27). The value of the self-diffusion coefficient of water results to be of about 4.5×10^{-10} $m^2\cdot sec^{-1}$ in the presence of the mixture of surfactants and 7×10^{-10} $m^2\cdot sec^{-1}$ in the presence of SPAN 80. This means that the transfer of water out of the dispersed aqueous phase and its diffusion through the continuous one is hampered more effectively when the mixture of surfactants is employed instead of SPAN. An interesting feature, which ensues from the comparison of the diffusion coefficient *vs.* time curves, is the behaviour of the portion of the curves close to the y axis. In the case of the SPAN 80 curve (see Fig. 3.27), with the exception of the first, all the points of the curve are parallel to the x axis, which means that the diffusion coefficient is constant with time. In the case of the mixture of surfactants, on the contrary, the first portion of the curve is characterised by a small positive gradient. The diffusion coefficient of water grows slightly during approximately the first five hours. This might mean that as the mixture of surfactants is more effective in preventing the passage of water from the dispersed to the continuous phase the time for the attainment of the stationary stage is longer.

While the experimental evidence offered by NMR diffusion coefficient measurements in the two surfactant systems give a quantitative evaluation of the difference in permeability to water molecules of the two surfactant films, it must be remembered that measurements were carried out at 25 °C. This is very different from the conditions experienced by emulsions during polymerisation, which is carried out at 60 °C. The diffusion coefficient is strongly dependant on temperature in the sense that it increases with temperature and we do not know how the two surfactant films respond, as far as permeability is concerned, to variation of temperature. It might be that differences in permeability of the two surfactant films to water molecules increases. On the other hand results of surface areas of foams prepared at different temperature do not seem to show to be influenced by temperature.

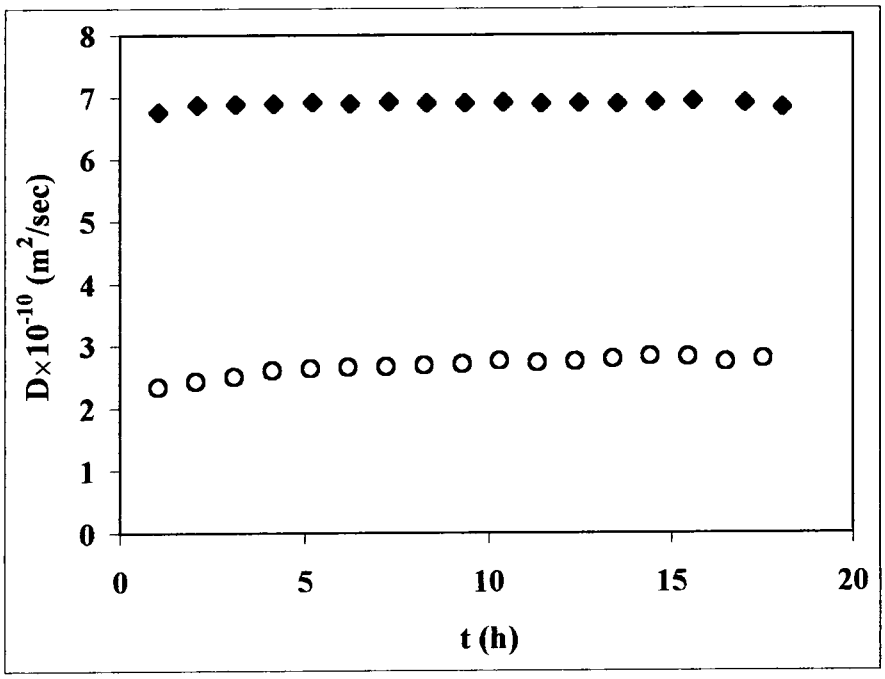

Fig. 3.27. Self-diffusion coefficient of water, at 25 °C, in two emulsions of the same composition of the continuous and dispersed phases (DVB 80% and CB) but incorporating two different kind of surfactants: (◆) SPAN 80; (○) mixture of SPAN 20, DDBSS and CTABr.

The measurement of the water diffusion coefficient was carried out also for emulsions characterised by different fractions, ϕ, of the dispersed phase, that is 0.75, 0.85 and 0.92 for both the surfactant systems. Diffusion curves at different ϕ were coincident for both sets of emulsions. This implies that for the emulsions containing either SPAN 80 or the mixture of surfactants and CB as a porogen, no difference in the surfactant excess at the interface should be expected, as the extent of diffusion is the same for all emulsions having different ϕ. The difference in surface areas, which as already pointed out previously depends on the quality of the solvent medium, should then be ascribed to differences in the extent of interaction among droplets of the dispersed phase (the parameter $f(\phi)$ in Eq. 5). Fig. 3.26a and b show that in the case of foams characterised by a pore volume of 75 and 85, droplets are on the average more separated than in the case of foams with higher pore volume (90 and 92%, Fig. 3.26c and d). As a consequence, the superimposition of diffusion spheres is less pronounced and the worsening of the quality of the solvent medium is less marked. As the volume fraction of the dispersed phase increases, water droplets come closer and closer and their diffusion domains superimpose to a greater extent. As a consequence, the local concentration of water molecules

3.3.7 Conclusions

The influence of different aromatic porogens used singularly or as 1:1 mixture on the morphology of DVB80% polyHIPE foams were studied.

The porogens affect the morphology and porosity of foams through the interplay of two mechanisms:

1.the porogens used tend to be co-adsorbed to a different extent at the oil-water interface together with the primary surfactant contributing to lower proportionally the interfacial tension;

2. the diffusion of the dispersed phase through the continuous one (Ostwald ripening).

Effect 1 determines the morphology of the polyHIPE foams in terms of cavities and interconnecting windows diameter and the thickness of wall cavities.

Effect 2 determines the level of porosities of foams walls and as a consequences their surface areas.

It was shown that the physical parameter of porogen molecules relevant to the described behaviour is represented by their three dimensional cohesion parameter. In particular the values of the polar and hydrogen bond components affects both to what extent porogens are adsorbed at the interface and the overall polarity of the continuous phase. This last feature determines the bulk solubility of water in the organic phase and as a consequence the magnitude of diffusion of water through the organic phase. The concentration of water in the monomer + porogen phase affects the quality of the reacting medium, determining the point at which the growing polymeric network phase separates and the final porous structure of the foam.

It was shown that the chemical structure of the surfactant used to stabilise the emulsion has a relevant influence as far as effect 2 is involved. When SPAN 80 was used, partitioning of porogen and water diffusion through the continuous phase is relatively high. This has been monitored for the different porogens used through measurements of N_2 porosimetry of the resulting foams. When the surfactant system was turned to a mixture of surfactants, that is SPAN 20, dodecylbenzene sulfonic acid, sodium salt and cetyltrimethylammonium bromide, partitioning and water diffusion were drastically reduced and surface areas resulted twice higher than those obtained for the same porogen when using SPAN 80.

Bibliography

[1] E.C. Peters, F. Svec, J.M.J. Freschet, *Adv. Mater.*, 1999, **11**, 1169.

[2] P. Haney, I.M. Huxam, B. Rowat, D.C. Sherrington, I. Tetley, *Macromolecules*, 1991, **24**, 117.

[3] S. Brunauer, P.H. Emmet, E. Teller *J. Am. Chem. Soc.* 1938, **60**, 309.

[4] *Porosity and pore size distribution of materials*, BS 7591: Part 2: 1992.

[5] K.S. Sing, D.H. Everett, R.A.W. Haul, L. Moscou, R.A. Pierotti, J. Roquerol, T. Siemieniewska, *Pure Appl. Chem.*, 1985, **57**, 603.

[6] J.M. Williams, A.J. Gray, M.H. Wilkerson, *Langmuir*, 1990, **6**, 437.

[7] D. Gregory, M. Sharples, J.M. Tucker, Eur. Pat., 299 762, 1989.

[8] N.R. Cameron, D.C. Sherrington, L. Albiston, D.P. Gregory, *Colloid Polym. Sci.* 1996, **274**, 592.

[9] T. Rohr, S. Knaus, H. Gruber, D.C. Sherrington, *Macromolecules*, 2002, **35**, 97.

[10] D.C. Sherrington, *Chem. Commun.*, 1998, 2275.

[11] D. Rabelo, F.M.B. Coutinho, *Polym. Bull.*, 1994, **33**, 493.

[12] D. Rabelo, F.M.B. Coutinho, *Polym. Bull.*, 1994, **33**, 487.

[13] D. Rabelo, F.M.B. Coutinho, *Eur. Polym. J.*, 1994, **30**, 675.

[14] I.C. Poinescu, C.-D. Vlad, *Eur. Polym. J.*, 1997, **33**, 1515.

[15] J. Brandrup, E.H. Immergut, E.A. Grulke, *Polymer Hanbook*, Wiley, New York, 1999.

[16] D.V. Kevrelan, *Properties of Polymesr*, 3rd ed.; Elsevier, Amsterdam, 1991; Chapter 7, p. 189.

[17] A. Boyde, *Scanning Electron Microscoppy*; O.C. Wells, ed.; McGraw-Hill: New York, 1974.

[18] A.S. Kabalnov, K.N. Makarv, A.V. Petsov, E.D. Shchukin, *J. Coll. Interface Sci.*, 1990, **138**, 98.

[19] J.M. Williams, D.A. Wrobleski, *Langmuir*, 1988, **4**, 656.

[20] P.A. Small, *J. Appl. Chem.*, 1953, **3**, 71.

[21] M.P. Aronson, M.F. Petko, *J. Coll. Interf. Sci.* 1993, **159**, 134.

[22] J. C. Ravey, M. J. Stebe, S. Sauvage, *Colloid Surf.* 1994, **91**, 237.

[23] R. Pons, J. C. Ravey, M. J. Stebe, P. Erra, C. Solans, *Prog. Colloid Polym. Sci.*, 1990, **82**, 218.

[24] R. Pons, J. C. Ravey, S. Sauvage, M. J. Stebe, P. Erra, C. Solans, *Colloid Surf.* 1993, **76**, 171.

[25] Pons, J. C. Ravey, M. J. Stebe, P. Erra, C. Solans, *J. Phys Chem.* 1993, **97**, 2320.

[26] R. O. Foyeke, O. Burgess, D.J. Burgess, *J. Coll. Inter. Sci.* 1998, **197**, 142.

[27] M.A. Krawczyk, D.T. Wasan, C.S. Shetty, *Ind. Eng. C Res.* 1991, **30**, 367.

[28] B. D. Binks, P.D.I Fletcher, D.I. Horsup, *Colloid Surf.* 1991, **61**, 291.

[29] B. Vonnegut, *Rev. Sci. Instr.* 1942, **6**, 13.

[30] B. P. Santora, M.R. Gagne`, K. G. Moloy, N. S. Radu, *Macromolecules*, 2001, **34**, 658.

[31] Guyot, in *Synthesis and Separation Using Functional Polymer*; D.C., Sherrington, P. Hodge, Eds; John Wiley: London, 1988; chap I.

[32] I. M. Lifshitz, V.V. Slezov, L., *Phys Chem. Solids*, 1961, **19**, *35*.

[33] C.Z. Wagner, *Elecktrochem.*, 1961, **581**, 65.

[34] A.S. Kabalanov, A.V. Pertsov, E.D. Shchukin, *Adv. Colloid Interface Sci.*, 1987, **118**, 590.

[35] D.J. Mitchel, B.W. Ninham, *J. Chem. Soc., Faraday Trans. 2*, 1981, **77**, 601.

[36] R. Aveyard, B.P. Binks, P.D.I. Fletcher, J.R. MacNab, *Langmuir*, 1995, **11**, 2515.

[37] A. Barbetta, N.R. Cameron, S.J. Cooper, *Chem. Commun.*, 2000, 221.

[38] M.J. Rosen, *Surfactant and Interface Phenomena*, 2nd edn., Wiley, 1989, p. 6.

[39] Th.F. Tadros, B. Vincent, in *Encyclopedia of Emulsion Technology*, ed. P. Becher, Marcell Dekker, Vol. 1, 1983.

[40] A.E. Alexander, J.H. Schulman, *Trans. Faraday Soc.*,1940, **36**,960.

[41] B.W. Barry, *Rheol. Acta,* 1971, **96,** 10.

[42] G.W. Hallworth, J.E. Carless, *J. Pharm. Pharmac.* 1972, *24*, Suppl., 71.

[43] R.M. Bass, T.F. Brownscombe, *WO9745479,* **1997**.

[44] P.A. Webb, C. Orr, *Analytical methods in fine particle technology*, 1997, Micromeritics Instrument Corp.

[45] W. I. Higuchi, A. H. Goldberg, *J. Pharm. Sci.*, 1969, **58**, 1342.

[46] T. Yotsuyanagi, W. I. Higuchi, A. H. Ghanem, *J. Pharm. Sci.*, 1973, **62**, 40.

[47] A. S. Kabal'nov, E. D. Shchuckin, *Adv. Colloid Interface Sci.* 1992, **38**, 69.

[48] A. Kari Nyhus, S. Hagen, A. Berge, *J. Polym. Sci.: Part A* 1999, **37**, 3973; Idem. *J. Appl. Polym. Sci.* 2000, **76**, 152.

[49] R.L. Albright, *React. Polym.*, 1986, **4**, 155.

[50] O. Okay, *Prog. Polym. Sci.*, 2000, **25**, 711.

[51] J.G. Weers in *Modern Aspects of Emulsion Science*, B.P. Binks Ed., The Royal Society of Chemistry, 1998.

[53] P.V. Voorhees, *J. Stat. Phys.*, 1985, **38**, 231.

[54] C.W. Beenakker, *Phys Rev. A,* 1986, **33**, 4482.

[55] J.A. Marquise, J. Ross, *J. Chem. Phys.*, 1984, **80**, 536.

[56] A.D. Brailsford, P. Wynblatt, *Acta Metall.*, 1972, **20**, 61.

[57] G. Venzl, *Ber. Bunzenges Phys. Chem.*, 1983, **87**, 318.

[58] P. A. Winsor, *Manuf. Chem.*, 1956, **89**, 130.

[59] K. Horbaschek, H. Hoffmann, C. Thunig, *J. Colloid Interf. Sci.*, 1998, **206**, 439.

[60] R.T Buwalda, M.C. Stuart, J.B.N. Engberts, *Langmuir*, 2000, **16**, 6780.

PREPARATION AND CHARACTERIZATION OF DVB AND 4-VINYLBENZYL CHLORIDE PolyHIPE MATERIALS

Chapter 4

PREPARATION AND CHARACTERIZATION OF DVB AND 4-VINYLBENZYL CHLORIDE PolyHIPE MATERIALS

4.1 Introduction

During the course of our work in developing novel PolyHIPE materials we undertook the preparation of species containing 4-vinylbenzyl chloride (VBC). This monomer is sufficiently hydrophobic to allow successful HIPE preparation, and results in material possessing reactive chloromethyl functionalities that are amenable to functionalization, potentially leading to a wide range of derivatized highly porous materials. VBC has been used previously to prepare HIPEs where it was present in either the droplet [1-3] or the continuous phase [4-7] leading to the production of agglomerates of particles or foams, respectively. However, the influence of VBC on the emulsion and resulting polymer morphology was not described. In general the initial properties of the emulsion-derived foam will depend most strongly on the physical properties of the starting monomer and on the presence of additives either in the organic or/and aqueous phase. For instance, in situation where water is the pore forming phase, solutes in the water phase can be used to affect emulsion properties. These solutes may take the form of solute salts or water phase miscible liquids. These materials affect both the overall system interface tension and partition themselves along the surfactant interface. On the other hand, additives in the organic phase such as aromatic compounds have the tendency to be adsorbed at the oil/water interface. For micellar solutions there is evidence that aromatic molecules are located in the polar interface layer in preference to the more hydrophobic regions of the aliphatic hydrocarbon chains of the surfactant [8]. The presence in the molecule of a polar functionality tends to confer to these compounds a more pronounced interfacial activity. When polar aromatic compounds bearing a chlorine atom are used as additives (porogens) in the organic phase, the effects on the final polyHIPE foam are quite dramatic (Chapter 3). The overall "openness" or interconnectivity and cavity dimension of the emulsion-derived foams resulted to be strongly affected by the choice of these additives.

This functional polyHIPE can lead to chemically modified supports. Of great interest is the ability to perform experiments by cross-flow through the polyHIPE structure without stirring which can damage conventional resin by abrasion. It is then possible to automate reactions with the help of a suitable pump which forces the medium to circulate through a monolithic polyHIPE. In that way the conversion rate may be easily improved without resin deterioration. Nevertheless cross-flow experiments remain quite expensive due to the large cell volume of PolyHIPEs: the filling of its voids by fluid phases involves a large amount of solvent and

components. Therefore it is of great interest to find a way to decrease the average cell size in order to obtain a PoyHIPE with low volume uptake. Another field of application might be represented by liquid chromatography. Also in this respect it is necessary to achieve a high degree of control over foam morphology. For instance, a wide distribution in window diameter is to be avoided because it is likely to result in an inhomogeneous flow of the mobile phase. This can be better understood by mean of the Poiseuille equation:

$$v = \frac{(P_0 - P_L)}{4\mu L} \sum_i R_i^2 \left[1 - \left(\frac{r}{R_i} \right)^2 \right] \qquad (1)$$

where $P_0 - P_L$ is the pressure drop along a tube, L its length and μ is the viscosity of the solvent. The summation is extended over all interconnecting windows of radius R_i, and r is the distance of a generic volume element of liquid from the centre of the hole i. This equation states that the velocity distribution for laminar incompressible flow in a tube is parabolic. If we imagine a chromatographic column filled with a foam made of VBC and DVB and a solvent carrying a solute or a mixture of solutes flowing through it, as in a chromatographic separation, it is to be expected that a wide distribution in window size will cause band broadening. This clearly represents a limitation to the possible applications of these materials.

4.2 Experimental section

4.2.1 Materials

4-vinylbenzylchloride (Aldrich), styrene (Aldrich), and divinylbenzene (Aldrich; 80 %vol *m*- and *p*-divinylbenzene, the remainder being *m*- and *p*-ethylstyrene), were purified by passing through a column of basic alumina to remove the inhibitor. Potassium persulfate (Aldrich), sorbitan monoleate (Aldrich; Span 80, HBL=4.3), calcium chloride dihydrate (Avocado) were used as supplied.

4.2.2 PolyHIPE Preparation

The experimental procedure followed for the preparation of PolyHIPE foams has already been described in the experimental section of chapter 3 (§ 3.3.2).

4.2.3 PolyHIPE Coding System

The content of 4-vinylbenzyl chloride and styrene monomers in the S-VBC polyHIPE foams are specified before the crosslink density, with V representing 4-vinylbenzyl chloride while S stands for styrene, for example V20S17.5X50PV90 is the code for a material

containing 20% 4-vinylbenzyl chloride, 17.5% styrene relative to total monomer and crosslinker content and X and PV represent the crosslink density and pore volume, respectively, as described before.

4.2.4 Mercury Porosimetry

Mercury porosimetry analysis was performed by using a Micromeritics AutoPore III. Samples were outgassed in vacuum at room temperature for 30 min before intrusion. Intrusion and extrusion mercury contact angles of 130° were used, measurements were conducted according to the set-time equilibration mode.

Penetrometers with a stem volume of 1.1310 ml were used. The intrusion volume was always comprised between 50 ÷ 85 % of the stem volume. Intrusion pressures never exceeded 1000 psi in order to avoid any specimen compression.

Polydispersities of the distributions are expressed as the 10-90% size distribution width divided by the median pore diameter [9].

4.2.5 SEM

A Hitachi S2400 electron microscope operating at 25 kV was used for studies of the morphology of the samples. Prior to analysis, specimens were sputter coated with a thin layer of gold to enhance conductivity.

4.2.6 Surface pressure-area (π-A) curves

Surface pressure *vs.* molecular area data were obtained using a Langmuir balance supplied by NIMA Technologies. Measurements were carried out on films spread on an aqueous solution of $CaCl_2$ (1.11% Wt.). The aqueous and organic phases that mimic the composition of the V-S-DVB HIPEs were pre-equilibrated by leaving them in contact overnight. This procedure was followed in order to avoid the partial dissolution of the components of the organic phase in the aqueous one. The organic phase was then dissolved in chloroform and 40 μl of this solution was spread on the water layer. Barrier speed was set to 200 cm/min.

4.2.7 Compression moduli measurements

Compression modulus measurements were performed on ~ 2-3 cm diameter × 3 cm high cylinders by using an Instron Model 4483 at a platen speed of 0.127 cm/min. Densities were determined by the ratio of weight to the volume of the cylindrical samples. The foam

modulus is obtained by linear regression of the linear compression region at small strains in the stress-strain region. The polymer modulus (E_p) has been related to the foam modulus (E_f), foam density (ρ_f) as seen in Eq. 4.2. E_f and ρ_f are measured experimentally, while ρ_p is expected to be in the neighborhood of 1g/cm^3 for the various polymers. The polymer compressive modulus was calculated using Eq. 4.1, assuming ρ_p = 1 g/cm^3

$$E_p = E_f\left(\frac{\rho_p}{\rho_f}\right)^2 \tag{2}$$

4.3 Results and discussion

For the reasons given in the introduction, it would be desirable to have a better and more predictable degree of control on both cell and window size and this control should be achieved through the variation of VBC concentration (the monomer carrying a functional group amenable to chemical modification).

Previously, Williams [10] found that increasing the DVB concentration in S-DVB PolyHIPE from 0 to 100% resulted in a decrease in average cell diameter by about 10 μm. He reasoned that DVB being more hydrophobic, was leading to more stable emulsions. To better study and put into evidence any correlation between the concentration of VBC and foam morphology and properties of the resulting polyHIPE foams three series of polyHIPE foams have been prepared and characterized by SEM microscopy and intrusion mercury porosimetry. Their mechanical properties were evaluated through the measurements of their compression moduli. In each of the series prepared, the amount of DVB was kept constant (10, 30, 50% on total volume of organic phase) while the volume ratio of VBC to S was varied, to give a range of foams in which the concentration of VBC increases gradually at the expense of S. This approach should allow to better reveal the separate influences of VBC and DVB on foam morphology.

4.3.1 Morphology

In Fig. 4.1 SEM micrographs of the foams of the VNSN'X10PV90 type are reported. They clearly show that the replacement of S with increasing amount of VBC in the formulation causes a marked decrease in both cell and interconnecting holes sizes. Foams containing a lower concentration of VBC (Fig. 4.1a and b) are characterized by a narrower cell and interconnecting average diameter distributions than those of foams with higher VBC content (Fig. 4.1c and d).

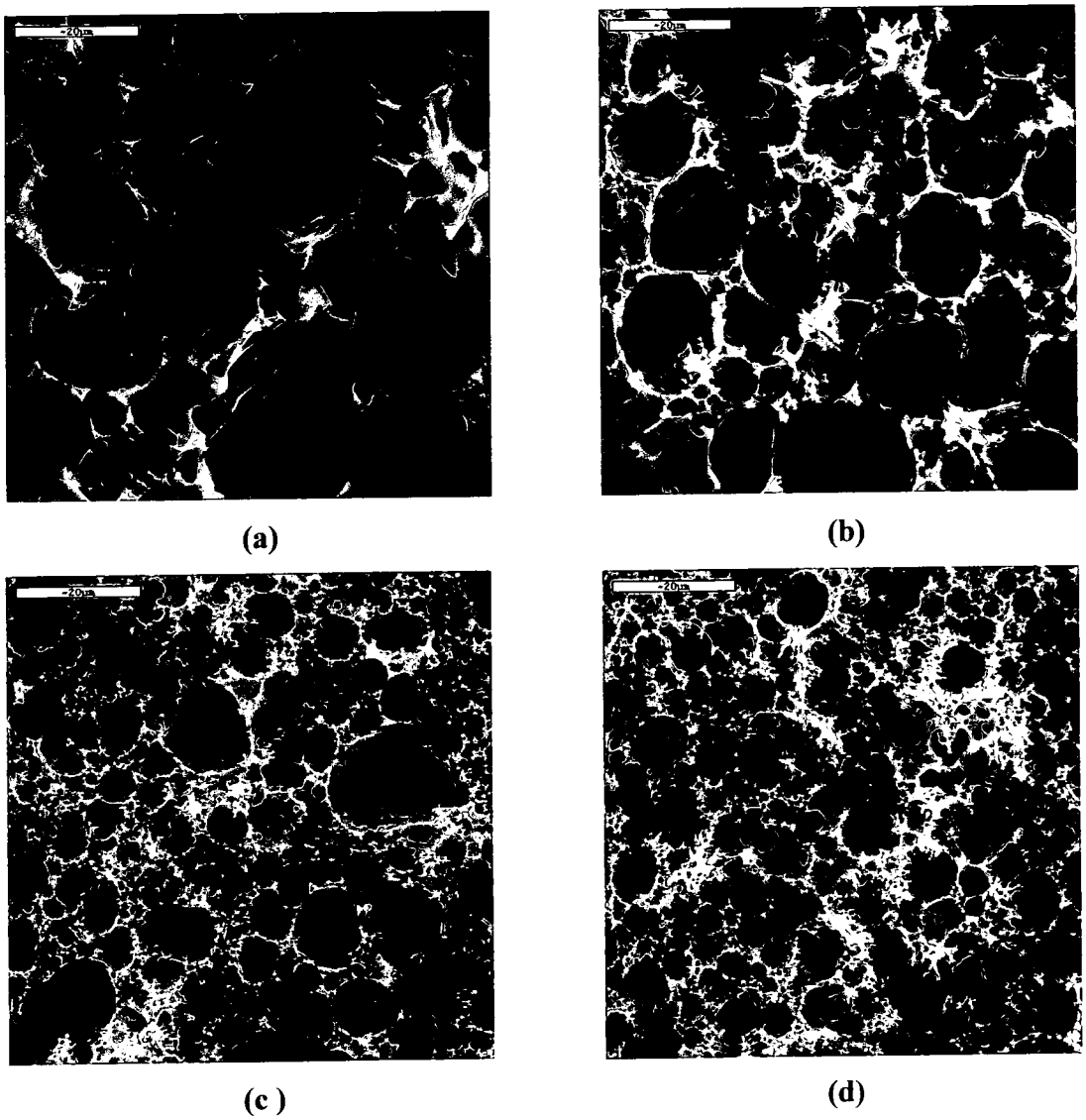

Fig. 4.1. Scanning electron micrographs of PolyHIPE foams prepared from S, DVB and VBC. (a) S87.5X10PV90; (b) V29.2S58.3X10PV90; (c) V58.3S29.2X10PV90; (d) V87.5X10PV90. Scale bar 20 μm.

A similar trend in the morphology is encountered in the foams belonging to the other two series, that is VNSN'X30PV90 (fig. 4.2) and VNSN'X50PV90 (Fig. 4.3). As the content of VBC increases in the foams, both the average cell and interconnecting windows diameters decrease. The qualitative comparison between the SEM micrographs referring to foams of different series indicate that the extent of this decrease is more consistent on variation of VBC concentration in foams prepared with a lower content of DVB. In foams prepared without VBC (Fig 4.1a, 4.2a, 4.3a), the increase of DVB concentration causes a decrease in cell size, in agreement with what has been observed by Williams [10]. The comparison of the morphology of the cells and interconnecting holes in foams belonging to the three series

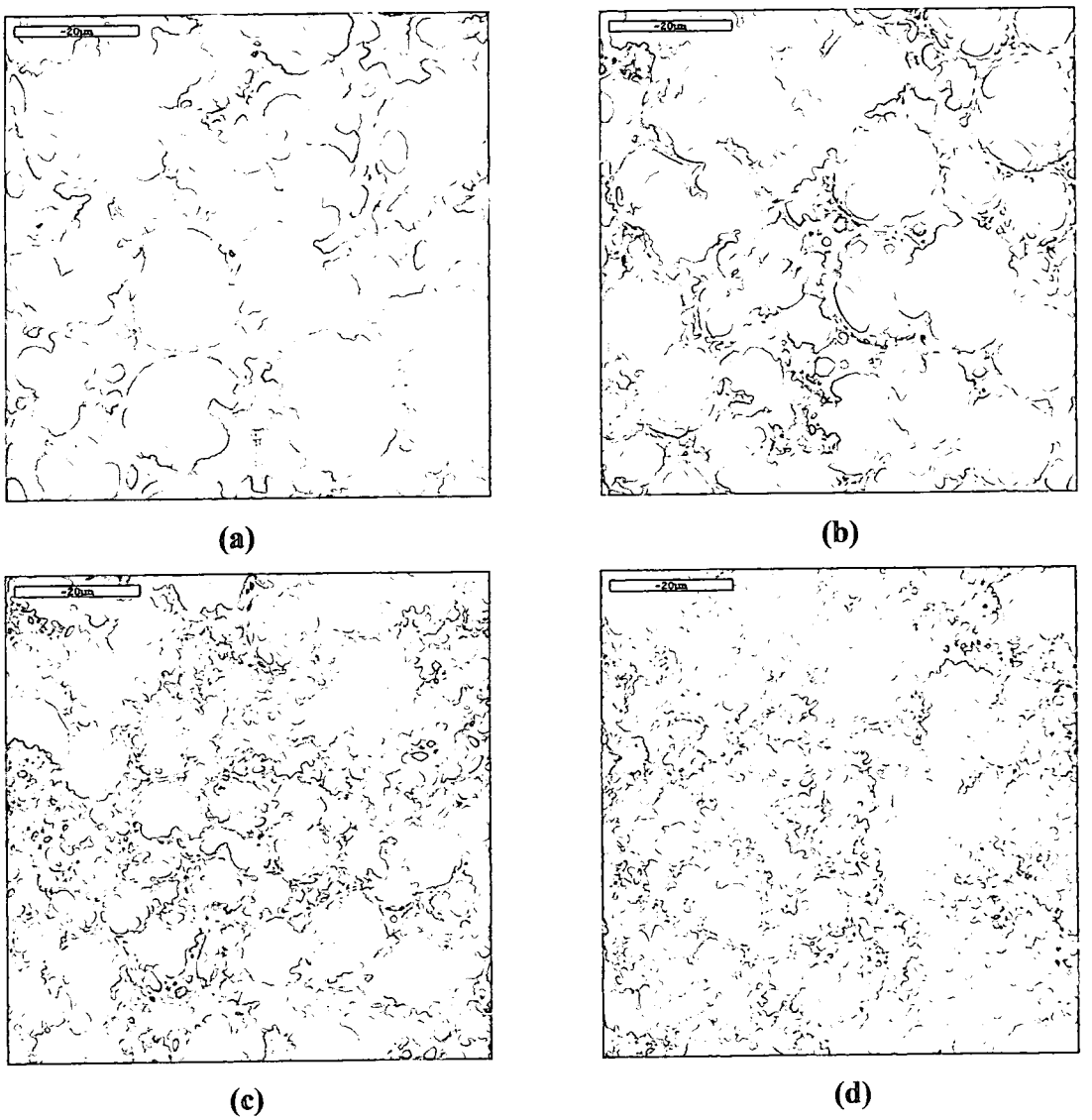

Fig. 4.2. Scanning electron micrographs of PolyHIPE foams prepared from styrene, divynilbenzene and 4-vinylbenzylchloride. (a) S62.5X30PV90; (b) V20S42.5X30PV90; (c) V40S22.5X30PV90; (d) V62.5X30PV90. Scale bar 20 μm.

examined here, show some other interesting features. Cells of the foams of the VNSN'X10PV90 type tend to be more markedly polyhedral, deviating considerably from a spherical symmetry. Also the shape of the interconnecting holes tend be ellipsoidal and it seems that deviation from a spherical shape is more accented for the larger holes. These features tend to be less pronounced in X30 and eventually disappear in X50 foams containing a larger concentration of DVB (Fig. 4.2 and 4.3). Thus, it seems that these characteristics in the morphology of foams is connected with DVB content. This concentration variable determines the time for the attainment of the gel point according to an inverse proportion relationship.

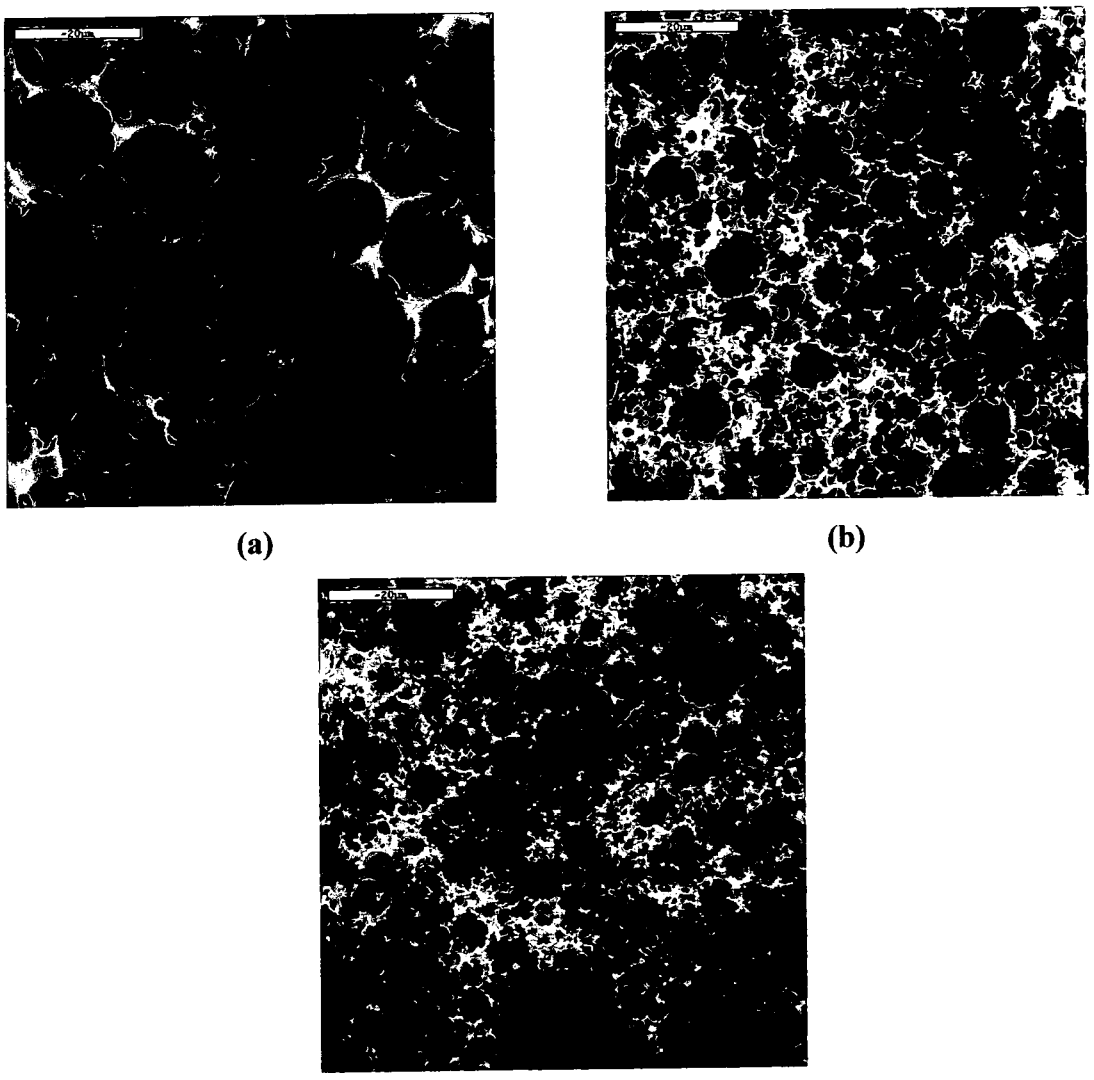

Fig. 4.3. Scanning electron micrographs of PolyHIPE foams prepared from S, DVB and VBC. (a) S37.5X50PV90; (b) V20S17.5X50PV90; (c) V37.5X50PV90. Scale bar 20 μm.

During the first stages of polymerisation when the emulsion is still fluid, because of their close contact (which is determined by the high volume fraction of the dispersed phase), and enhanced thermal agitation (the temperature of polymerisation is 60 °C), droplets collide with each other and are subject to deformations which cause the creation of flat boundaries among them. These deformations are more pronounced, in emulsions belonging to the VNSN'X10PV90 series, for larger droplets than for the smaller ones (compare micrographs a with c in Fig. 4.1) because on the average larger droplets are surrounded by a higher number of neighbouring droplets and the probability of suffering deformations will be, as a consequence, higher than for the smaller droplets. A direct consequence of this is that near the gel point when interconnect holes start to appear [11] the holes at the edge of two such flat

regions will assume a slit like symmetry. In emulsions whose organic phase contains a higher concentration of DVB the combined effects of smaller average droplets diameters and a shorter interval of time necessary for the attainment of the gel point will result in an attenuation of the effect described above.

4.3.2 Intrusion mercury porosimetry results

The qualitative observations made on SEM micrographs find quantitative support from the cell size distributions determined by intrusion mercury porosimetry (Fig. 4.4). It can be seen that in each series as the concentration of VBC increases the distributions shift on the whole towards lower diameters and as a result their average cell diameters decrease markedly (Table 4.I). The most consistent decrease in the average diameter takes place upon the first additions of VBC then, values of the average diameter tend to level off.

The closer examination of the pore size distributions allow to discern a few trends inside each series in connection with the concentration of VBC in the organic phase. For instance, within VNSN'X10PV90 series it can be seen that distributions become broader and broader as the concentration of VBC increases. This feature is expressed quantitatively by the polydispersity index (Table 4.I). V87.5X10PV90 in this respect represents an exception as its polysispersity is only higher than that of S87.5X10PV90. The increasing values of polydispersities reflect the increasing contribution taken on in the distributions by the tails that are present in the low diameter side. Both the range of diameters spanned by the tails and their intensities seem to be directly proportional to VBC content. Both S87.5X10PV90 and V58.3S29.2X10PV90 distributions are bimodal. In the former case the intensity of the peak positioned to the left of the main one is negligible, while in the latter they are approximately of the same intensity. V87.5X10PV90 distribution presents a shoulder positioned to the left of the main peak. All distributions have a small tail extending towards the high diameter side.

The same overall features are met with the foams belonging to the other two series. The comparison among foams of the SNXMPV90 type (M = 10, 30 ,50) show that as the concentration of DVB increase the relative pore size distributions tend to shift towards low diameters and as a result their average diameters decrease in the same fashion. These curves are more bimodal in character as the weight of the low intensity peak grow in importance. This is reflected in the polydispersities that passing from S87.5X10PV90 to S37.5X50PV90, doubles (Table 4.I). In foams with an increasing content of DVB (X30, X50), variations in the concentration of VBC between adjacent members of the series is reduced. For instance in VNSN'X10PV90 is of about 30%, while in both VNSN'X30PV90 and VNSN'X50PV90

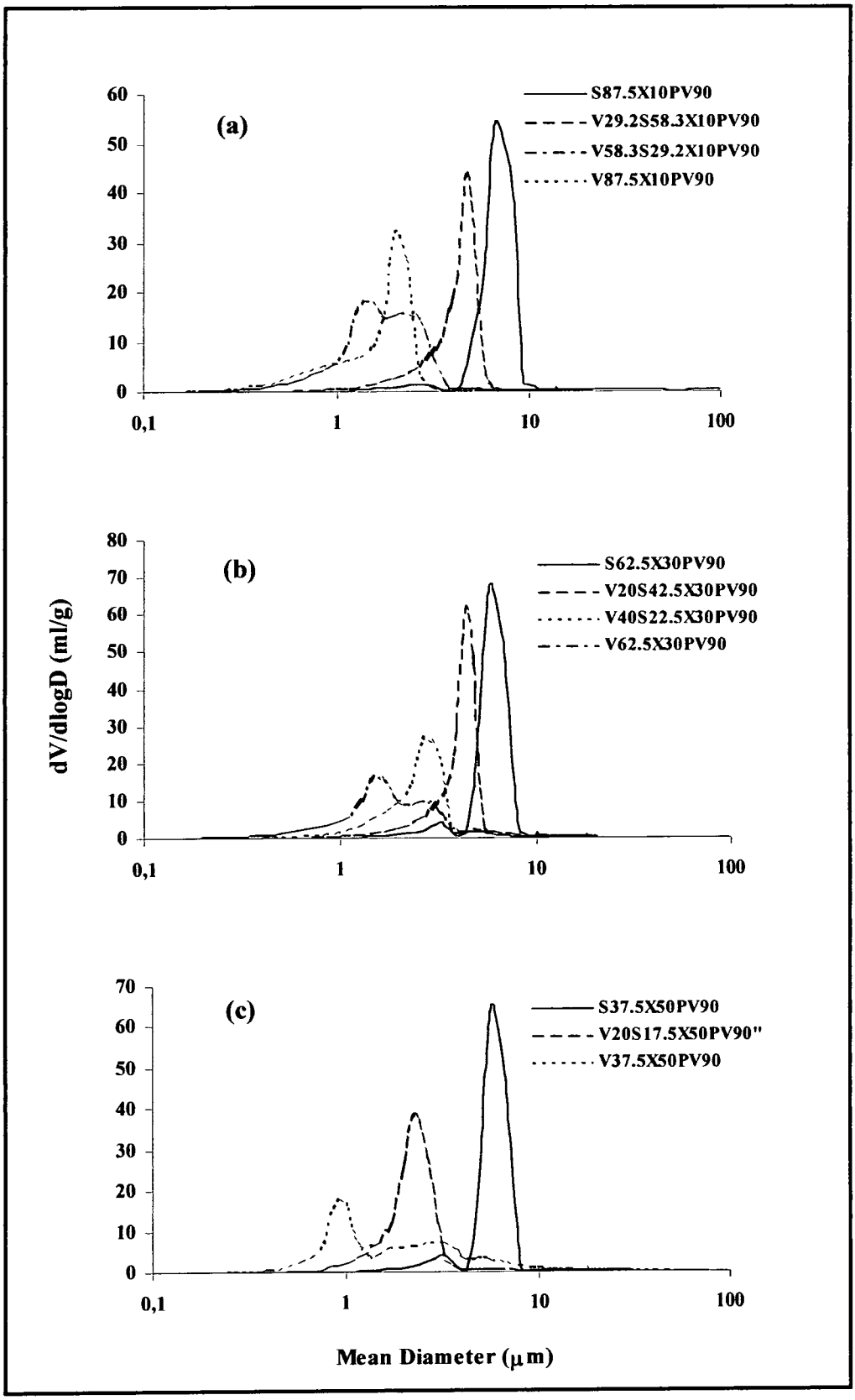

Fig. 4.4. Pore size distributions determined by intrusion mercuri porosimetry of PolyHIPE foams based on VBC, S and DVB 80%. (a) VNSN'X10PV90; (b) VNSN'X30PV90; (c) VNSN'X50PV90.

Table 4.I. Density, total intrusion volume, average pore diameter, cell size polydispersities and compression strengths of VBC/S/DVB PolyHIPE foams.

SAMPLE	Density	Intrusion Volume (ml/g)	Pore Diameter (μm)	Polydispersity	Compression Moduli (kPa)	Specific. Compr. Moduli (kPa ml/g)
V87.5X10PV90	0.105	8.0	1.1	2.0	174	1657
V58.3S29.2X10PV90	0.099	8.6	1.3	6.5	94	949
V29.2S58.3X10PV90	0.093	8.8	3.3	4.1	111	1193
S87.5X10PV90	0.083	9.0	5.9	1.4	137	1651
V62.5X30PV90	0.106	7.4	1.3	8.7	51	481
V40S22.5X30PV90	0.102	7.8	2.0	4.7	30	283
V20S42.5X30PV90	0.095	9.1	3.3	3.4	81	853
S62.5X30PV90	0.089	9.1	4.5	2.3	101	1135
V37.5X50PV90	0.105	8.1	1.3	14.5	47	290
V20S17.5X50PV90	0.101	8.6	1.9	5.1	54	535
S37.5X50PV90	0.093	8.9	4.4	2.7	118	1124

is of about 20%. In spite of this the effect of variation of VBC concentration on pore size distributions is more marked: shift apart among curves of X30 and X50 type is relatively more pronounced as evidenced by the decrease in the average diameters (Table 4.I). On the other hand, the comparison within each series of the lower diameter portion of the distribution curves show that the range covered by the tails diminishes proportionally with the content of VBC. The extent of this contraction is more important in X50 and to a lesser extent in X30 series. The influence of VBC content on polydispersity in X30 and X50 series of foams is more pronounced in a way which is clearly dependant on DVB concentration. For instance, the polydispersities of the pore size distribution in foams characterised by a comparable content of VBC as V40S22.5X30PV90, V37.5X50PV90 and V20S42.5X30PV90, V20S17.5X50PV90, polydispersities are 4.7, 14.5 and 3.4, 5.1, respectively. In spite of the decreasing contribution taken on by the tails extending towards the low diameter side, the polydipsersitiy index increase with crosslinker content. The increase in polydispersity in X30 and X50 series of foams is due to a tail which appears in the high diameter side and grow in importance as the concentration of VBC increases within these series. For instance, if we consider the distribution curve referring to S62.5X30PV90, this tail is negligible but as the amount of VBC that replace S increases it acquires more and more importance both as far as range spanned and intensities are concerned (V62.5X30PV90). This trend is more pronounced in the distributions of VNSN'X50PV90 type foams. Again, in the case of S37.5X50PV90 the tail extending towards the high diameter side is negligible, but it becomes substantial in V37.5X50PV90. As a consequence, the corresponding distribution is very broad and characterised by a polydispersity index of 14.5 (Table 4.I).

Pore volumes (Table 4.I) tend to decrease within each series of foams as the concentration of VBC increases. This might be due to partial foam collapse during drying. The extent of the decrease in intrusion volume is more relevant in foams in which the amount of VBC is higher as for instance V87.5X10PV90, V58.3S29.2X10PV90 and V62.5X30PV90. This might be a symptom of the increase thinning that foam wall undergo as a result of the reduction of the interfacial tension (see subsequent section). Foams density follow a behaviour which matches according to an inverse relationship with intrusion volume data: the lower is the pore volume of a foam the higher is its density.

4.3.3 Surface pressure measurements

It is well known that droplet size decreases with increasing emulsion stability since the

surface energy per unit area is lower. A decrease in emulsion droplet leads to a decrease in polyHIPE cell size since the foam is effectively a replica of the emulsion structure immediately prior to gel formation. In the present case increasing VBC concentration causes a decrease in the average cell size of the resulting foam. This implies that increasing amount of VBC leads to more stable emulsions.

The major differences between the molecules normally found in the oil phase are their polarity and chain length. The interfacial tension at an oil-water interface decreases as the polarity of oil molecules increases, which would be expected to influence droplet coalescence and Ostwald ripening [12, 13]. The water solubility in a hydrocarbon medium increases as their chain length decreases or their polarity increases [14], which would be expected to decrease the rate of Ostwald ripening.

In order to find a correlation between the observed trend in morphology of foams as evidenced by SEM and emulsion composition we have evaluated the three dimensional cohesion parameter δ_t which considers the contribution from dispersive, δ_d, dipolar, δ_p, and hydrogen bonding, δ_h, interactions for the compounds used in this study:

$$\delta_t^2 = \delta_d^2 + \delta_P^2 + \delta_h^2 \qquad (3)$$

With the exception of styrene, data regarding three dimensional cohesion parameter for the other molecules present in the organic phase of the emulsions are not available in literature. They were calculated by applying a group contribution method according to Hoftyzer-Van Krevrelen and Hoy [15, 16]. Both methods are of the same order of accuracy, and it has been suggested that these should be averaged [15]. Both methods used alone yielded similar relationships, but the scattering of data points was significantly reduced using average values from both methods. The values of three dimensional cohesion parameter reported in Table 4.III are in accordance with common physical sense. For instance, styrene which bears only one vinyl group has a value of the dipolar component, δ_p, higher than those of both *m*-DVB and *p*-DVB where there is a partial compensatory effect due to the inherent symmetry of the molecules. On the other hand, the hydrogen bond component, δ_h, of styrene is lower than *m*-DVB and *p*-DVB because in the latter there are the contributions from two vinyl groups instead of one. VBC as a molecule combines a relatively high polarity and hydrogen bonding formation capabilities.

The data reported in Table 4.II were used in the calculation the average cohesion parameters of mixtures of the same composition found in the organic phase of the emulsions precursor of the foams studied here through the use of Eq. 4:

Table 4.II. Three dimensional cohesion parameter δ_t of the components used in the preparation of PolyHIPE foams. The contribution due to dispersive δ_d, dipolar δ_p and hydrogen bonding δ_h, are included.

COMPOUND	δ_t	δ_d	δ_p	δ_h
VBC	19.9	17.7	7.4	3.8
Styrene	19.1	17.4	5.2	3.2
***p*-DVB**	18.6	16.4	4.5	4.7
***m*-DVB**	18.5	16.4	4.7	4.7
***p/m*-ES**	18.5	17.1	4.4	3.1

$$\bar{\delta}_k = \sum_i \phi_i \delta_{ki} \qquad k = t,\ d,\ p,\ h \tag{4}$$

where φ is the volume fraction of the various components and the summation is extended over the contributions to the cohesion parameter.

Table 4.III. Average cohesion parameters δ_t and contributions due to dispersive δ_d, dipolar δ_p and hydrogen bonding δ_h, of the organic phases of the emulsions listed below.

SAMPLE	$\bar{\delta}_t$	$\bar{\delta}_d$	$\bar{\delta}_p$	$\bar{\delta}_h$
V87.5X10PV90	19.7	17.6	7.0	3.9
V58.3S29.2X10PV90	19.5	17.5	6.4	3.7
V29.2S58.3X10PV90	19.3	17.4	5.8	3.5
S87.5X10PV90	19.0	17.3	5.1	3.4
V62.5X30PV90	19.4	17.3	6.3	4.0
V40S22.5X30PV90	19.2	17.2	5.8	3.9
V20S42.5X30PV90	19.1	17.1	5.4	3.9
S62.5X30PV90	18.9	17.1	5.0	4.0
V37.5X50PV90	19.1	17.0	5.6	4.2
V20S17.5X50PV90	18.9	16.9	5.2	4.1
S37.5X50PV90	18.8	16.9	4.8	4.0

As can be seen in Table 4.III the polarity in each of the three series follows a trend which is dictated by the concentration of VBC in the organic phase. Variation in polarity are more pronounced down VNSN'X10PV90 series in which variation in VBC concentration between adjacent members is of about 30%. As far as hydrogen bonding is involved, variation within

each series are more limited. This is due to a "buffering" effect exerted by DVB. As shown in Table 4.II DVB has the highest value of δ_h among the chemical species considered in Table 4.II. In VNSN'X10PV90 series where the concentration of DVB is low (10% vol.), as the concentration of VBC decreases, the values of δ_h decrease as well but to a limited extent. In VNSN'X30PV90 and VNSN'X50PV90 on the contrary, where the concentration of DVB is relatively higher, δ_h is constant.

Polarity and hydrogen bond forming capabilities are likely to be the features that confer to the molecules reported in Table II their interfacial activity.

In order to evaluate quantitatively the correlation between the emulsion concentration of VBC and the lowering in the interfacial tension caused by its adsorption at an interface we tried to measure the interfacial tension of the pre-equilibrated organic and aqueous phases by mean of the spinning drop method. Unfortunately the densities of the two phases are very close to each other, differing less than 1%, and this drawback prevented the successful application of this technique. For this reason we have resorted to a Langmuir trough. This technique is less suitable than the spinning drop method because it allows measurements of the dynamic surface pressure at the air/water interface. On the other hand, it provide a simple and reliable method for investigating the adsorption of organic liquid at the surface under compression, a condition most likely to represent the condensed surfactant layer present at the oil-water interface on the droplet surface in HIPEs. Since both air and oil are hydrophobic phases, we felt we were justified in applying the trough data to emulsion interface. Steps, such as pre-equilibrating the two phases and carrying out the measurement at the maximum speed, were taken in order to limit dissolution of organic phase components into the aqueous phase and evaporation of the organic components during measurements. Using the trough we measured the surface pressure against area (π-A) curves of film of Span 80 alone, and of solutions that mimic the HIPE continuous phase in emulsion of VNSN'X10PV90 types. The interfacial behaviour of the various components can be inferred form their π-A curves (Fig. 4.5). Span 80 displays the behaviour of a typical surfactant: the surface pressure is low and constant until critical film compression is reached, whereupon it increases drastically. The area corresponding to this compression represents the area of the condensed interfacial film where the surfactant molecules are densely packed. The adsorption of the other species (S, DVB, VBC) at the interface will cause greater crowding and lead to an increase in π at higher area (lower compression), which is indeed observed. From Fig. 4.5 it can be inferred that the adsorption of VBC at the interface increases proportionally with its concentration in the

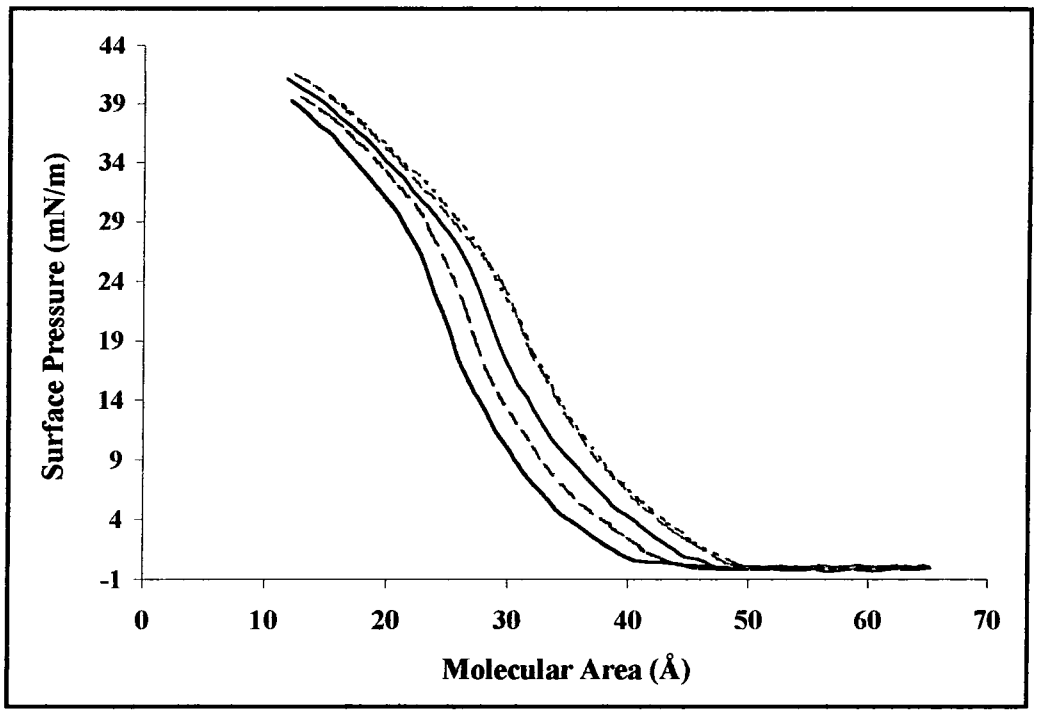

Fig. 4.5. π-*A* curves for films containing SPAN 80 alone (———), and SPAN 80 plus divinylbenzene 80% (10% vol.) and different % vol. of 4-vinylbenzyl chloride and styrene: S87.5 (– – – –), V29.2S58.3 (———), V58.5S29.2 (– – – –), V87.5 (·····).

spread film. The coincidence between π-*A* curves corresponding to V58.2S29.2X10PV90 and V87.5X10PV90 seems to indicate that the interface is close to saturation at a VBC concentration in the HIPE of around 55÷60%.

The mechanism by which VBC may enhance stabilization in the emulsion here studied is not known, but in the literature analogous system have been studied with some detail. It is known that single-tailed surfactants usually form globular micelles in aqueous solution above their critical micellar concentration (CMC). An increase in surfactant concentration may induce the formation of wormlike micelles. Similarly, addition of organic or inorganic counterions, uncharged compound such as aromatic hydrocarbon [17] can transform spherical micelles into wormlike micelles. In the case of cationic surfactant aggregates, upon changing the counterions to aromatic ones which usually display higher counterion binding, micellar growth already occurs at low surfactant and counterion concentrations [18, 19]. However, not only high counterion binding is a prerequisite for micellar growth, but also the orientation of substituents on the aromatic ring is important [20]. It was shown that the aromatic ring of salicylate is located between the headgroups of the surfactant molecules and that the OH and COO^- substituents protrude out of the micellar surface [21-23]. Theoretical studies showed that

wormlike micelles are long and flexible and that they undergo transformations on relatively short time scales [24]. The presence of wormlike micelles in aqueous solutions is often reflected by an increase in relative viscosity [25]. Upon increase of the surfactant concentration an entangling network of wormlike micelles is formed which displays viscoelastic behaviour.
We have observed during emulsification a marked increase of the viscosity and it seemed that such an increase was correlated and proportional to the content of VBC in the organic phase.
Pore size distribution features are consistent with a morphology which was determined by viscosity. A multimodal distribution is usually associated with the changing of the rheological properties during the emulsification process. During the first stages of emulsification at low water-to-oil ratio the viscosity is relatively low and this coupled with the low interfacial tension favours the creation of a fine dispersion of droplets. The size of the droplets formed at this stage correspond to the lower diameter portion of the pore size distribution. As the volume ratio increases, following the addition of the aqueous phase, the viscosity of the emulsions increase more and more. At high viscosities, the shear stress of mixing is not able to break up the large droplets. It is thus difficult to generate a uniform fine dispersion of the aqueous phase in those HIPEs that are highly viscous at high water/oil ratios [26, 27]. Thus, on one hand, the increase in VBC content reduces interfacial tension, and thus reduce cell dimensions. On the other hand, the increase in VBC content increases the viscosity at high water-in-oil ratios and makes it more difficult to generate the mixing shear stress needed to create a fine dispersion of the aqueous phase, yielding large droplets in the last stage of HIPE preparation. The size of the droplets formed at this stage correspond to the higher diameter portion of the distribution. Viscosity thus plays an important role in determining cell size and size distribution. This explains the presence of the tails positioned in the low diameter side of the distributions and their relationship between extension, intensity and the content of VBC. The presence of a bimodal/multimodal type of distribution at high concentration of VBC is particularly significant symptom of the influence of viscosity in determining the pore size distribution [28].
The initial pore size distributions resulting immediately after emulsification is modified by other phenomena such as coalescence [29-35] and Ostwald ripening [36-42]. Coalescence is the process by which two or more droplets fuse to form a single larger droplet. Emulsions begins deteriorating immediately after their preparation. Although the number average droplet size increase significantly, the distribution begins tailing towards larger droplet sizes. The tail increases with time and the distribution broadens [43]. Conversely, Ostwald ripening is the process by which larger droplets grow at the expense of smaller ones due to differences in

their chemical potential. In molecular diffusion, the growth occurs by diffusion of the dispersed phase through the continuous phase.

The stability of emulsions of aliphatic hydrocarbon (C_6 – C_{12}) in water in the presence of surfactant has been studied in detail: in general the stability increases with an increase in chain length of alkanes, and molecular diffusion rather than coalescence tends to occur for droplets of shorter chain alkanes and polar oils. In this respect, the mass transport rate of molecules through an organic solution depends on their organic solubility, and therefore the growth of droplets due to Ostwald ripening depends on the composition of the organic phase [44-46]. The size distribution *g(u)* of the droplets in the steady-state regime of the ripening process, where u is the normalised droplet size, r/r_c is governed by the following Eq.:

$$g(u) = \frac{81e}{\sqrt{32}} u^2 (3+u)^{-7/3} (1.5-u)^{-1/3} \exp\left[\frac{1}{\left(\frac{2u}{3}-1\right)}\right] \qquad (5)$$

for $u < 1.5$ and

$g(u) = 0$ for $u \geq 1.5$

The normalised form of this distribution [40] is represented by a curve characterised by a long tail extending towards the low diameter side. The distribution is time invariant so that whilst the critical radius increases with time, the form of the size distribution as a function of u does not change. The asymmetry of the curve has been shown theoretically to depend markedly [47] on the volume fraction of the dispersed phase: as this variable increases the maximum of the distribution curve decreases and the distribution broadens becoming more and more skewed. The rate of ripening will be affected by the droplet size distribution if the steady state regime has not been reached where Eq. 5 hold true. A wider distribution of sizes will lead to an enhanced rate. Thus those emulsions characterised by a high overall polarity and possessing hydrogen bond forming capabilities will undergo a faster ripening process which tend to increase the mean radius with time according to Eq. 17, § 1.4, chapter 1 and the distribution will narrow with time. The effects of ripening on pore size distributions is partially offset by the reduction of interfacial tension as evident from Eq 17 of chapter 1 and by the rate of network gelation. In foams containing a higher concentration of DVB the attainment of the gel point occurs after a shorter time interval from the beginning of polymerisation. As a result the influence of diffusion on the cell size distribution of the final foam will be less pronounced.

It is not clear why cell size of the foam series VNSN'X50PV90 are so broad. Also in this

case we observed a marked increase in viscosity with VBC content but the overall concentration of VBC in this series is lower than that in the other two series of foams. From Table 3.III we can see that the organic medium becomes increasingly less polar as the VBC content decreases and so relatively more hydrophobic. It is possible that a more hydrophobic environment will enhance the transfer of VBC molecules from the bulk of the continuous phase to the interface where the polar and hydrogen bond interactions with the dispersed aqueous phase represent for VBC molecules a more energetically favourable situation.
We can conclude that the main variable affecting pore size distribution are interfacial tension and viscosity of the emulsions.

4.3.4 Mechanical Properties

The mechanical properties of the foam samples were evaluated as a compression strength. Table 3.I presents the compression strength results and includes the foam densities and a specific compression value. The foam sample densities varies slightly due to variation in volume shrinkages during the drying process. Therefore, to obtain a more accurate comparison of the foam performances, a specific compression strength was calculated by dividing the compression strength with the foam density. The compressive strain-stress curves (Fig. 4.6) are typical three stages foam compressive strain-stress curves: a linear elastic region, a plateau region and a bulk compression region [48]. Linear elasticity is controlled by cell wall bending and Young's modulus is obtained from the initial slope of the stress strain curve. The plateau is associated with collapse of the cells – by elastic buckling in elastomeric foams; by the formation of plastic hinges in a foam which yields; and by brittle crushing in a brittle foam. When the cells have almost completely collapsed opposing cell walls touch, and further strain compresses the solid itself, giving the final region of rapidly increasing stress. Increasing the relative density of the foam increases Young's modulus, raises the plateau stress and reduces the strain at which densification starts. The initial linear elasticity is caused by cell bending, plus stretching if the cell is closed. In the elastomeric foam larger strains rotate the cell edges towards the tensile axis, increasing the stiffness of the structure. The cell walls in the plastic foam, too, rotate towards the tensile axis (by plastic bending), giving a yield point followed by a rising stress-strain curve which is ultimately truncated by fracture. In the brittle foam a crack nucleates at a weak cell wall or pre-existing flaw and propagates catastrophically, giving fast brittle fracture [49].
Fig. 4.6 shows representative stress-strain plots of three foams characterised by different

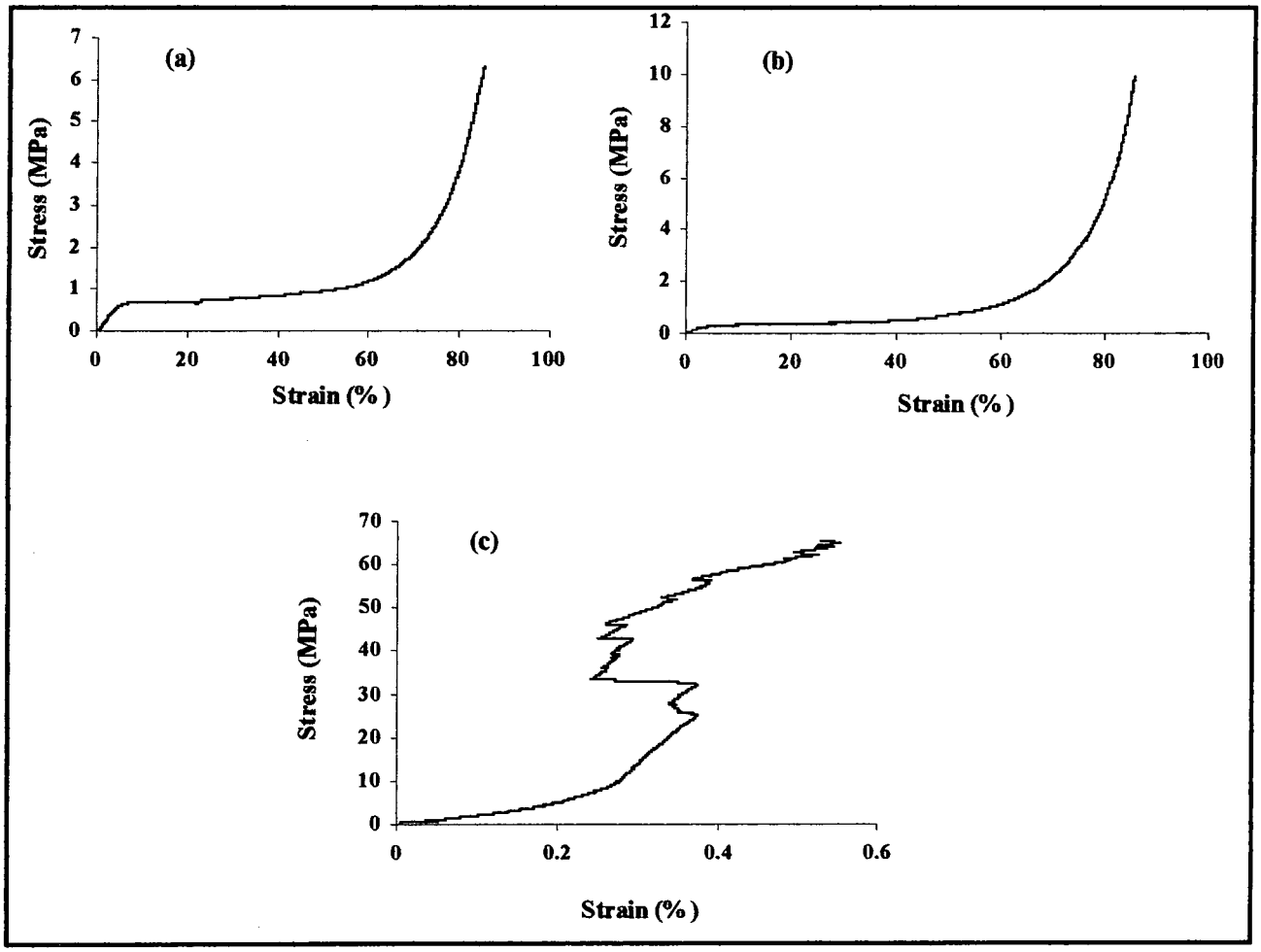

Fig. 4.6. Compressive stress-strain curves for (a) S87.5X10PV90; (b) V20S42.5X30PV90; (c) V37.5X50PV90

crosslink density.

Stress-strain curves of X10 and X30 foams type are very similar to each other and exhibit a behaviour typical of a elastomeric open foam cell. In the case of X50 type foams, the shape of the stress-strain curve is characteristic of elastic brittle foam: it consists of an initial linear portion which corresponds to the elastic bending of the foam walls followed, beyond a critical value of the stress, by an indented part which indicates that fracture events are taking place. SEM micrographs (Fig. 4.3) clearly show the presence of cracks within the walls of the X50 type foams. The presence of such cracks represent stress concentration sources [50] that under the regime of a compression mode deformation propagate leading to the partial failure of the structure. Under compressive loading, crack propagation is somewhat inhibited by compressive stresses and this explains the absence of a truncated stress-strain curve.

The results regarding compression moduli reported in Table 3.I and in Fig. 4.7 show that the moduli are relatively independent of crosslink content, reflecting the relative insensitivity of

the polymer to the degree of crosslinking. The highest moduli are obtained for foams containing a 10 % of DVB. Similar results were obtained by Williams and co-workers with S-DVB foams [10].

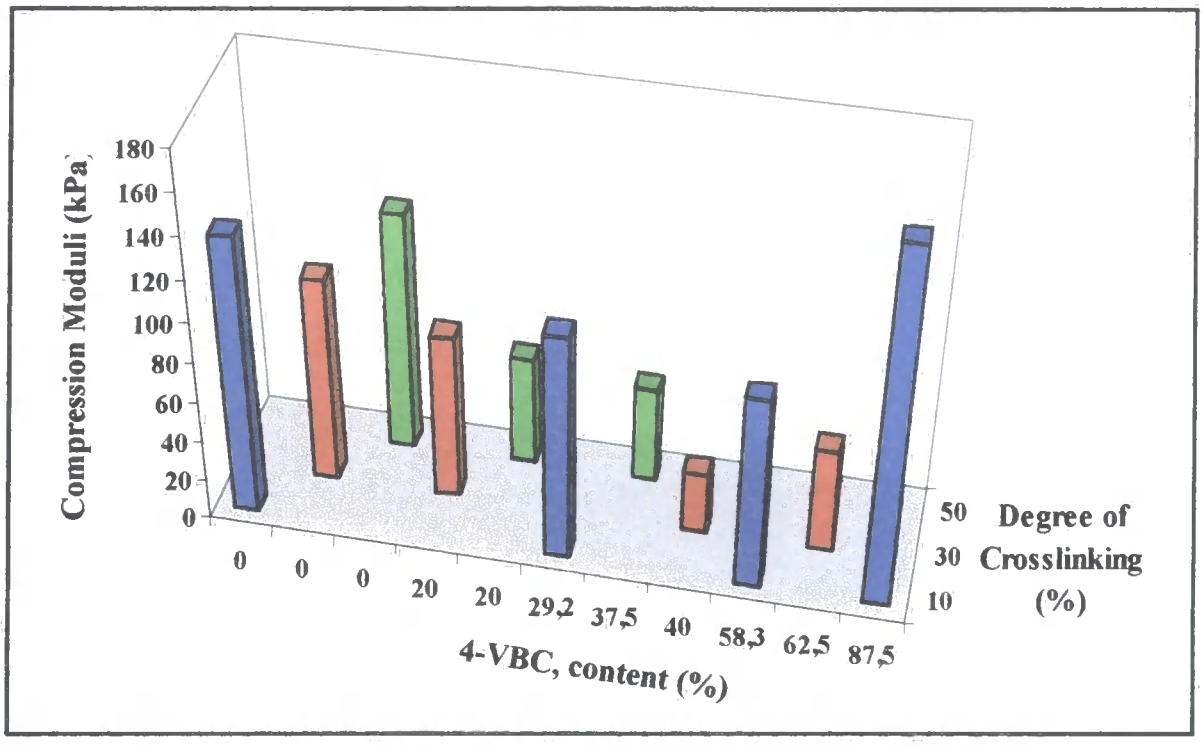

Fig. 4.7. Compressive modulus of PolyHIPE foams as function of VBC content and crosslinker levels.

Within each series the dependence of the compressive modulus on foam densities follows a parabolic trend (Fig. 4.8). The upward curve was expected since the moduli of these foams follow a square dependence, [49, 51] Eq. 4.2. Differences in mechanical properties can in theory ensue from the monomer sequencing composition in the polyHIPEs which depends on the reactivity ratios of the monomers employed. The reactivity ratio of styrene (r_1) and *p*-chloromethylstyrene (r_2) are 0.6 and 1.66 respectively [52] which means that especially in foams in which the ratio of VBC to S is high, such as V58.3S29.2X10PV90 and V40S22.5X30PV90, polymer segments between crosslink points tend to be rather blocky copolymers of poly(VBC) and polystyrene. This might be the source of differences in mechanical properties among foams with a different chemical composition. Considerations based on the intrinsic rigidities of poly(VBC) and polystyrene allow out this possibility to be ruled out because the glass transition temperatures for these two polymers are practically coincident ($T_g \cong 100^\circ$ C).

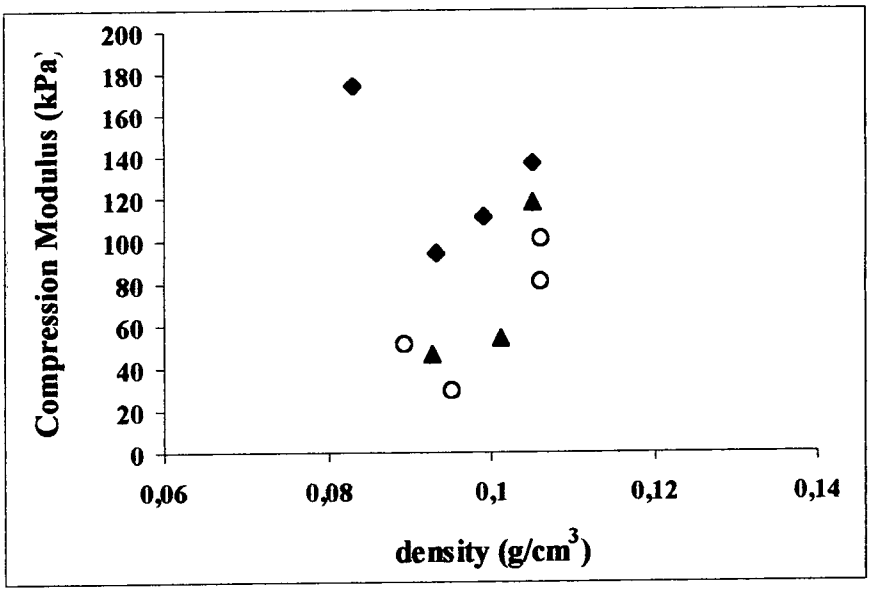

Fig. 4.8. Dependence of compression moduli on density. (♦) VNSN'X10PV90; (○)VNSN'X30PV90; (▲)VNSN'X50PV90.

The compression moduli trend observed within each series of foams can be explained in term of foam morphology and keeping in mind the interfacial behaviour exhibited by VBC. The interfacial activity put into evidence by π-A measurements showed that the content of VBC in the organic phase of the emulsions, determined the extent of the concomitant decrease in interfacial tension. This phenomenon is accompanied, as illustrated in chapter 3, by the thinning of the film of the continuous phase surrounding the droplets of the dispersed phase together with a marked decrease in average droplet size. The morphologies of the foams belonging to the three series as evidenced by SEM (Fig 4.1, 4.2, 4.3) are consistent with such a hypothesis. This implies that the thickness of the walls of the foams is inversely proportional to VBC content. This feature is expected to influence the mechanical performances of the foams [53].

This can be better understood if we refer to a simple model based on scaling arguments [49]. An open cell may be idealised into its simple form, as a cubic array of members of length l and square cross-section of side t, as shown in Fig. 4.9. The relative density of the cell ρ_f/ρ_p is related to t and l by

$$\frac{\rho_f}{\rho_l} \propto \left(\frac{t}{l}\right)^2 \tag{6}$$

and the second moment of area of a member, I, is

$$I \propto t^4 \tag{7}$$

When a load is applied at the midpoint of a member, the deflection is proportional to Fl^3/E_pI where E_p is the elastic modulus for the material of the beam. The remote stress σ is related to this force by $F \propto \sigma l^2$ and the remote strain ε is related to the displacement by $\varepsilon \propto \delta/l$. It follows that the elastic modulus for the foam is

$$E_f = \frac{\sigma}{\varepsilon} \propto \frac{E_p I}{l^4} \propto \frac{E_p t^4}{l^4} \propto E_p \left(\frac{\rho_f}{\rho_p}\right)^2 \propto E \left(\frac{t}{l}\right)^2 \tag{8}$$

This simple model allow to predict that foams characterised by thinner wall (smaller t) will bent more easily and hence possess smaller compression moduli.

In this respect V87.5X10PV90 and V62,5X30PV90 represent exceptions as their compression moduli are the highest among foams of their respective series. A possible explanation might be that because of the extreme thinning of their wall within the foams, foam collapse upon drying has occurred to a larger extent. This is evidenced by the values of their pore volumes which are the lowest in their respective series. Densification of the foam structure consequent to this shrinkage may partially offset the intrinsic weakness of foams walls. The effect of cell size on the elastic modulus has been shown to be negligible.

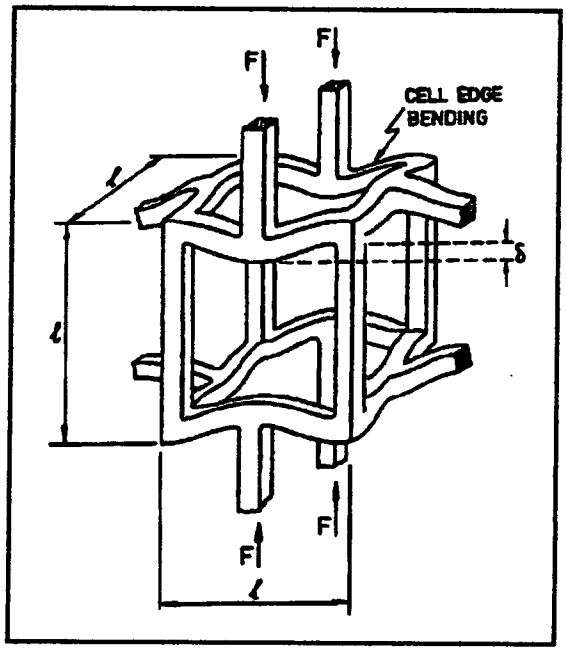

Fig. 4.9. Cell edge bending of an idealised foam cell (from ref. 49).

4.3.5 Conclusions

In this charter polyHIPE foams containing a monomer amenable to functionalization, 4-vinylbenzylchloride, and divinylbenzene as a crosslinker were prepared and characterized.

The influence of VBC concentration on the morphology and mechanical properties of the corresponding foams were studied. It was shown that VBC, a relatively polar molecule, exhibits a pronounced ability to be co-adsorbed at the interface together with SPAN 80, the primary surfactant used to stabilise the emulsions.

The morphology of the foams were investigated by SEM and intrusion mercury porosimetry which revealed that the increase of the concentration of VBC in the organic phase of the emulsions caused a decrease in both the cavities and interconnecting windows diameters.

The mechanical performances of the foams were evaluated through measurements of their compression modulus. Their values were a function, for low values of the crosslinker content, of the thickness of foams walls. For higher concentration of DVB, foams response to compression was dictated mainly by the increasing brittleness of the walls of the foams.

Bibliography

1 L.Hong, E. Ruckenstein, *Polymer*, 1992, **33**, 1968.

2 L.Hong, E. Ruckenstein, *React. Polym.*, 1991/1992, **16**, 181.

3 E. Ruckenstein, L.Hong, *Chem. Mater.*, 1992, **4**, 1032.

4 K. Jones, B.R. Lothian, A. Martin, G. Taylor, Z. Haq, *U.S. Pat. 4,668,709*, 1987.

5 H.F.M. Schoo, G. Challa, B. Rowatt, D.C. Sherrington, *React. Polym.*, 1991/1992, **16**, 125.

6 B.C. Benicewicz, G.D. Jarvinen, D.J. Kathios, B.S. Jorgensen, *J. Radioanal. Nucl. Chem.*, 1998, **235**, 31.

7 S.D. Alexandratos, R. Beauvais, J.R. Duke, B.S. Jorgensen, *J. Appl. Polym. Sci.*, 1998, **68**, 1911.

8 Boyde A., *Scanning Electron Microscopy*; Wells, O.C. Ed. Mc Graw-Hill: New York, 1974.

9 I. Aranberri, K.J. Beverley, B.P. Binks, J.H. Clint, P.D.I. Fletcher, *Langmuir*, 2002, **18**, 3471.

10 Williams, A.J. Gray, M.H. Wilkerson, *Langmuir*, 1990, **6**, 437.

11 N.R. Cameron, D.C. Sherrington, L. Albiston, D.P. Gregory, *Colloid Polym Sci.* 1996, **274**, 592.

12 C.Z. Wagner, *Elektrochem.*, 1961, **65**, 581.

13 I.M. Lifshitz, V.V. Slyozov, *J. Phys. Chem. Solids,* 1961, **19**, 35.

14 Tanford, C. "*The Hydrophobuc Effect: Formation of Micelles and Biological Membranes*", Krieger Publishing Co., Malabar, FL, 1991.

15 Grulke, E. A. In *Polymer Handbook*, 4th ed.; Brandrup, J., Immergut E. H., Grulke, E. A., Eds.; Wiley-Interscience: New York, 1999; Chapter VII, p. 675.

16 Van Krevrelen, D. W. In *Properties of Polymers*, 3rd ed.; Elsevier: New York, 1990; Chapter 7, p. 189.

17 A.J. Hyde, D.W.M. Johnstone, *J. Colloid Interf. Sci.*, 1975, **53**, 349.

18 S. Gravsholt, *J. Colloid Inter. Sci.*, 1976, **57**, 575.

19 T. Imae, R. Kamiga, S. Ikeda, *J. Colloid Interf. Sci.*, 1985 **108**, 215.

20 K. Horbaschek, H. Hofmann, C. Thunig, *J. Colloid Interf. Sci.*, 1998, **206**, 439.

21 U.R.K. Rao, C. Manohar, B.S. Valaulikar, R.M. Iyer, *J. Phys. Chem.*, 1987, **91**, 3286.

22 U. Olsson, O. Söderman, P. Guéring, *J. Phys. Chem.*, 1986, **90**, 5223.

23 C. Manohar, U.R.K. Rao, Valaulikar, R.M. Iyer, *J. Chem. Soc.*, 1996, 379.

[24] M.S. Turner, C. Marques, M.E. Cates, *Langmuir*, 1993, **6**, 695.

[25] B. Lindmann, H. Wennerström, *Topics Curr. Chem.*, 1980, **87**, 1.

[26] H. Tai, A. Sergienko, M.S. Silverstein, *Polym. Eng. Sci.*, 2001, **41**, 1540.

[27] H. Tai, A. Sergienko, M.S. Silverstein, M.S. Silverstein, *Polymer*, 2001, **42**, 4473.

[28] C. Orr, in *Encyclopedia of Emulsion Science and Technology*, chapter 6, ed. P. Becher, Marcell Dekker, Vol. 1, 1983.

[29] Deshikan, S.R.; Papadopolous, K.D., *J. Colloid Interf. Sci.*, 1995, **174**, 302.

[30] Deshikan, S.R.; Papadopolous, K.D., *J. Colloid Interf. Sci.*, 1995, **174**, 313.

[31] Chen, J.D., Hahn P.S., Slattery J.C., *ALChE J.*, 1984, **30**, 622.

[32] Chen, J.D., *J. Colloid Interf. Sci.*, 1985, **107**, 209.

[33] Chen, J.D., Hahn P.S., Slattery J.C., *ALChE J.* 1988, **34**, 140.

[34] Derjaguin, B.V., London, L.D., *Acta Physicochim. URSS,* 1941, **14**, 633.

[35] Verwey, E.J.W.; Overbeek J.Th.G., *Theory of the Stability of Lyophobic Colloids*, Elsevier, Amsterdam, 1948.

[36] Ostwald W., *Z. Phys. Chem.* (Leipzig), 1900, **34**, 295.

[37] Lifshitz I.M., Slezov, V.V., *Sov. Phys. JETP,* 1959, **35**, 331.

[38] Wagner, C., *Z. Electrochem.*, 1961, **35**, 581.

[39] Taylor, P. *Colloids Surf., A,* 1995, **99**, 175.

[40] Taylor P. *Adv. Colloid Inter. Sci.*, 1998, **75**, 107.

[41] Higuchi, W.I., Misra J., *J. Pharm. Sci.*, 1962, **51**, 459.

[42] Thomson W. (Lord Kelvin) *Philos. Mag.*, 1871, **42**, 448.

[43] M.P. Aronson, M.F. Petko, *J.Coll. Interf. Sci.*, 1993, **159**, 134.

[44] Kabalnov, A.S., Shchukin, E.D., *Adv. Colloid Interf. Sci.*, 1992, **38**, 69.

[45] Weiss, J., Hermann, N., Mc Clements, D.J., *Langmuir,* 1999, **15**, 6745.

[46] De Smet, Y., Denemaeker L., Finsy, R., *Langmuir,* 1999, **15**, 6745.

[47] J.A. Marqusee, J. Ross, *J. Chem. Phys*, 1984, **80** , 536.

[48] Klemper D, Frisch K. C., *Handbook of polymeric foam and foam Technology*, New York: Oxford University Press, 1996.

[49] L.J. Gibson, M.F. Ashby, *Cellular Solids, Structure & Properties,* Pergamon Press: New York, 1988.

[50] R.W. Rice, *J. Mater. Sci.*, 1997, **32**, 4731.

[51] J.M. Williams, D.A. Wroblesky, *Langmuir*, 1988, **4**, 656.

[52] D. Braun, W. Czerwinski, G. Dusselhoff, F. Tudös, T. Kelen, B. Turcsanyi, *Angew. Makromol. Chem.*, 1984, **125**, 161.

[53] G. Lu, G.Q. Lu, Z.M. Xiao, *J. Porous Mater.*, 1999, **6**, 359.

Conclusions and future work

The work described in this thesis has shown for the first time what are the relevant processes responsible for the morphologies and porous structure exhibited by PolyHIPE foams possessing high surface areas (~ 700 m^2/g). In particular, it was shown that the polarity and hydrogen bond forming abilities of the components of the organic phase determined the degree of their adsorption at the interface and as a consequence cooperated together with the primary surfactant to the value of the interfacial tension. This effect translates into morphological features in the final foams such as the size of the cells and the thickness of foam walls (the size of the interconnecting windows is influenced by this last feature of the foams).

A more subtle effect, also related with continuous phase polarity, is represented by the molecular diffusion of the dispersed phase through the continuous one (Ostwald ripening). This effect affects the quality of the reacting medium in which polymerisation occurs and in final terms the porosity of the walls of the foams. Because of Ostwald ripening there is not a direct relationship between thermodynamic affinity of the porogen for the polymeric network and surface areas of the resulting PolyHIPE foams but the quality of the organic medium is the outcome of the interplay among a few factors:

1) porogen-polymer affinity;

2) interfacial activity of the porogen;

3) influence of the porogen on surfactant c.μ.c and as a consequence on its degree of covering and packing at the interface;

4) the influence of porogen on Ostwald ripening.

The comprehension of the phenomena described above allowed to devise strategies for attaining control over foam morphology (dimension of cells and of interconnecting holes) and to obtain materials with very high surface areas.

In the case of foams prepared with VBC monomer there are strong clues that the morphological features of the foams obtained in the experimental conditions stated, are dictated primarily by emulsion viscosity which in turn seems to be determined by the concentration of VBC in the organic phase. Mechanical performances are a direct consequence of the morphology and chemical compositions of the foams.

Materials with hierarchical porosity have attracted much attention recently because they combine the advantages of high surface area with the accessible diffusion pathways associated with macroporous structures [1-5].

The polyHIPE materials described in this thesis are expected to be of interest to processes traditionally associated with chromatographic separation and supported phase synthesis or catalysis. In applications such as catalysis and sorption, high porosity and high internal surface area improve efficiency. Macropores facilitate material transport to mesoporous internal regions where reactions or separation can take place

At the macroscale level the performance of sorbents for chromatographic separation and solid-phase catalysis depends on the size, porosity, texture and mechanical strength of the matrix. Simultaneously, high surface areas and monodispersed pore sizes are needed to obtain the necessary space-flow velocity and molecular selectivity.

Attempts were pursued in order to find applications for the high surface areas polyHIPE foams described in this thesis in the field of reversed phase chromatography. The approach devised to this end, consisted of filling a chromatographic column with a HIPE and polymerising the emulsion at 60 C in a oven at 60 °C. In practice, the implementation of this strategy is constrained by several limitations. A few are of practical nature: concentrated macro-emulsions are inherently thermodynamically unstable systems that undergo breaking to some extent. This means that at the end of polymerisation on top of a emulsion there is always a thin layer of water phase which has separated out of the emulsion. This translates into a void space at the top end of the column. This inconvenience can be circumvented by using moulds clamped at both ends of the chromatographic column. At the end of the polymerisation, the moulds are removed and the rod of polymeric foam protruding out of the column is cut. This ensures that the column will be completely filled with the stationary phase. Emulsion breaking processes cause also the appearance inside the bulk of the foam of small voids which are detrimental to separations. For these reason it is important to use as much kinetically stable as possible emulsion systems that minimize the breaking processes. Another problem is represented by porogen evaporation during polymerisation that causes a radial gap to appear at both ends of the column. High boiling porogens (for instance, CB and C_2B better than T) are preferred in this respect. The occurrence of porogen evaporation can be drastically reduced by the application of a positive pressure on the polymerising system. For instance, the column filled with the emulsion can be placed in a vacuum oven connected to a nitrogen cylinder so as to increase the pressure inside the oven above room pressure.

By applying these precautions we succeeded to circumvent the above shortcomings and to prepare columns filled with X80PV90(0.75CB)S20AD (1:0.75 monomer to porogen ratio). Separation tests conducted on a mixture of low molecular weights compounds (mainly aromatics) demonstrated that this PolyHIPE material was effective as a separation medium.

The main advantage consisted of the possibility of carrying out the analysis at very high flow rates without meeting relevant backpressures. Conversely, peak resolution was not as good as that provided by a conventional chromatographic column packed with silica. Despite of the high surface area possessed by X80PV90(0.75CB)S20AD (~ 600 m^2/g) the number of theoretical plates is rather low (~ 2000 plates/m). Possible reasons for this not optimal performance are as follows:

-the material in spite of its high crosslinking density is not rigid but may undergo shrinking or swelling in response to the thermodynamic quality of the mobile phase used. This translates into changes of its porous structure. The figure of surface area reported, refers to the dry state;

-it can also be wondered whether PolyHIPE possess an intrinsically suitable morphology for chromatographic separations. This can be deduced from the flow pattern imparted by PolyHIPE matrixes on a liquid flowing through it. It may be envisaged that the presence of a plurality of interconnecting windows of different dimensions will result in a distribution of flow rates which will cause band broadening and poor peak resolution. In addition, the relatively large volume characterising a cavity of average dimension will cause the partition equilibrium of analytes between stationary and mobile phases to shift in favour of the latter.

For these reasons an improvement in foam morphology may involve a narrowing in the polydispersity of windows diameter and a reduction in cell size. This goal can be achieved through the following strategies:

1) the addition of increasing amount of salt in the aqueous phase of the emulsion tend to lower the diameter of the interconnecting windows and their polydispersity[6];

2) a novel route which has not been tested yet with HIPEs is based on the phase inversion technique introduced by Shinoda [7-9]. An O/W emulsion at room temperature stabilised by a non-ionic surfactant of the polyoxyethylene type (for instance, Brj 30)[10, 11] undergoes phase inversion at higher temperature producing a finely dispersed W/O emulsion. In such a system the average diameter of the droplets of the dispersed phase is of the order of 100 nm and is characterised by a narrow polydispersity. This methodology may be adapted to the DVB(Por) system in order to produce foam with smaller average diameter. Such porous matrixes could represent an advancement compared to existing polyHIPE foams which are characterised by relatively large and polydispersed cells (~ 10 μm) and applications like chromatographic separations and solid-phase synthesis would benefit of the lower volume of solvent necessary to fill a cavity and as a consequence should guarantee better separations and adequate conversion rate of reagents into products. These positive aspects would be partially offset by the corresponding increase in the backpressure connected with pumping liquids through the

matrix.

To better characterise the porous structure of the polyHIPE foams produced and monitor their performances in the operative conditions, that is in the wet state, it would be advisable to use additional techniques to those used in this thesis. The traditional methods for measuring pore size distributions such as N_2 sorption and mercury intrusion porosimetry, suffer from disadvantages mainly associated with the preliminary drying of the samples.

Conversely, inversion size exclusion chromatography (ISEC) [12-15] and nuclear magnetic resonance (NMR) [16-19] allow to probe non destructively the pore size distribution of porous, wet solids.

ISEC is used to determine the pore-size distribution of column packing by monitoring the residence times of solutes of varying molecular diameters. A monodisperse solute is injected into a column packed with the porous material and is used to probe the pores that are larger than the solute size. Each monodisperse standard provides the average pore-size within the range of pores sizes up to the next larger monodisperse standard. While solutes with a larger molecular size have fewer chances to penetrate the macropores of the adsorbent and thus have a smaller retention time, smaller solutes penetrate more pores and are retained longer in the column.

The nuclear magnetic resonance behaviour of liquids confined in pores is used to infer information about the structure of porous materials. This method is based on the lowering of the freezing point of liquids embedded in capillary pores. The NMR signal attributed to the liquid part of the solvent is recorded as a function of decreasing temperature. The solvent inside the pore structure of the sample remains liquid well below the normal freezing point of bulk solvent. The lowering of the freezing point of an adsorbed liquid is well known, and many formulas have been proposed in the literature. In addition, the interaction between liquid molecules and pore surfaces, and motion restriction due to pore geometry, are often quantified using NMR through the spatial measurements of spin density and relaxation time.

The fluid flow through a polyHIPE matrix can be characterised using three dimensional microimaging and pulsed gradient stimulated ordinary echo NMR. Microimaging in particular, yields structural information and, specifically, a reduced radial distribution function for the structure of the void space [21-22].

Bibliography

1 F.M. Menger, T. Tsuno, *J. Am. Chem. Soc.* 1990, **112**, 1263.

2 B.T. Holland, L. Abrams, A. Stein, *J. Am. Chem. Soc.* 1999, **121**, 4308.

3 A. Imhof, D.J. Pine, *Nature*, 1997, **389**, 948.

4 Q. Huo, J. Feng, F. Schüth, G.D. Stucky, *Chem. Mater.*, 1997, **9**, 14.

5 H.F. Zhang, G.C. Hardy, M.J. Rosseinsky, A.I. Cooper, *Adv. Mater.*, 2003, **15**, 78.

6 D.P. Gregory, *EU0299762*, 1987.

7 K. Shinoda, H, Saito, *J. Colloid Interface Sci.* 1968, **26**, 70.

8 K. Shinoda, H, Saito, *J. Colloid Interface Sci.* 1969, **30**, 258.

9 K. Shinoda, H. Kunieda, In *Encyclopedia of Emulson Technology*; P. Becher, Ed.; Marcel Dekker: New York, 1983; Vol. 1 pp 337-367.

10 A. Forgianini, J. Esquena, C. Gonzalez, C. Solans *Langmuir*, 2001, **17**, 2076.

11 P. Izquierdo, J. Esquena, Th. F. Tadros, C. Dederen, M.J. Garcia, N. Azemar, C. Solans, *Langmuir*, 2002, **18**, 26.

12 N. V. Saritha, G. Madras, *Chem. Eng. Sci.*, 2001, **56**, 6511.

13 M. Al-Bokari, D. Cherrak, G. Guiochon, *J. Chrom. A*, 2002, **975**, 275.

14 Ousalem, X.X. Zhu, J. Hradil, *J. Chrom. A*, 2000, **93**, 13.

15 M. Goto, B.J. McCoy, *Chem. Eng. Sci.*, 2000, 55, 723.

16 S.H. Strange, M. Rahman, E.G. Smith, *Phys Rev. Lett.*, 1993, **71**, 3589.

17 F. Milia, M. Fardis, G. Papavassilion, A. Leventis, *Magnetic Resonance Imaging*, 1998, **16**, 677.

18 P. Porion, A.M. Fangère, P. Levitz, H. Van Damme, A. Raoof, J.P. Guilband, F. Chevor, *Magnetic Resonance Imaging*, 1998, **16**, 679.

19 B. Issa, P. Gibbs, R. Hodjskinson, C.M. Langton, L.W. Turnbull, *Magnetic Resonance Imaging*, 1998, **16**, 651.

20 B. Manz, P. Alexander, P.B: Warren, L.F. Gladden, *Magnetic Resonance Imaging*, 1998, **16**, 673.

21 K.J. Packer, J.J. Tessier, *Molecular Physics*, 1996, **87**, 267.

22 B.R. Locke, M. Acton, S.J. Gibbs, *Langmuir*, 2001, **17**, 6771.

Acknowledgments

My first thanks is for my supervisor, dr Neil R. Cameron, who gave me the opportunity to work in an intellectually stimulating environment and to a scientifically interesting and sound research project.

A heartily thanks is for dr Audrey M. Cameron for being my friend and for the help and support given during the three years of my PhD.

I wish also to thank my colleague and "fellow traveller" Wendy Busby for the help given to me.

Finally a big thanks goes to the "Italian contingent" of Durham University and in particular to Edoardo, Claudia, Dimitri and Cinzia.